

ON ADAPTIVE MIMO SPACE-TIME PROCESSING

CENTRE FOR NEWFOUNDLAND STUDIES

**TOTAL OF 10 PAGES ONLY
MAY BE XEROXED**

(Without Author's Permission)

JASON R. LEE



On Adaptive MIMO Space-Time Processing

Submitted By

Jason R. Lee
(ID#: 008908980)

In partial fulfillment of the requirements for the

Degree of Master of Engineering

Faculty of Engineering & Applied Science

Memorial University of Newfoundland
St. John's, Newfoundland

Copyright 2005, Jason R. Lee



Library and
Archives Canada

Bibliothèque et
Archives Canada

Published Heritage
Branch

Direction du
Patrimoine de l'édition

395 Wellington Street
Ottawa ON K1A 0N4
Canada

395, rue Wellington
Ottawa ON K1A 0N4
Canada

Your file *Votre référence*
ISBN: 978-0-494-19415-7
Our file *Notre référence*
ISBN: 978-0-494-19415-7

NOTICE:

The author has granted a non-exclusive license allowing Library and Archives Canada to reproduce, publish, archive, preserve, conserve, communicate to the public by telecommunication or on the Internet, loan, distribute and sell theses worldwide, for commercial or non-commercial purposes, in microform, paper, electronic and/or any other formats.

The author retains copyright ownership and moral rights in this thesis. Neither the thesis nor substantial extracts from it may be printed or otherwise reproduced without the author's permission.

AVIS:

L'auteur a accordé une licence non exclusive permettant à la Bibliothèque et Archives Canada de reproduire, publier, archiver, sauvegarder, conserver, transmettre au public par télécommunication ou par l'Internet, prêter, distribuer et vendre des thèses partout dans le monde, à des fins commerciales ou autres, sur support microforme, papier, électronique et/ou autres formats.

L'auteur conserve la propriété du droit d'auteur et des droits moraux qui protègent cette thèse. Ni la thèse ni des extraits substantiels de celle-ci ne doivent être imprimés ou autrement reproduits sans son autorisation.

In compliance with the Canadian Privacy Act some supporting forms may have been removed from this thesis.

Conformément à la loi canadienne sur la protection de la vie privée, quelques formulaires secondaires ont été enlevés de cette thèse.

While these forms may be included in the document page count, their removal does not represent any loss of content from the thesis.

Bien que ces formulaires aient inclus dans la pagination, il n'y aura aucun contenu manquant.


Canada

The undersigned hereby recommended to the School of Graduate Studies acceptance of the thesis

On Adaptive MIMO Space-Time Processing

Submitted by Jason R. Lee
In partial fulfillment of the requirements for the
Degree of Master of Engineering

Thesis Supervisor
Dr. Mohamed Hossam Ahmed

Associate Dean, Graduate Studies & Research
Dr. R. Venkatesan

ABSTRACT

In this thesis, we develop a novel adaptive MIMO space-time processing method which adapts to changes in the wireless environment for the maximization of wireless link *performance*.

First, we develop a fully simulated MIMO wireless environment in Matlab[®] to facilitate algorithm development and performance benchmarking. Second, we develop the theory supporting an adaptive MIMO layered space-time processing method called adaptive BLAST (A-BLAST). Thirdly, known non-adaptive diversity and spatial multiplexing layered space-time processing techniques are implemented and benchmarked under simulated MIMO channels using two element, four element, and eight element antenna arrays respectively. Fourth, we implement and benchmark an A-BLAST approach under equivalent simulated MIMO channels. Finally, simulation results are provided which demonstrate a performance improvement using A-BLAST over the non-adaptive benchmarks.

The main contributions of this thesis include the creation of a highly parameterized MIMO simulation environment in Matlab[®], as well as, the development of a novel A-BLAST layered space-time processing algorithm complemented with adaptation based on reference BER data obtained under MIMO channels of varying spatial rank using the developed simulation environment. The A-BLAST code structure developed provides additional space-time codeword mappings not previously defined through traditional non-adaptive BLAST methods. These additional codeword mappings are shown to provide more granular control over the relative weighting of spatial multiplexing gain and diversity order and are better suited to a broader range of MIMO channel environments. Using estimates of the MIMO channel spatial rank and receive signal-to-noise ratio, combined with a residual bit error rate threshold, the developed adaptation algorithm is shown to be able to automatically select an A-BLAST codeword mapping from the available A-BLAST codeword set, improving MIMO link performance when compared with non-adaptive BLAST techniques which are optimized for the spatial multiplexing and diversity encoding respectively.

ACKNOWLEDGEMENT

I would like to thank Dr. Heys and Dr. Moloney for agreeing to support my application to the School of Graduate Studies in 2001. I sincerely appreciate the confidence shown and support given as I began my graduate work at Memorial University.

I would like to thank both Dr. Heys and Dr. Gosine for convincing me to take a one year leave of absence rather than withdrawing entirely from the School of Graduate Studies in the fall of 2002. The leave of absence allowed me to focus entirely on being successful at adjusting to the new roles and increased project management responsibilities at Aliant Mobility. In addition, the leave of absence provided time needed as a father to assist at home with the arrival of our second child, Noah. For helping me make the right decision in 2002, I will always be grateful.

I would like to thank Dr. Ahmed for agreeing, in the fall of 2003, to supervise my research. Since that time, your supervision, direction, and tutelage in the areas of MIMO space-time processing and wireless communications have been a tremendous help. Your recommendation, in the fall of 2004, that I take Matrix Computations 6910 in the Computational Sciences Department was both well timed and a great help, allowing me to effectively grasp and efficiently complete the literature review that would follow. Our discussions during the development of the A-BLAST space-time processing method and adaptation algorithm were most enjoyable. I regard this time as tremendously valuable and rewarding.

I would like to thank Reza Shahidi for taking the time from his busy PhD. studies, during my initial days at CERL, to show me how to launch simulations from the server *cluster*. I used this server near continuously during my research and found it to be a very valuable research tool.

I would like to thank Dave Brown of Aliant Mobility and Trevor Macleod of Bell Mobility for their combined support, both financially and professionally, of my application for educational leave and NSERC-IPS scholarship in 2005. For the financial assistance and educational leave given, I will always be grateful.

Finally, I would like to thank my beautiful wife Kelly and children Hannah and Noah for their support and sacrifices made while I completed this work.

TABLE OF CONTENTS

ABSTRACT.....	III
ACKNOWLEDGEMENT.....	IV
LIST OF FIGURES.....	VIII
LIST OF TABLES.....	XI
LIST OF ACRONYMS.....	XII
LIST OF SYMBOLS.....	XIV
1 INTRODUCTION.....	1
1.1 THESIS MOTIVATION.....	2
1.2 THESIS OBJECTIVES.....	4
1.3 THESIS ORGANIZATION.....	4
2 MIMO OVERVIEW.....	6
2.1 INTRODUCTION.....	6
2.2 BASIC MIMO CHANNEL MODEL.....	6
2.2.1 <i>Full Rank Channel</i>	8
2.2.2 <i>Rank Deficient Channel</i>	9
2.2.3 <i>Low Signal-to-Noise Ratio Channel</i>	9
2.3 MIMO PERFORMANCE GAINS.....	10
2.3.1 <i>Array Gain</i>	10
2.3.2 <i>Diversity Gain</i>	10
2.3.3 <i>Spatial Multiplexing Gain</i>	11
2.4 MIMO SPATIAL MULTIPLEXING METHODS.....	12
2.4.1 <i>Vertically Encoded Bell Labs Layered Space Time Codes (V-BLAST)</i>	12
2.5 MIMO DIVERSITY METHODS.....	13
2.5.1 <i>Diagonally Encoded Bell Labs Layered Space Time Codes (D-BLAST)</i>	13
2.5.2 <i>Orthogonal Space-Time Block Codes (OSTBC)</i>	14
2.6 MIMO ADAPTIVE SPACE-TIME PROCESSING METHODS.....	16
2.6.1 <i>Switched Mode Transmission (SMT)</i>	16
2.6.2 <i>Rank Adaptive Transmission (RAT)</i>	18
2.6.3 <i>Linear Dispersion Code (LDC)</i>	20
2.7 SUMMARY.....	21
3 SIMULATED MIMO WIRELESS ENVIRONMENT (SMWE).....	23
3.1 SMWE INPUT PARAMETERS.....	23
3.2 SMWE ARCHITECTURE.....	24
3.2.1 <i>Space-Time Transmitter Subsystem (STS)</i>	26
3.2.1.1 Random Data Source.....	26
3.2.1.2 ST Mapper.....	27
3.2.1.3 Precoder.....	31
3.2.2 <i>Space-Time Receiver Subsystem (SRS)</i>	32
3.2.2.1 Precoder.....	33
3.2.2.2 ST Demapper.....	34
3.2.2.3 Random Data Sink.....	34
3.2.3 <i>MIMO Channel Subsystem (MCS)</i>	35
3.2.3.1 Block Fading MIMO Channel.....	36
3.2.3.2 Time-Correlated Continuous Fading MIMO Channel.....	37

3.2.3.3	Spatial Correlation	37
3.2.3.4	Line-of-Sight (LOS) Signal Propagation.....	37
3.2.3.5	Antenna Cross-Polarization Discrimination.....	38
3.2.4	<i>Adaptive Controller Subsystem (ACS)</i>	38
3.2.5	<i>Performance Analysis Subsystem (PAS)</i>	42
3.3	SUMMARY	44
4	LAYERED SPACE-TIME (LST) PROCESSING PERFORMANCE BENCHMARKS	46
4.1	LST SPATIAL MULTIPLEXING METHODS.....	46
4.1.1	<i>V-BLAST (M = N = 2)</i>	47
4.1.2	<i>V-BLAST (M = N = 4)</i>	47
4.1.3	<i>V-BLAST (M = N = 8)</i>	48
4.2	LST DIVERSITY METHODS.....	49
4.2.1	<i>D-BLAST (M = N = 2)</i>	50
4.2.2	<i>D-BLAST (M = N = 4)</i>	50
4.2.3	<i>D-BLAST (M = N = 8)</i>	51
4.3	SUMMARY	52
5	ADAPTIVE MIMO SPACE-TIME PROCESSING RESEARCH.....	53
5.1	ADAPTIVE BLAST (A-BLAST).....	53
5.1.1	<i>Space-Time Codec Description</i>	53
5.1.2	<i>Adaptation (Mode Selection)</i>	56
5.1.3	<i>A2-BLAST Implementation (M = N = 2)</i>	58
5.1.3.1	Performance Results.....	60
5.1.3.1.1	Residual BER Threshold of 10^{-1}	61
5.1.3.1.2	Residual BER Threshold of 10^{-2}	63
5.1.3.1.3	Residual BER Threshold of 10^{-3}	65
5.1.3.2	Summary	66
5.1.4	<i>A4-BLAST Implementation (M = N = 4)</i>	68
5.1.4.1	Performance Results.....	71
5.1.4.1.1	Residual BER Threshold of 10^{-1}	72
5.1.4.1.2	Residual BER Threshold of 10^{-2}	76
5.1.4.1.3	Residual BER Threshold of 10^{-3}	80
5.1.4.2	Summary	84
5.1.5	<i>A8-BLAST Implementation (M = N = 8)</i>	85
5.1.5.1	Performance Results.....	89
5.1.5.1.1	Residual BER Threshold of 10^{-1}	90
5.1.5.1.2	Residual BER Threshold of 10^{-2}	93
5.1.5.1.3	Residual BER Threshold of 10^{-3}	96
5.1.5.2	Summary	99
5.1.6	<i>Implementation Issues</i>	99
5.1.6.1	Side Channel Feedback Bandwidth Requirements.....	100
5.1.6.2	Channel Estimation	103
5.1.6.2.1	Effect of Noise Perturbation.....	103
5.1.6.3	Rank Estimation.....	105
5.1.6.3.1	Effect of Noise Perturbation.....	105
5.1.6.3.2	Effect of Reducing Rank Percentage Power Threshold (τ).....	108
5.1.6.4	Antenna Array Mutual Coupling and Spatial Correlation.....	110
5.1.6.5	Implementation Complexity.....	114
6	CONCLUSIONS AND FUTURE WORK	116
	REFERENCES.....	118
	APPENDIX A – SMWE SOURCE FILE LISTING	122
	APPENDIX B – SUPPLEMENTARY A-BLAST MODE SUMMARY DATA.....	124

EXAMPLE CALCULATION OF CODE RATE [S/CU] AND DIVERSITY ORDER	124
A2-BLAST (M = N = 2).....	124
A3-BLAST (M = N = 3).....	125
A4-BLAST (M = N = 4).....	126
A5-BLAST (M = N = 5).....	127
A6-BLAST (M = N = 6).....	129
A7-BLAST (M = N = 7).....	131
A8-BLAST (M = N = 8).....	134

LIST OF FIGURES

FIGURE 2-1 MIMO CHANNEL MODEL (EQUIVALENT BASEBAND).....	6
FIGURE 2-2 MIMO CHANNEL TO I TH RECEIVER.....	8
FIGURE 2-3 MIMO CHANNEL FROM J TH TRANSMITTER.....	8
FIGURE 2-4 V-BLAST ENCODING (M=N=4).....	13
FIGURE 2-5 D-BLAST ENCODING (M=N=4).....	14
FIGURE 2-6 OSTBC ENCODING.....	15
FIGURE 2-7 ADAPTIVE STP - DIVERSITY VS. SPATIAL MULTIPLEXING LATTICE.....	16
FIGURE 2-8 SMT BLOCK DIAGRAM.....	17
FIGURE 2-9 RAT BLOCK DIAGRAM.....	19
FIGURE 3-1 SMWE ARCHITECTURE.....	25
FIGURE 3-2 ST TRANSMITTER SUBSYSTEM.....	26
FIGURE 3-3 RANDOM DATA SOURCE.....	27
FIGURE 3-4 ST RECEIVER SUBSYSTEM.....	32
FIGURE 3-5 RANDOM DATA SINK.....	34
FIGURE 3-6 MIMO CHANNEL SUBSYSTEM.....	35
FIGURE 3-7 MIMO CHANNEL REALIZATION GENERATION.....	36
FIGURE 3-8 ACS PSEUDO CODE.....	41
FIGURE 3-9 PERFORMANCE MONITOR LOG FILE (SAMPLE).....	44
FIGURE 4-1 V-BLAST BER VS. SNR (M=N=2, QPSK).....	47
FIGURE 4-2 V-BLAST BER VS. SNR (M=N=4, QPSK).....	48
FIGURE 4-3 V-BLAST BER VS. SNR (M=N=8, QPSK).....	48
FIGURE 4-4 D-BLAST BER VS. SNR (M=N=2, QPSK).....	50
FIGURE 4-5 D-BLAST BER VS. SNR (M=N=4, QPSK).....	51
FIGURE 4-6 D-BLAST BER VS. SNR (M=N=8, QPSK).....	51
FIGURE 5-1 A-BLAST BLOCK DIAGRAM.....	54
FIGURE 5-2 A-BLAST DIVERSITY VS. SPATIAL MULTIPLEXING BALANCING.....	56
FIGURE 5-3 A2-BLAST MODE SUMMARY (M=N=2).....	58
FIGURE 5-4 A2-BLAST REFERENCE BER CURVES (RALEIGH FADING).....	59
FIGURE 5-5 A2-BLAST REFERENCE BER CURVES (AVERAGE RANK 1).....	59
FIGURE 5-6 A2-BLAST RESIDUAL BER (RALEIGH FADING, BER <1E-1).....	61
FIGURE 5-7 A2-BLAST GOODPUT (RALEIGH FADING, BER <1E-1).....	61
FIGURE 5-8 A2-BLAST RESIDUAL BER (AVERAGE RANK 1, BER <1E-1).....	62
FIGURE 5-9 A2-BLAST GOODPUT (AVERAGE RANK 1, BER <1E-1).....	62
FIGURE 5-10 A2-BLAST RESIDUAL BER (RALEIGH FADING, BER <1E-2).....	63
FIGURE 5-11 A2-BLAST GOODPUT (RALEIGH FADING, BER <1E-2).....	63
FIGURE 5-12 A2-BLAST RESIDUAL BER (AVERAGE RANK 1, BER <1E-2).....	64
FIGURE 5-13 A2-BLAST GOODPUT (AVERAGE RANK 1, BER <1E-2).....	64
FIGURE 5-14 A2-BLAST RESIDUAL BER (RALEIGH FADING, BER <1E-3).....	65
FIGURE 5-15 A2-BLAST GOODPUT (RALEIGH FADING, BER <1E-3).....	65
FIGURE 5-16 A2-BLAST RESIDUAL BER (AVERAGE RANK 1, BER <1E-3).....	66
FIGURE 5-17 A2-BLAST GOODPUT (AVERAGE RANK 1, BER <1E-3).....	66
FIGURE 5-18 A4-BLAST MODE SUMMARY (M=N=4).....	68
FIGURE 5-19 A4-BLAST REFERENCE BER CURVES (RALEIGH FADING).....	69
FIGURE 5-20 A4-BLAST REFERENCE BER CURVES (AVERAGE RANK 3).....	69
FIGURE 5-21 A4-BLAST REFERENCE BER CURVES (AVERAGE RANK 2).....	70
FIGURE 5-22 A4-BLAST REFERENCE BER CURVES (AVERAGE RANK 1).....	70
FIGURE 5-23 A4-BLAST RESIDUAL BER (RALEIGH FADING, BER <1E-1).....	72
FIGURE 5-24 A4-BLAST GOODPUT (RALEIGH FADING, BER <1E-1).....	72
FIGURE 5-25 A4-BLAST RESIDUAL BER (AVERAGE RANK 3, BER <1E-1).....	73
FIGURE 5-26 A4-BLAST GOODPUT (AVERAGE RANK 3, BER <1E-1).....	73
FIGURE 5-27 A4-BLAST RESIDUAL BER (AVERAGE RANK 2 BER <1E-1).....	74
FIGURE 5-28 A4-BLAST GOODPUT (AVERAGE RANK 2 BER <1E-1).....	74

FIGURE 5-29 A4-BLAST RESIDUAL BER (AVERAGE RANK 1 BER <1E-1).....	75
FIGURE 5-30 A4-BLAST GOODPUT (AVERAGE RANK 1 BER <1E-1)	75
FIGURE 5-31 A4-BLAST RESIDUAL BER (RALEIGH FADING, BER <1E-2).....	76
FIGURE 5-32 A4-BLAST GOODPUT (RALEIGH FADING, BER <1E-2).....	76
FIGURE 5-33 A4-BLAST RESIDUAL BER (AVERAGE RANK 3, BER <1E-2).....	77
FIGURE 5-34 A4-BLAST GOODPUT (AVERAGE RANK 3, BER <1E-2)	77
FIGURE 5-35 A4-BLAST RESIDUAL BER (AVERAGE RANK 2 BER <1E-2).....	78
FIGURE 5-36 A4-BLAST GOODPUT (AVERAGE RANK 2, BER <1E-2)	78
FIGURE 5-37 A4-BLAST RESIDUAL BER (AVERAGE RANK 1, BER <1E-2).....	79
FIGURE 5-38 A4-BLAST GOODPUT (AVERAGE RANK 1, BER <1E-2)	79
FIGURE 5-39 A4-BLAST RESIDUAL BER (RALEIGH FADING, BER <1E-3)	80
FIGURE 5-40 A4-BLAST GOODPUT (RALEIGH FADING, BER <1E-3).....	80
FIGURE 5-41 A4-BLAST RESIDUAL BER (AVERAGE RANK 3, BER <1E-3).....	81
FIGURE 5-42 A4-BLAST GOODPUT (AVERAGE RANK 3, BER <1E-3)	81
FIGURE 5-43 A4-BLAST RESIDUAL BER (AVERAGE RANK 2, BER <1E-3).....	82
FIGURE 5-44 A4-BLAST GOODPUT (AVERAGE RANK 2, BER <1E-3)	82
FIGURE 5-45 A4-BLAST RESIDUAL BER (AVERAGE RANK 1, BER <1E-3).....	83
FIGURE 5-46 A4-BLAST GOODPUT (AVERAGE RANK 1, BER <1E-3)	83
FIGURE 5-47 A8-BLAST MODE SUMMARY (M=N=8).....	85
FIGURE 5-48 A8-BLAST REFERENCE BER CURVES (RALEIGH FADING)	86
FIGURE 5-49 A8-BLAST REFERENCE BER CURVES (AVERAGE RANK 6).....	86
FIGURE 5-50 A8-BLAST REFERENCE BER CURVES (AVERAGE RANK 5).....	87
FIGURE 5-51 A8-BLAST REFERENCE BER CURVES (AVERAGE RANK 4).....	87
FIGURE 5-52 A8-BLAST REFERENCE BER CURVES (AVERAGE RANK 3).....	88
FIGURE 5-53 A8-BLAST REFERENCE BER CURVES (AVERAGE RANK 2).....	88
FIGURE 5-54 A8-BLAST REFERENCE BER CURVES (AVERAGE RANK 1).....	89
FIGURE 5-55 A8-BLAST RESIDUAL BER (RALEIGH FADING, BER<1E-1).....	90
FIGURE 5-56 A8-BLAST GOODPUT (RALEIGH FADING, BER<1E-1).....	90
FIGURE 5-57 A8-BLAST RESIDUAL BER (AVERAGE RANK 4, BER<1E-1)	91
FIGURE 5-58 A8-BLAST GOODPUT (AVERAGE RANK 4, BER<1E-1)	91
FIGURE 5-59 A8-BLAST RESIDUAL BER (AVERAGE RANK 1, BER<1E-1)	92
FIGURE 5-60 A8-BLAST GOODPUT (AVERAGE RANK 1, BER<1E-1)	92
FIGURE 5-61 A8-BLAST RESIDUAL BER (RALEIGH FADING, BER<1E-2).....	93
FIGURE 5-62 A8-BLAST GOODPUT (RALEIGH FADING, BER<1E-2).....	93
FIGURE 5-63 A8-BLAST RESIDUAL BER (AVERAGE RANK 4, BER<1E-2)	94
FIGURE 5-64 A8-BLAST GOODPUT (AVERAGE RANK 4, BER<1E-2)	94
FIGURE 5-65 A8-BLAST RESIDUAL BER (AVERAGE RANK 1, BER<1E-2)	95
FIGURE 5-66 A8-BLAST GOODPUT (AVERAGE RANK 1, BER<1E-2)	95
FIGURE 5-67 A8-BLAST RESIDUAL BER (RALEIGH FADING, BER<1E-3).....	96
FIGURE 5-68 A8-BLAST GOODPUT (RALEIGH FADING, BER<1E-3).....	96
FIGURE 5-69 A8-BLAST RESIDUAL BER (AVERAGE RANK 4, BER<1E-3)	97
FIGURE 5-70 A8-BLAST GOODPUT (AVERAGE RANK 4, BER<1E-3)	97
FIGURE 5-71 A8-BLAST RESIDUAL BER (AVERAGE RANK 1, BER<1E-3)	98
FIGURE 5-72 A8-BLAST GOODPUT (AVERAGE RANK 1, BER<1E-3)	98
FIGURE 5-73 PARTIAL CSI BANDWIDTH (FDD AIR INTERFACE, $\log_2(q_q) = 8, M=N=4$).....	101
FIGURE 5-74 PARTIAL CSI BANDWIDTH (TDD AIR INTERFACE, M=N=4).....	102
FIGURE 5-75 AVERAGE CSI ERROR (LS ESTIMATION, RALEIGH FADING, M=N=4).....	104
FIGURE 5-76 EFFECT OF CSI ERROR ON BER (A4-BLAST).....	105
FIGURE 5-77 AVERAGE RANK VS. K ($\tau=0.99, M=N=4$).....	106
FIGURE 5-78 AVERAGE RANK ESTIMATION ERROR ($\tau=0.99, M=N=4$)	107
FIGURE 5-79 GOODPUT VS. RANK POWER THRESHOLD (A4-BLAST)	108
FIGURE 5-80 RESIDUAL BER VS. RANK POWER THRESHOLD (A4-BLAST)	109
FIGURE 5-81 EFFECT OF SPATIAL CORRELATION ON RANK ESTIMATION (A4-BLAST)	110
FIGURE 5-82 EFFECT OF SPATIAL CORRELATION ON GOODPUT (A4-BLAST)	111

FIGURE 5-83 EFFECT OF SPATIAL CORRELATION ON RESIDUAL BER (A4-BLAST).....	112
FIGURE 5-84 RESIDUAL BER PERFORMANCE - RICEAN FADING VS. SPATIAL CORRELATION (A4-BLAST).	113
FIGURE 5-85 GOODPUT PERFORMANCE - RICEAN FADING VS. SPATIAL CORRELATION (A4-BLAST).....	113
FIGURE 110 A2-BLAST MODE SUMMARY (M=N=2)	124
FIGURE 111 A3-BLAST MODE SUMMARY (M=N=3)	125
FIGURE 112 A4-BLAST MODE SUMMARY (M=N=4)	126
FIGURE 113 A5-BLAST MODE SUMMARY (M=N=5)	128
FIGURE 114 A6-BLAST MODE SUMMARY (M=N=6)	130
FIGURE 115 A7-BLAST MODE SUMMARY (M=N=7)	133
FIGURE 116 A8-BLAST MODE SUMMARY (M=N=8)	136

LIST OF TABLES

TABLE 3-1 SMWE PROGRAMMABLE PARAMETERS	24
TABLE 3-2 ST MAPPING FUNCTIONS	30
TABLE 3-3 ST TRANSMITTER PRECODING FUNCTIONS	32
TABLE 3-4 ST RECEIVER PRECODING FUNCTIONS.....	34
TABLE 3-5 ACS DATABASE.....	40
TABLE 3-6 PAS DATABASE.....	42
TABLE 5-1 A-BLAST CSI SUMMARY	100
TABLE 8 SMWE SOURCE FILE LISTING.....	123
TABLE 9 A2-BLAST MODE SUMMARY (M=N=2)	124
TABLE 10 A3-BLAST MODE SUMMARY (M=N=3)	125
TABLE 11 A4-BLAST MODE SUMMARY (M=N=4)	126
TABLE 12 A5-BLAST MODE SUMMARY (M=N=5)	127
TABLE 13 A6-BLAST MODE SUMMARY (M=N=6)	130
TABLE 14 A7-BLAST MODE SUMMARY (M=N=7)	132
TABLE 15 A8-BLAST MODE SUMMARY (M=N=8)	135

LIST OF ACRONYMS

A-BLAST	Adaptive Bell Labs Layered Space-Time Coding
ACS	Adaptive Controller Subsystem
AP	Access Point
AWGN	Additive White Gaussian Noise
BCD	Binary Coded Decimal
BCH	Bose-Chadhuri-Hocquenghem
BER	Bit Error Rate
BLAST	Bell Labs Layered Space-Time Coding
BS	Base Station
BWA	Broadband Wireless Access
CDMA	Code Division Multiple Access
CPE	Customer Premise Equipment
CODEC	Coder-Decoder
CSI	Channel State Information
DB	Decibel
DBM	Decibel with Respect to a Milliwatt
DFT	Discrete Fourier Transform
DOA	Direction of Arrival
DSP	Digital Signal Processor
D-BLAST	Diagonally Layered BLAST
EVD	Eigen Value Decomposition
FDD	Frequency Division Duplex
FEC	Forward Error Correction
FFT	Fast Fourier Transform
FSL	Free Space Loss
FWA	Fixed Wireless Access
GCB	Gray Coded Binary
H-BLAST	Horizontally Layered BLAST
IEEE	Institute of Electrical and Electronics Engineers
IIR	Infinite Impulse Response
ITU	International Telecommunications Union
IMT-2000	International Mobile Telecommunications-2000
LAN	Local Area Network
LDC	Linear Dispersion Codes
LOS	Line-of-Sight
LS	Least Squares
LST	Layered Space-Time
MAC	Media Access Control
MAN	Metropolitan Area Network
MCS	MIMO Channel Subsystem
MIMO	Multiple-Input Multiple-Output
MISO	Multiple-Input Single-Output

ML	Maximum Likelihood
MPSK	M-ary Phase Shift Keying
MMSE	Minimum Mean Squared Error
MSI	Multi-Stream Interference
NLOS	Non-Line-of-Sight
OFDM	Orthogonal Frequency Division Multiplexing
OSTBC	Orthogonal Space-Time Block Coding
OSUC	Ordered Successive Cancellation
PAS	Performance Analysis Subsystem
PHY	Physical Layer
PSK	Phase Shift Keying
QAM	Quadrature Amplitude Modulation
RCVR	Receiver
RF	Radio Frequency
RFI	Radio Frequency Interference
RSL	Receive Signal Level
SER	Symbol Error Rate
SIMO	Single-Input Multiple-Output
SINR	Signal-to-Interference & Noise Ratio
SISO	Single-Input Single-Output
SMWE	Simulated MIMO Wireless Environment
SNR	Signal-to-Noise Ratio
SRS	Space-Time Receiver Subsystem
STBC	Space-Time Block Coding
STC	Space-Time Coding
STP	Space-Time Processing
STS	Space-Time Transmitter Subsystem
SVD	Singular Value Decomposition
TDD	Time Division Duplex
V-BLAST	Vertically Layered BLAST
WCDMA	Wideband CDMA
WiMAX	Worldwide Interoperability Microwave Access
WLAN	Wireless Local Area Network
XCVR	Transceiver
XTMR	Transmitter
ZF	Zero Forcing
ZMCSCG	Zero Mean Circularly Symmetric Complex Gaussian
3G	Third Generation
4G	Fourth Generation

LIST OF SYMBOLS

B	Composite Channel Bandwidth
B_c	Coherence Bandwidth
C	Channel Capacity
D_c	Coherence Distance
E_s	Energy Per Symbol
$E\{\cdot\}$	Expected Value Operator
G_r	Receive Antenna Gain
G_t	Transmit Antenna Gain
\mathbf{H}	MIMO Channel Matrix
\mathbf{H}_{iid}	Raleigh MIMO Channel Matrix
\mathbf{H}_p	Row Permuted MIMO Channel Matrix
\mathbf{H}_r	Ricean MIMO Channel Matrix
K	Ricean Power Factor
L	Ancillary Path Loss
M	Number of Transmitter Antennas
N	Number of Receiver Antennas
N_0	Noise Power Spectral Density
P_r	Receive Power Level
P_t	Transmit Power Level
R	Wireless Path Length
\mathbf{R}_{rr}	Receiver Spatial Covariance Matrix
\mathbf{R}_{tt}	Transmitter Spatial Covariance Matrix
T_c	Coherence Time
$Tr(\cdot)$	Trace Operator
$Q(\cdot)$	Complementary Error Function
W	Channel Bandwidth
\mathbf{X}_p	Antenna Cross-polarization Discrimination Matrix
α	Temporal Correlation Factor
λ	Wavelength
\mathbf{H}	Hermitian Transpose
\mathbf{T}	Transpose
$\ \cdot\ _2$	Matrix Two Norm
$\ \cdot\ _F$	Matrix Frobenius Norm

1 INTRODUCTION

Wireless communications, particularly broadband wireless access (BWA) and wireless local area networks (WLAN), is a rapidly growing market sector. With rapid growth, managing the capacity and quality of the wireless air interface becomes a challenge. This challenge becomes even greater as the users expectation of quality, mobility, and application bandwidth increase as wireless service offerings evolve and become more sophisticated over time. Wireless communications in general offer advantages over traditional wired solutions, most often as it relates to speed and cost of deployment, as well as, opportunity for reuse and user mobility. Wireless communications has typically been disadvantaged when compared against wired solutions from the standpoint of capacity and reliability. Multiple-Input Multiple-Output (MIMO) antenna systems and Space-Time (ST) coding methods are complementary technologies that enable wireless systems to operate with improved reliability and increased spectral efficiency over traditional wireless systems. The ability of MIMO enhanced wireless systems, under appropriate environments, to exploit the spatial domain and achieve potential linear increase in link information theoretic capacity has drawn substantial interest in the research community, both within academia and the wireless communications industry. The technology is attracting much attention for its potential performance benefits to future BWA, WLAN, and mobility networks. Several standards development bodies have begun to include aspects of MIMO in wireless standards related to future deployments of cellular systems (e.g. ITU IMT-2000 WCDMA), WLAN (e.g. IEEE 802.11n), and BWA (e.g. IEEE 802.16d/e) [1-4].

Typical of many engineering problems, potential performance gains within MIMO systems must be traded off against one another depending on the desired behavior of a given system. The simultaneous maximization of link reliability with link capacity through MIMO space-time processing methods are competing performance objectives. The relative weighting of importance of reliability versus capacity gains depends on the particular system requirements. When circumstances dictate that extent of coverage and quality, rather than per user throughput are required, the appropriate MIMO system should maximize diversity gain. However, when the performance objective is to achieve higher capacity, the appropriate MIMO system should maximize capacity gain. In addition, the ability of any practical MIMO wireless system to achieve these performance gains depends on many factors such as antenna array dimension and geometry, channel fading statistics, receive signal level, noise & interference levels,

bit error rate (BER) constraints, not to mention, allowable transceiver complexity and channel state information (CSI) overhead bandwidth.

The questions, ‘*What is an optimal MIMO system?*’ and ‘*How much improvement is provided by an optimal MIMO system?*’ are not necessarily easy questions to answer. Knowledge of the deployment environment and service requirements are essential to understanding how MIMO can best be adapted for the improvement of wireless system performance. This thesis will attempt to address these questions by investigating adaptive MIMO space-time processing methods, of realizable complexity, which adapt, based on the deployed environment, for optimal, or near optimal, MIMO link performance.

1.1 Thesis Motivation

Most research published to date has been concerned with evaluating the performance or complexity of non-adaptive MIMO coding techniques under specific channel conditions such as independent channel fading versus correlated fading, high signal-to-noise (SNR) versus SNR limiting, or spatially white versus time-varying and spatially colored additive noise [5-10]. In practice, all wireless channels are time varying and depend to a great extent on the surrounding environment. The ability of any specific non-adaptive space-time coding technique to exploit array gain, diversity gain, or spatial multiplexing gain will vary depending on the environmental conditions of the particular deployment. Knowledge of the trade-offs between diversity order and spatial multiplexing gain under various operating environments is essential if one expects to understand how a given space-time processing method will perform versus another. Work in this area has been performed by several researchers and has been published in [11][12].

More recently, research focus has shifted toward adaptive space-time processing techniques. Research published in [13] introduces a generic framework for implementing adaptive BLAST transmission utilizing a side feedback channel, while implementing either dominant eigenmode transmission when full CSI is known at both the transmitter and receiver or simply data rate adjustment when CSI is unknown at the transmitter. Each mode of operation however has substantially divergent complexity requirements and performance points. Authors in [14] propose a generic framework which explicitly switches between Alamouti diversity coding and BLAST spatial multiplexing methods, based on instantaneous channel conditions, while jointly varying the modulation order to maintain constant bit rate. This method, although conceptually simple, involves the implementation of entirely separate space-time coding approaches while introducing a somewhat coarse switch between diversity and spatial

multiplexing modes of operation. Authors in [15] propose linear dispersion codes, based on frame theory [16], which attempt to bridge the performance gap between full diversity versus spatial multiplexing methods. The main drawback of such codes is their requirement for high complexity maximum likelihood (ML) based receivers. Others have taken an approach similar to antenna selection diversity where an optimal, or near optimal, subset of available antennas are selected based on channel conditions as to obtain maximum diversity gain [17].

Adaptive MIMO is an interesting and promising area for further study, which to-date has been far less researched when compared with non-adaptive space-time processing methods. This research is motivated toward developing a fully self-conforming, of realizable complexity, adaptive MIMO space-time processing algorithm. Through the research and development of the algorithm, the following are design goals under consideration:

- 1) Algorithm stability.
- 2) Implementation complexity.
- 3) Adaptive granularity in spatial multiplexing gain and diversity gain.
- 4) Channel state information feedback overhead requirements.
- 5) Algorithm ability to partition the channel for spatial multiplexing versus diversity performance objectives.
- 6) Self-conforming to a wide range of potential wireless environments.

Accordingly, the research is targeted toward benchmarking the performance of known and widely accepted non-adaptive space-time coding techniques, determining the operating conditions under which specific techniques outperform, and developing a new and novel adaptive switched or hybrid space-time processing algorithm, of realizable complexity, that automatically adapts to the wireless channel conditions for the maximization of wireless link performance.

We define the wireless link performance metric as link *goodput*¹, a measure of useful throughput as seen at the output of the MIMO receiver. This definition provides a single measure of link performance which includes the combined BER improvement effect of array gain and diversity order, as well as the spectral efficiency improvement offered through spatial multiplexing gain. Ideal adaptation should

¹ $goodput = (1 - BER) * Throughput * (1 - \%Outage)$

converge toward the correct balance of diversity encoding and spatial multiplexing gain necessary to maximize link goodput while keeping residual BER below a tolerable outage threshold.

1.2 Thesis Objectives

The principle objective of this research is to develop an adaptive MIMO space-time processing algorithm that maximizes MIMO link performance, defined as MIMO link *goodput*, under highly variable wireless channel environments. The channel variability being controlled through system parameters such as i) average receive signal level (RSL), ii) antenna spatial correlation, iii) channel coherence time, iv) Ricean power factor, and v) antenna cross polarization discrimination. The research plan is summarized as follows:

- 1) Develop the programmable MIMO simulation framework in Matlab[®].
- 2) Obtain performance curves of optimal non-adaptive MIMO spatial multiplexing and diversity coding methods using the framework developed in 1).
- 3) Research and develop an adaptive MIMO space-time processing algorithm which meets the design goals outlined in §1.1.
- 4) Demonstrate the performance improvement of the algorithm developed in 3) against the non-adaptive benchmarks recorded in 2), under varying MIMO channel environments.

1.3 Thesis Organization

The thesis is organized as follows:

- 1) Chapter 2 presents background information necessary to understand the basic concepts underlying MIMO wireless systems.
- 2) Chapter 3 describes the Simulated MIMO Wireless Environment (SMWE) developed within Matlab[®].
- 3) Chapter 4 documents the performance results of known non-adaptive space-time processing methods obtained through the SMWE and used as comparative performance benchmarks.
- 4) Chapter 5 introduces the adaptive space-time processing research. The A-BLAST design and implementation is described with performance results obtained through simulation using the SMWE. Comparative performance analysis is completed against the non-adaptive benchmarks

documented in Chapter 4. A discussion of implementation issues as well as side channel feedback overhead bandwidth is also provided.

- 5) Chapter 6 provides conclusions related to this thesis and suggests potential future research areas relevant to this area of study.

2 MIMO Overview

2.1 Introduction

Multiple-Input Multiple-Output or MIMO describes any wireless communication system which employs antenna arrays, complemented with space-time digital signal processing, at the transmitter and/or receiver for the improvement of wireless link performance. Wireless link performance being defined in terms of the link reliability (i.e. residual bit error rate) and spectral efficiency in bit-per-second per Hertz [bps/Hz].

2.2 Basic MIMO Channel Model

The basic MIMO wireless channel is illustrated in the following figure:

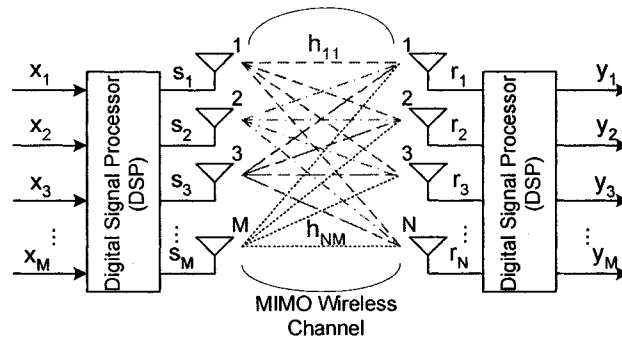


Figure 2-1 MIMO Channel Model (Equivalent Baseband)

As shown in Figure 2-1, the $M \times 1$ input data vector \mathbf{x} is processed through a digital signal processor (DSP) and mapped to the $M \times 1$ transmit symbol vector \mathbf{s} which is forwarded to the transmit antenna array for transmission across the MIMO wireless channel. Typically, the transmit symbol vector \mathbf{s} is complex with elements belonging to an M -ary digital modulation scheme such as Quadrature Phase Shift Keying (QPSK), Quadrature Amplitude Modulation (e.g. 16-QAM), etc. In a general sense, the transmitted symbols are perturbed during transmission by the diffraction, scattering, and reflection characteristics of the wireless channel, as well as noise inherent in the channel. The MIMO channel itself is modeled as an $N \times M$ matrix $\mathbf{H} = (\mathbf{h}_1, \mathbf{h}_2, \dots, \mathbf{h}_M)$:

$$\mathbf{H} = \begin{pmatrix} h_{11} & h_{12} & \cdots & h_{1M} \\ h_{21} & h_{22} & \vdots & \vdots \\ \vdots & \cdots & \ddots & h_{N-1M} \\ h_{N1} & \cdots & h_{NM-1} & h_{NM} \end{pmatrix} \quad (1)$$

The channel matrix \mathbf{H} is typically random with complex elements representing the time varying composite channel gain and phase lag between the i^{th} receive and j^{th} transmit antennas. The elements of \mathbf{H} are modeled as zero mean circularly symmetric complex Gaussian (ZMCSCG) (i.e. $h_{ij} \in CN(0,1)$). It is assumed that the receive power at each receive antenna element is equal to the total transmitted power E_s [18]. Although not explicitly shown in Figure 2-1, the transmitted symbols are perturbed by additive noise during transmission. In most environments, an $N \times 1$ channel noise vector \mathbf{n} is modeled as ZMCSCG with noise power N_0 (i.e. $n_i \in CN(0, N_0)$) at each receive antenna element. The receiver antenna array produces an $N \times 1$ receive vector \mathbf{r} , expressed efficiently through vector-matrix notation as:

$$\mathbf{r} = \mathbf{H}\mathbf{s} + \mathbf{n} \quad (2)$$

It should be noted that Figure 2-1 is highly simplified to emphasize the MIMO specific components of the narrowband wireless system in equivalent baseband. The input vector \mathbf{x} is generated by the application specific modules which would typically include the source coder, channel coder, data interleaver, input multiplexer, etc. The digitally modulated symbols in practice would also be upconverted to radio frequency (RF) and amplified prior to transmission.

From Figure 2-1 and the MIMO composite channel matrix of (1), the composite channel power gain between the i^{th} receive and j^{th} transmit antennas is given simply as $|h_{ij}|^2$. Similarly, the composite channel power gain, from the transmit array, as seen by the i^{th} receive antenna is given as the square of $\|\cdot\|_2$ of the i^{th} row of \mathbf{H} :

$$g_{r_i} = \left\| \mathbf{h}_i^T \right\|_2^2 = \sum_{j=1}^M |h_{ij}|^2 \quad (3)$$

This is illustrated in Figure 2-2:

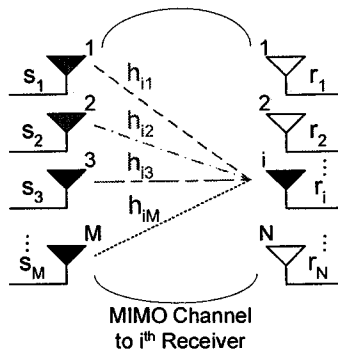


Figure 2-2 MIMO Channel to i^{th} Receiver

The composite channel power gain from the j^{th} transmit antenna, as seen at the receive antenna array is computed as the square of $\|\cdot\|_2$ of the j^{th} column of \mathbf{H} :

$$g_r = \left\| \mathbf{h}_j \right\|_2^2 = \sum_{i=1}^N |h_{ij}|^2 \quad (4)$$

This is illustrated in Figure 2-3:

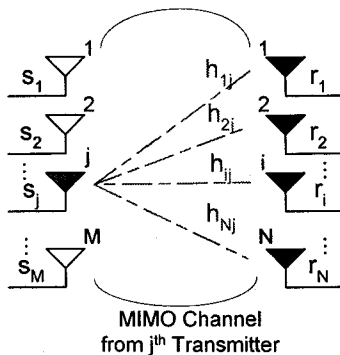


Figure 2-3 MIMO Channel from j^{th} Transmitter

The total composite channel power gain of the MIMO system is given as the square of $\|\cdot\|_F$ of \mathbf{H} or $\text{Tr}(\mathbf{H}\mathbf{H}^H)$ [18].

2.2.1 Full Rank Channel

In non-line-of-sight (NLOS) propagation environments with significant local scattering, the channel matrix of (1) may exhibit random spatially uncorrelated microscopic fading. That is to say, for a given coherence time, the time over which the channel realization may be assumed to be fixed, for each realization of the channel \mathbf{H} , the elements h_{ij} become independent identically distributed (i.i.d.) Gaussian random variables. In such cases, known to be typical of many indoor and outdoor urban propagation environments, the channel fading exhibits a Rayleigh distribution, given by the following probability density function:

$$f(x) = \frac{2x}{\Omega} e^{-\frac{x^2}{\Omega}} u(x) \quad (5)$$

where Ω is the average received power and $u(x)$ is the unit step function [18]. Under Rayleigh fading conditions, the channel matrix achieves full rank and the columns of \mathbf{H} span the entire r dimensional

vector space, where r is given as $\min(N, M)$ [19]. As will be introduced in §2.3.3, this environment is optimal for exploiting the r spatial degrees of freedom available in the MIMO channel for the improvement of link spectral efficiency through spatial multiplexing space-time processing.

2.2.2 Rank Deficient Channel

In many practical environments, mutual coupling exists between antenna elements of an antenna array. With antenna element separation below the channel correlation distance, spatial correlation is introduced between antenna elements. With insufficient local scattering, the direction-of-arrival (DOA) of received signals over the available MIMO transmission paths has small angular spread and fading becomes spatially correlated. The existence of spatial correlation within the MIMO propagation environment introduces linear dependence within each realization of the channel matrix \mathbf{H} . As the microscopic fading correlation increases between antenna elements, the channel matrix \mathbf{H} becomes rank deficient and the spatial degrees of freedom available for improving link spectral efficiency through spatial multiplexing is reduced. Under this environment, a shift toward space-time processing methods which emphasize diversity and array gain are preferred.

References [18][20] provide a thorough summary of the negative performance impacts associated with spatial correlation in the MIMO channel.

2.2.3 Low Signal-to-Noise Ratio Channel

The average path loss, assuming a free space loss (FSL) propagation model, is given by the well known Friis transmission formula [18]:

$$P_r = \frac{P_t G_t G_r \lambda^2}{(4\pi R)^2} \quad (6)$$

where P_r is the receive power, P_t is the transmit power, G_t is the transmitter composite gain, G_r is the receiver composite gain, λ is the carrier wavelength, and R is the LOS distance between the transmit and receive antennas. In highly obstructed or long propagation paths, the macroscopic fading in the far field may substantially reduce average SNR levels across the receiver antenna array. Most MIMO space-time processing methods require CSI which must be estimated through some form of training communicated over the MIMO channel. In low SNR environments therefore, errors in CSI estimation degrade MIMO performance by perturbing receive symbol detection. This degradation is known to more negatively impact spatial multiplexing space-time processing methods, which by definition include less symbol

redundancy. For this reason, at low average SNR, diversity based space-time processing methods, which provide some degree of symbol redundancy for symbol detection, are preferred.

References [9][10] provide a thorough analysis of the performance of space-time processing methods in the low SNR regime.

2.3 MIMO Performance Gains

Wireless communications systems are increasingly under pressure to provide higher data rates at superior levels of quality of service. Wireless communication systems employing multi-antenna configurations have the ability to provide additional performance gains, not available to traditional single antenna transceiver configurations. These additional gains may be classified as either (i) array gain, (ii) diversity gain, or (iii) spatial multiplexing gain and each may be used to improve link performance [18][21-24].

2.3.1 Array Gain

The term array gain comes from the ability to improve the average SNR at the output of a receiver combiner by coherently combining signals received across multiple antennas of an antenna array. Array gain may be obtained at the transmitter as well, prior to signal transmission, provided the transmitter has knowledge of the MIMO channel transfer function and appropriately weights the individual signal transmissions for coherent combining at the receiver. In all cases, CSI is required to perform the coherent combining. The benefit of array gain is improved average receiver SNR and therefore improved range of communication. The array gain may be thought of as additional gain, included in G_t or G_r of the Friis transmission formula (6), thereby for a fixed transmit power P_t , improving the overall link budget and providing additional fade margin. Array gain through coherent combining is available regardless of the channel fading statistics.

2.3.2 Diversity Gain

Diversity gain is achieved primarily by replicating transmitted data in space, time, or frequency domain and is used to combat microscopic fading across a wireless channel. Under multipath propagation environments microscopic fading, caused by the vector cancellation of out of phase receive signals at a particular receive antenna, can cause deep fades below the receiver detection threshold, resulting in periods of very low instantaneous SNR and poor BER performance. All diversity techniques attempt to combat microscopic fading by providing to the receiver independently fading replicas of the transmitted

data such that the probability that all replicas experiencing a fade simultaneously is very small. The effectiveness of diversity techniques is dependent on the fading statistics of the wireless channel as well as the design of the diversity scheme employed.

Spatial diversity, obtained through the transmitter and receiver antenna arrays of MIMO systems offer potentially a full MN improvement in diversity order over that of a Single-Input Single-Output (SISO) system [18]. To be effective and provide diversity gain, and therefore ensure independent fading, antenna separation must be larger than the channel coherence distance. If fading becomes correlated across antennas, the available diversity gain is diminished and only array gain is available to enhance receiver SNR.

Similar to array gain, diversity gain acts to improve the average receiver SNR by reducing the null depths of microscopic fading. Accordingly, both may be thought of as providing an improvement in overall receive signal quality. The frequency normalized information theoretic capacity of an additive white Gaussian noise (AWGN) channel, as derived in the seminal paper by Shannon in 1948 [25], is well known to be:

$$\frac{C}{W} = \log_2(1 + \text{SNR}) \quad (7)$$

As seen in (7), a linear increase in SNR provides only a logarithmic improvement in link spectral efficiency [bps/Hz]. The potential of MIMO systems to provide linear increase in spectral efficiency, and therefore link capacity, for band-limited/power-limited wireless communications is not provided by the combined SNR enhancement effects of array and diversity gain alone.

2.3.3 Spatial Multiplexing Gain

The concept of spatial multiplexing was first introduced by Foschini in 1996 [26]. Spatial multiplexing gain combines the spatial diversity provided through MIMO systems with rich scattering in the environment in order to exploit spatial data pipes for the benefit of linear increase in channel capacity [18]. To be more precise, as introduced in §2.2.1, the r dimensional vector space described by a realization of the channel matrix \mathbf{H} may be viewed as a system of r linearly independent equations, allowing the receiver to recover estimates of the transmitted symbols through appropriate space-time linear processing. Assuming for the moment that the MIMO receiver is able to track the channel through some form of channel estimation, symbol recovery involves the following minimization problem:

$$\mathbf{s}_{\text{est}} = \min_{\mathbf{s}_i} \|\mathbf{r} - \mathbf{H}_{\text{est}} \mathbf{s}_i\|_2^2 \quad (8)$$

In (8), for the receive vector \mathbf{r} of (1), using the channel estimate \mathbf{H}_{est} , the optimal symbol vector estimate \mathbf{s}_{est} from the available symbol vector set $\{\mathbf{s}_i\}$ is that which minimizes the resultant error, introduced through channel estimation and signal transmission by the ZMCSCG noise perturbation. If the propagation environment is Raleigh fading as described in §2.2.1, then \mathbf{s}_{est} is unique, allowing for the transmission of r independent data symbols per channel use. The MIMO channel spectral efficiency is maximized when the transmitter, with CSI, employs “*Dominant Eigenmode Transmission*” with dynamic power allocation across the transmit antenna array using the “*Water-Pouring Principle*” [18][27]. In this environment, the MIMO channel spectral efficiency is given as:

$$\frac{C}{W} \leq \frac{\max}{\sum_1^r \gamma_i} \sum_{i=1}^r \log_2 \left(1 + \frac{E_s \gamma_i}{M N_0} \lambda_i \right) \quad (9)$$

where E_s is the average energy per transmitted symbol, M is the number of transmit antennas, N_0 is the noise power, λ_i is the i^{th} eigenvalue of the composite MIMO channel realization \mathbf{H} , and γ_i is the power ratio allocation applied the i^{th} eigenmode through the “*water pouring algorithm*”. The improvement in spectral efficiency ($\frac{C}{W}$) is the sum of r SISO channels, each having a power gain of $(\gamma_i \lambda_i)$ and transmit power ($\frac{E_s}{M}$). For this reason, in highly scattered environments with adequate fade margin, spatial multiplexing through MIMO space-time processing introduces a complementary performance improvement emphasizing capacity gain over signal quality within the wireless communication system.

2.4 MIMO Spatial Multiplexing Methods

Initially proposed in [26], Layered Space-Time (LST) architectures may be implemented to exploit spatial multiplexing gain within a highly scattered MIMO environment. The most widely known non-adaptive LST architecture is the Bell Labs Layered Space-Time (BLAST) architecture [26][28].

2.4.1 Vertically Encoded Bell Labs Layered Space Time Codes (V-BLAST)

Vertically layered BLAST (V-BLAST) is a vertically encoded BLAST LST architecture which has been shown to approach the MIMO channel capacity of (9) in highly scattered MIMO environments [20]. The V-BLAST encoding is illustrated in Figure 2-4:

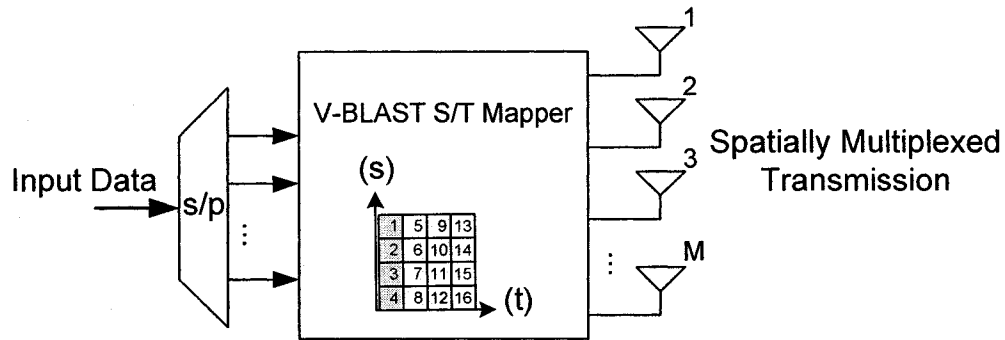


Figure 2-4 V-BLAST Encoding ($M=N=4$)

Through V-BLAST encoding, independent data streams are multiplexed in space (i.e. across antenna array elements) and time (i.e. across symbol periods) to achieve capacity enhancement over non-spatially multiplexed space-time coding methods. The detection technique employed for V-BLAST is based on Ordered Successive Cancellation (OSUC). In practice, V-BLAST transmission, by its very nature, is susceptible to self interference, often referred to as multi-stream interference (MSI). OSUC based receivers process the V-BLAST reception in rows across the space-time codeword, in order of decreasing signal-to-interference-and-noise ratio (SINR). As each row is detected, its MSI effect is canceled from the remaining rows and the process repeats until all rows in the V-BLAST space-time transmission has been recovered.

2.5 MIMO Diversity Methods

MIMO diversity space-time coding methods are designed primarily to exploit the rich spatial diversity that exists within the MIMO environment. Unlike spatial multiplexing approaches, diversity methods are employed to improve the reliability of MIMO communications and therefore minimize link residual BER. It is beneficial to view diversity methods as a complementary space-time coding approach to that of spatial multiplexing. Two non-adaptive diversity space-time coding methods will be considered in this section, each capable of achieving the maximum diversity order of MN , D-BLAST, which is an LST architecture and Orthogonal Space-Time Block-Coding (OSTBC).

2.5.1 Diagonally Encoded Bell Labs Layered Space Time Codes (D-BLAST)

Diagonally layered BLAST (D-BLAST) is a diagonally encoded BLAST LST architecture which has been shown to provide maximum diversity order of MN while achieving a code rate of one symbol per channel use [18][26]. The D-BLAST encoding is illustrated in Figure 2-5:

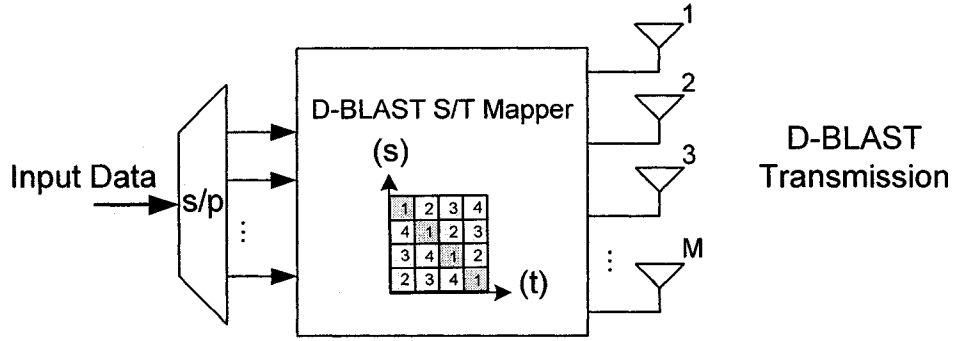


Figure 2-5 D-BLAST Encoding (M=N=4)

Through D-BLAST encoding, parallel data streams are replicated across space and time through diagonal layering within the space-time codeword. Following reception of an entire space-time transmission block, the D-BLAST receiver is provided with replicas of the transmitted symbols which have traversed all possible MN spatial paths within the composite MIMO channel, thereby providing the maximum achievable diversity protection against spatially uncorrelated microscopic fading. Similar to V-BLAST, with CSI, D-BLAST reception is performed using a combination of OSUC, joint soft symbol detection, and diversity combining [18].

2.5.2 Orthogonal Space-Time Block Codes (OSTBC)

Orthogonal Space-Time Block Codes (OSTBC) first became popular through the work of Alamouti [6]. Alamouti proposed a novel orthogonal transmit diversity scheme, employing two transmit antennas and any number of receive antennas, that provided a full MN (i.e. $M = 2$) diversity order improvement without the requirement for CSI at the transmitter, while achieving a code rate of one symbol per channel use. Since the development of the Alamouti OSTBC, much work has been performed researching and developing more generalized OSTBC methods employable over any number of transmit antennas while capable of achieving the Alamouti code rate, this remains an open field of research.

The authors of [27] identify the orthogonality requirement of generalized OSTBC as:

$$\mathbf{Z}\mathbf{Z}^H = c\|\mathbf{s}\|_2^2 \mathbf{I}_M \quad (10)$$

where $\mathbf{Z} \in \mathbb{C}^{M \times P}$ is the OSTBC, c is a real constant, $\mathbf{I}_M \in \mathbb{R}^{M \times M}$ is an identity matrix, and $\mathbf{s} \in \mathbb{C}^K$ belonging to the underlying M-ary symbol set. As illustrated in Figure 2-6, the input symbol vector \mathbf{s} is mapped to the OSTBC codeword \mathbf{Z} through the OSTBC Mapper block. The elements of \mathbf{s} encode $n = \log_2(M)$ bits of

information. The OSTBC Mapper block buffers k symbols to be transmitted, or equivalently kn bits of information for encoding:

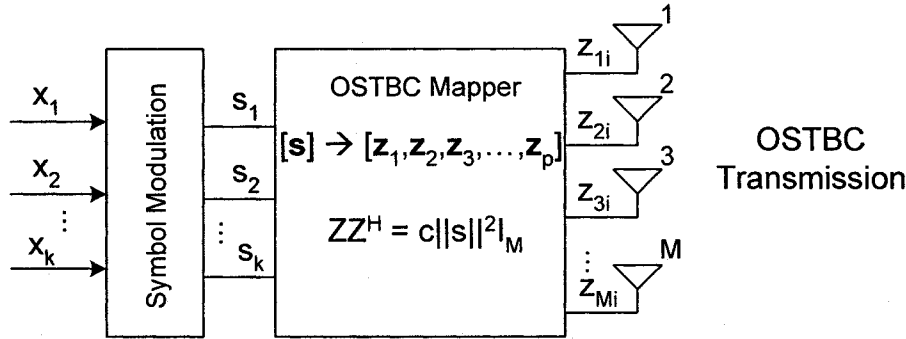


Figure 2-6 OSTBC Encoding

The elements of \mathbf{Z} are selected to be linear combinations of the buffered k symbols and their conjugates. The p columns in \mathbf{Z} represent the number of symbol periods required for transmission of one entire OSTBC via the transmit antenna array. The code rate of the OSTBC is given as the ratio of input symbols to transmission periods required to process the code:

$$R_o = \frac{k}{p} \quad (11)$$

The code rate influences the spectral efficiency of the OSTBC. The spectral efficiency (η) may be related to the code rate R as:

$$\eta = \frac{r_b}{B} \cong \frac{nr_s R_o}{r_s} \Leftrightarrow \frac{nk}{p} \quad (12)$$

Here r_b is the input bit rate [bit/sec], r_s is the input symbol rate [symbol/sec] and B is the required composite system bandwidth in Hertz. Clearly, as the number of transmission intervals p increases, the OSTBC spectral efficiency is reduced.

Because OSTBC employ orthogonal designs, the inner product of any two columns of \mathbf{Z} are mutually orthogonal, that is to say, their inner products are zero. As such, elements of \mathbf{Z} may be recovered through appropriate linear processing. With CSI at the receiver, OSTBC decoding is performed using a combination of linear processing, joint soft symbol detection, and diversity combining [18].

2.6 MIMO Adaptive Space-Time Processing Methods

The motivation behind adaptive space-time processing is simply the goal of maintaining consistent and superior performance over a broader range of operating environments than can be achieved through non-adaptive space-time processing methods. Adaptive space-time processing techniques recognize that as the wireless environment changes, so too must the coding method if performance levels are to be regulated. Figure 2-7 is a qualitative illustration of this methodology, as signal quality levels and spatial fading statistics change over time, so does the relative diversity (D) versus spatial multiplexing (S) requirements of the MIMO air interface:

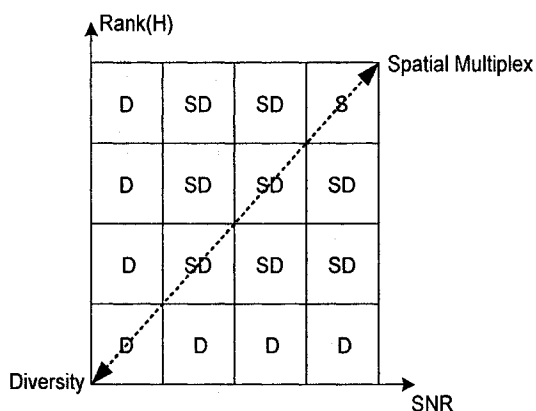


Figure 2-7 Adaptive STP - Diversity vs. Spatial Multiplexing Lattice

As mentioned in §1.1, research focus has shifted toward adaptive space-time processing techniques. The following subsections provide a more thorough summary of some of the adaptive methods surveyed.

2.6.1 Switched Mode Transmission (SMT)

One approach to adaptive space-time processing is to explicitly switch between diversity and spatial multiplexing modes of operation based on MIMO channel conditions. Authors in [14] propose a generic framework, using a low bit rate side channel, to explicitly switch between linear diversity and spatial multiplexing methods in a frequency flat fading i.i.d. MIMO channel environment where the number of transmit antennas (M) is less than or equal to the number of receive antennas (N). The switching of mode and space-time modulation order is performed as to maintain a constant data rate (R) while minimizing residual symbol error rate (P_e):

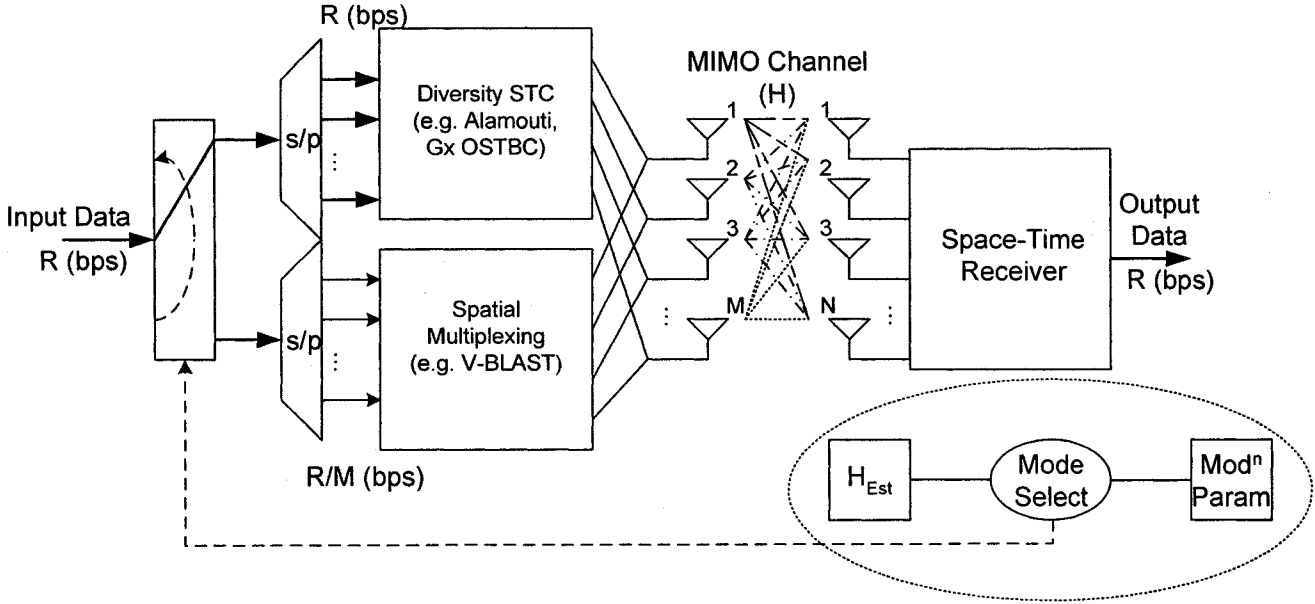


Figure 2-8 SMT Block Diagram

In [14], upper bounds on symbol error probability for diversity and spatial multiplexing modes are approximated and used to develop a mode switching criteria based on the minimum Euclidean distance of the transmit symbol vector set. It is shown in [14] that the upper bound on diversity mode symbol error probability, for an M_d point transmit symbol vector constellation, with minimum Euclidean distance $d_{\min,d}^2$, is approximately:

$$P_{e,d} < (M_d - 1)Q \left(\sqrt{\frac{E_s}{2N_o} \frac{\|\mathbf{H}\|_F^2}{M} d_{\min,d}^2} \right) \quad (13)$$

As seen in (13), error performance in diversity mode is a function of the overall channel power gain expressed as the square of the Frobenius norm of the MIMO channel realization ($\|\mathbf{H}\|_F^2$). Similarly, the upper bound on spatial multiplexing mode symbol error probability, with minimum Euclidean distance $d_{\min,sm}^2$, is approximately:

$$P_{e,sm} = (|S_{SM}| - 1)Q \left(\sqrt{\frac{E_s}{2N_o} \frac{\lambda_M^2 d_{\min,sm}^2}{M}} \right) \quad (14)$$

Here S_{SM} is the set of all possible transmit symbol vectors and λ_M is the smallest singular value of the MIMO channel realization. As seen in (14), the error performance in spatial multiplexing mode is a

function of the weakest channel eigenmode (λ_M), which decays to zero as the MIMO channel becomes rank deficient.

The authors go on to define the MIMO channel condition number (K) as the ratio of maximum to minimum channel singular values ($\lambda_i : i \in \{1..M\}$):

$$K = \frac{\lambda_1}{\lambda_M} \quad (15)$$

Expressed in terms of diversity and spatial multiplexing minimum Euclidean distances, an upper bound on the channel condition number, below which identifies MIMO channels that are better suited for spatial multiplexing than diversity coding for a given data rate (R) in terms of minimum residual symbol error rate (P_e) is given as:

$$K \leq \sqrt{\frac{d_{\min,sm}^2}{d_{\min,d}^2} - 1} \quad (16)$$

The SMT method, although conceptually simple, suggests the implementation of entirely separate space-time coding approaches while introducing a somewhat coarse switch between diversity and spatial multiplexing modes of operation. In addition, as the number of transmit and receive antennas increase, in highly scattered propagation environments with full rank ($r = \min(N,M)$) and adequate fade margin, spatial multiplexing methods are preferred. The ability of diversity coding methods to maintain the spectral efficiency of spatial multiplexing techniques requires very high modulation order with ever smaller minimum symbol vector Euclidean distances ($d_{\min,d}^2$), reducing the set of available MIMO channel realizations for which diversity coding techniques are preferred.

2.6.2 Rank Adaptive Transmission (RAT)

As discussed previously in §2.3.3, it is well understood that the ability of spatial multiplexing space-time processing methods to achieve a linear increase in wireless link spectral efficiency is directly related to the effective rank (r) of the MIMO channel. Authors in [13] introduce a generic framework for implementing a Rank Adaptive Transmission (RAT) scheme utilizing a side feedback channel.

Through an eigenvalue decomposition of the MIMO channel matrix [19], the MIMO channel rank (r) is estimated by comparing the eigenvalue ratios, obtained by dividing the maximum eigenvalue (λ_1) by the

remaining eigenvalues ($\lambda_i, i \in [2..\min(N,M)]$), with a predetermined threshold (τ). The MIMO channel capacity of (9) is maximized when the power distribution across the available (r) eigenmodes is constant:

$$\prod_{i=1}^r \left(1 + \frac{E_s \gamma_i}{MN_o} \lambda_i \right) \leq \left\{ \frac{\sum_{i=1}^r \log_2 \left(1 + \frac{E_s \gamma_i}{MN_o} \lambda_i \right)}{r} \right\}^r \quad (17)$$

When full CSI is known at the transmitter and receiver, “*Dominant Eigenmode Transmission*” with “*Water-Pouring Principle*” dynamic power allocation [18][27], known to maximize the MIMO channel capacity and achieve equality in (17) is suggested. This method, although optimal, requires maximum CSI feedback overhead as well as space-time transceiver complexity.

When full CSI is unknown at the transmitter, side feedback of rate information based on the estimated MIMO channel rank (r) is suggested such that the transmitter may regulate the offered data rate according to the MIMO channel’s ability to support spatial multiplexing:

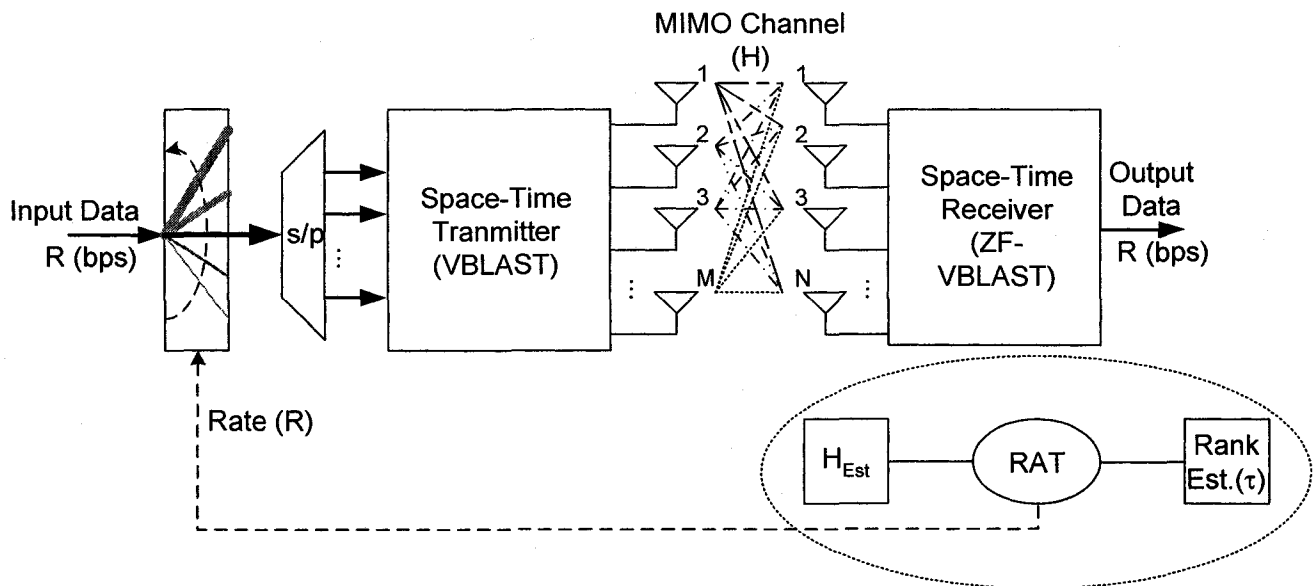


Figure 2-9 RAT Block Diagram

Simulation results for this reduced complexity RAT technique using 4x4 VBLAST in a WCDMA system with Zero Forcing (ZF) detection [18] are given in [13]. An improvement in BER and data throughput at $\frac{E_b}{N_o} \geq 4\text{dB}$ is demonstrated in rank deficient environments. The RAT technique as

described in [13] identifies a means to regulate transmission rate in rank deficient MIMO environments that cannot fully support spatial multiplexing. The RAT technique however fails to identify methods to exploit diversity gain, also available in rank deficient MIMO environments for the improvement of link reliability. As will be discussed in §5, the research carried out in this thesis proposes a single adaptive space-time processing method that attempts to achieve, with realizable implementation complexity, the correct balance and transition between diversity and spatial multiplexing gains over a wide range of operating environments for the maximization of wireless link performance.

2.6.3 Linear Dispersion Code (LDC)

For practical MIMO based wireless communications, a balance is required between diversity gain and spatial multiplexing gain allowing systems to achieve necessary improvements in spectral efficiency while maintaining an acceptable level of link reliability. Unlike OSTBC's and spatial multiplexing methods that are each optimized to deliver maximum reliability and spectral efficiency respectively, Linear Dispersion Codes (LDC's) attempt to bridge these performance objectives.

Authors in [29] have developed LDC's that are optimized with respect to spectral efficiency, which is to say that the resulting codes maximize the information theoretic channel capacity of (9). Authors in [15] however propose LDC's, based on frame theory [16], that are slightly suboptimal with respect to spectral efficiency but maintain some degree of diversity order over fully spatial multiplexed MIMO wireless communications.

For a complex m -ary input symbol sequences $\mathbf{s} = (s_1 \ \dots \ s_Q)^T \in C^{Q \times 1}$, the LDC approach is to disperse across space and time the input symbols to form a space-time codeword $\mathbf{S} \in C^{M \times T}$. By doing so, each input symbol is potentially spread across some combination of available transmit antennas (M) over the codeword duration (T). The resulting LDC code rate in bit-per-second [bps] is given as:

$$R_{\text{LDC}} = \frac{Q \log_2 m}{T} \quad (18)$$

The LDC codeword is formed through a linear combination of basis dispersion matrices ($\mathbf{X}_k \in C^{M \times Q}$) where $k \in [1..T]$:

$$\mathbf{S} = (\mathbf{X}_1 \mathbf{s} \ \dots \ \mathbf{X}_T \mathbf{s}) \in C^{M \times T} \quad (19)$$

Accordingly, the LDC is completely defined through the set of linear dispersion matrices ($\mathbf{X}_k \in C^{M \times Q}$) while the codeword (\mathbf{S}) is determined by the linear weighting provided through the input symbol sequences $\mathbf{s} = (s_1 \ \dots \ s_Q)^T$. Because the codeword is linear with respect to the input symbols $s_q = \alpha_q + j\beta_q$, space-time linear decoding techniques such as OSUC or ML decoding may be employed at the receiver [18].

The main design parameters are T , Q , and the set of dispersion matrices $\{\mathbf{X}_k\}$ where $k \in [1..T]$. Assuming $M \leq N$, the design method involves the selection of Q and T such that $Q \leq MT$. The dispersion matrices are selected to maximize channel capacity while in addition conforming to the system power constraint given as:

$$E\{tr(\mathbf{S}\mathbf{S}^H)\} = TM \quad (20)$$

The dispersion matrices may additionally be designed to ensure each symbol s_q is transmitted with equal power at each of the T symbol periods or each symbol s_q is dispersed with equal energy in all spatial and temporal directions.

By selecting $Q = MT$, the capacity optimal LDC (i.e. $R_{LDC} = M \log_2 m$) may be obtained with appropriate selection of linear dispersion matrices $\{\mathbf{X}_k\}$. Selecting $Q < MT$ results in a capacity suboptimal LDC (i.e. $R_{LDC} < M \log_2 m$). In this case, the linear dispersion matrices $\{\mathbf{X}_k\}$ provide a representation of input symbols $\mathbf{s} = (s_1 \ \dots \ s_Q)^T$ which includes redundancy (i.e. $T > \frac{Q}{M}$) and therefore potential to provide diversity order improvement. Authors in [30] provide an analytical survey on the design of LDC's.

Performance results for the capacity optimal LDC are provided in [18], for $M = N = 2$ and $R_{LDC} = 4$ [bps], which show a BER improvement against V-BLAST at high SNR when ML detection is employed.

The main drawback however of the LDC approach stems for the complexities resulting from a requirement for ML detection as well as difficulty in obtaining dispersion matrices suitable for a broad range of operating environments.

2.7 Summary

This chapter provides for the reader an introduction to the theory and concepts underlying basic MIMO wireless systems and space-time processing techniques. A description of the basic MIMO channel model is given along with specific deployment environments of particular significance such as the

Raleigh fading, the rank deficient channel, and low SNR environments. Basic performance gains, applicable to MIMO systems, have been introduced. The reader is also introduced to basic non-adaptive space-time coding methods that are optimized for either spatial multiplexing or diversity encoding purposes. Finally, the chapter concludes with a review of some of the relevant research completed in the area of adaptive space-time processing including a switched mode technique, rank adaptive method, and linear dispersion codes.

3 Simulated MIMO Wireless Environment (SMWE)

To facilitate performance benchmarking and adaptive space-time algorithm development, a fully simulated MIMO wireless environment was developed in Matlab[®]. The Matlab[®] environment was selected for its ease of programmability, robust support for vector and matrix computations, and rich signal processing and communications support libraries. Throughout the remainder of this document, the simulated MIMO wireless environment is referred to simply as the SMWE. The remainder of this chapter discusses the design, implementation, and capabilities of the developed SMWE.

The SMWE is implemented in equivalent baseband with baud rate sampling. As such, simulation of up/down conversion to/from RF spectrum is not performed. It is understood that the RF portion of the MIMO transceiver is essential in any practical system and influences the cost and complexity of real world implementation. However, for the purposes of research and development of adaptive ST processing algorithms, it may be removed if linearity and time-invariance of the RF section is assumed.

3.1 SMWE Input Parameters

To aid in the analysis and expedite the benchmarking process, the SMWE is parameterized allowing for the efficient simulation of various modes of operation under highly variable operating conditions. The SMWE programmability includes:

Parameter	Description												
BER_UT	Outage BER threshold to be maintained throughout simulation. Supported BER thresholds are 10^{-1} , 10^{-2} , 10^{-3} , etc.												
COH_TIME_UT	Coherence time of the simulated MIMO channel in ST-Blocks (T_c).												
DUR_UT	Duration of the simulation run in ST-Blocks.												
H_RICEAN_UT	Simulated Ricean channel matrix (H_r).												
K_RICEAN_UT	Ricean power factor (K).												
MODE_UT	Simulation mode of operation. Supported modes include: <table border="1" data-bbox="435 1437 1477 1860"> <thead> <tr> <th>Mode</th> <th>Description</th> </tr> </thead> <tbody> <tr> <td>MODE_FORCE_ABLAST1</td> <td>MxN ABLAST mode of operation. Code rate M, ($M = N$, $M > 1$).</td> </tr> <tr> <td>MODE_FORCE_ABLAST2</td> <td>MxN ABLAST mode of operation. Code rate M-1, ($M = N$, $M > 1$).</td> </tr> <tr> <td>MODE_FORCE_ABLAST3</td> <td>MxN ABLAST mode of operation. Code rate M-2, ($M = N$, $M > 2$).</td> </tr> <tr> <td>MODE_FORCE_ABLAST4</td> <td>MxN ABLAST mode of operation. Code rate M-3, ($M = N$, $M > 3$).</td> </tr> <tr> <td>MODE_FORCE_ABLAST5</td> <td>MxN ABLAST mode of operation. Code rate M-4, ($M = N$, $M > 4$).</td> </tr> </tbody> </table>	Mode	Description	MODE_FORCE_ABLAST1	MxN ABLAST mode of operation. Code rate M, ($M = N$, $M > 1$).	MODE_FORCE_ABLAST2	MxN ABLAST mode of operation. Code rate M-1, ($M = N$, $M > 1$).	MODE_FORCE_ABLAST3	MxN ABLAST mode of operation. Code rate M-2, ($M = N$, $M > 2$).	MODE_FORCE_ABLAST4	MxN ABLAST mode of operation. Code rate M-3, ($M = N$, $M > 3$).	MODE_FORCE_ABLAST5	MxN ABLAST mode of operation. Code rate M-4, ($M = N$, $M > 4$).
Mode	Description												
MODE_FORCE_ABLAST1	MxN ABLAST mode of operation. Code rate M, ($M = N$, $M > 1$).												
MODE_FORCE_ABLAST2	MxN ABLAST mode of operation. Code rate M-1, ($M = N$, $M > 1$).												
MODE_FORCE_ABLAST3	MxN ABLAST mode of operation. Code rate M-2, ($M = N$, $M > 2$).												
MODE_FORCE_ABLAST4	MxN ABLAST mode of operation. Code rate M-3, ($M = N$, $M > 3$).												
MODE_FORCE_ABLAST5	MxN ABLAST mode of operation. Code rate M-4, ($M = N$, $M > 4$).												

	MODE_FORCE_ABLAST6	MxN ABLAST mode of operation. Code rate M-5, (M = N, M > 5).								
	MODE_FORCE_ABLAST7	MxN ABLAST mode of operation. Code rate M-6, (M = N, M > 6).								
	MODE_FORCE_ABLAST8	MxN ABLAST mode of operation. Code rate M-7, (M = N, M > 7).								
	MODE_FORCE_ALAMOUTI	2xN Alamouti mode of operation.								
	MODE_FORCE ESTRANK	Channel rank data collection mode.								
	MODE_FULLY_ADAPTIVE	Fully adaptive MxN ABLAST mode of operation (M = N, M > 1).								
PWR_UT	Percentage power threshold used in channel rank estimation (e.g. 0.99).									
RX_CORR_UT	Receiver spatial covariance matrix (\mathbf{R}_r).									
SNR_UT	Average signal-to-noise in dB.									
TRAIN_TIME_UT	Training period in ST-Blocks.									
TRAIN_TYPE_UT	Training type employed through channel estimation. Supported training modes include:									
	<table border="1"> <thead> <tr> <th>Mode</th> <th>Description</th> </tr> </thead> <tbody> <tr> <td>PERFECT_CSI</td> <td>CSI is perfect.</td> </tr> <tr> <td>LSE_CSI</td> <td>CSI is obtained through training employing OSTBC and LS estimation [18].</td> </tr> <tr> <td>MMSE_CSI</td> <td>CSI is obtained through training employing OSTBC and MMSE estimation [18].</td> </tr> </tbody> </table>		Mode	Description	PERFECT_CSI	CSI is perfect.	LSE_CSI	CSI is obtained through training employing OSTBC and LS estimation [18].	MMSE_CSI	CSI is obtained through training employing OSTBC and MMSE estimation [18].
Mode	Description									
PERFECT_CSI	CSI is perfect.									
LSE_CSI	CSI is obtained through training employing OSTBC and LS estimation [18].									
MMSE_CSI	CSI is obtained through training employing OSTBC and MMSE estimation [18].									
TXRX_ANT_UT	Transmitter & receiver antenna array dimensions (M, N).									
TX_CORR_UT	Transmitter spatial covariance matrix (\mathbf{R}_t).									
T_BLOCK_UT	ST-Block length in symbol periods.									
T_CORR_FACT_UT	Temporal correlation factor for simulated continuous fading MIMO channel (α).									
X_POL_UT	Transmitter and receiver cross-polarization discrimination matrix (\mathbf{X}_p).									

Table 3-1 SMWE Programmable Parameters

It should be noted that simulations of V-BLAST are achieved through the simulation mode MODE_FORCE_ABLAST1. Similarly, simulations of D-BLAST are achieved for the M=N MIMO environment through the appropriate mode MODE_FORCE_ABLAST{M}, where $M=N \in [2..8]$.

3.2 SMWE Architecture

The SMWE is developed as five major subsystems, these are:

- 1) Space-Time Transmitter Subsystem
- 2) Space-Time Receiver Subsystem
- 3) MIMO Channel Subsystem

- 4) Adaptive Controller Subsystem
- 5) Performance Analysis Subsystem

The SMWE architecture is illustrated in Figure 3-1:

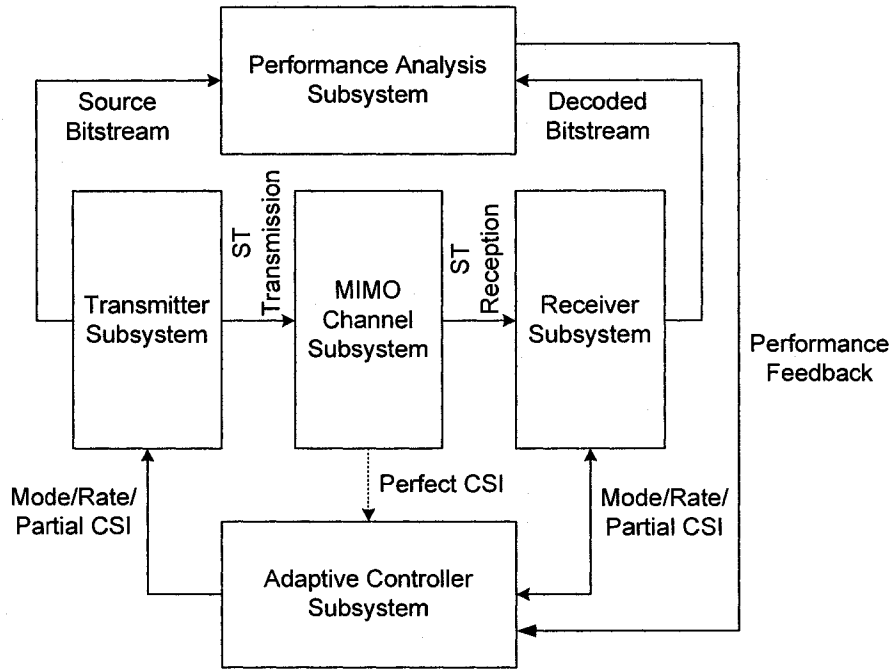


Figure 3-1 SMWE Architecture

The operation of the SMWE is conceptually simple. In data transmission mode, the transmitter subsystem generates random source data for transmission across the simulated MIMO channel. The receiver subsystem upon reception of the ST transmission performs the required decoding and passes the decoded data to the performance analysis subsystem for performance monitoring. The performance analysis subsystem is provided with the original source data as reference. The performance analysis subsystem provides performance feedback to the adaptive controller subsystem. The adaptive controller subsystem, with inputs from the performance analysis and receiver subsystems adjusts the mode of operation based on the employed adaptive algorithm under test. In training mode, the transmitter, receiver, and controller subsystems are also responsible for performing periodic channel estimation, necessary for the generation and dissemination of required CSI and precoding data within the SMWE.

3.2.1 Space-Time Transmitter Subsystem (STS)

The ST Transmitter Subsystem (STS) is illustrated in Figure 3-2. There are three modules which implement ST transmitter functionality, the Random Data Source, the ST Mapper, and the Precoder module.

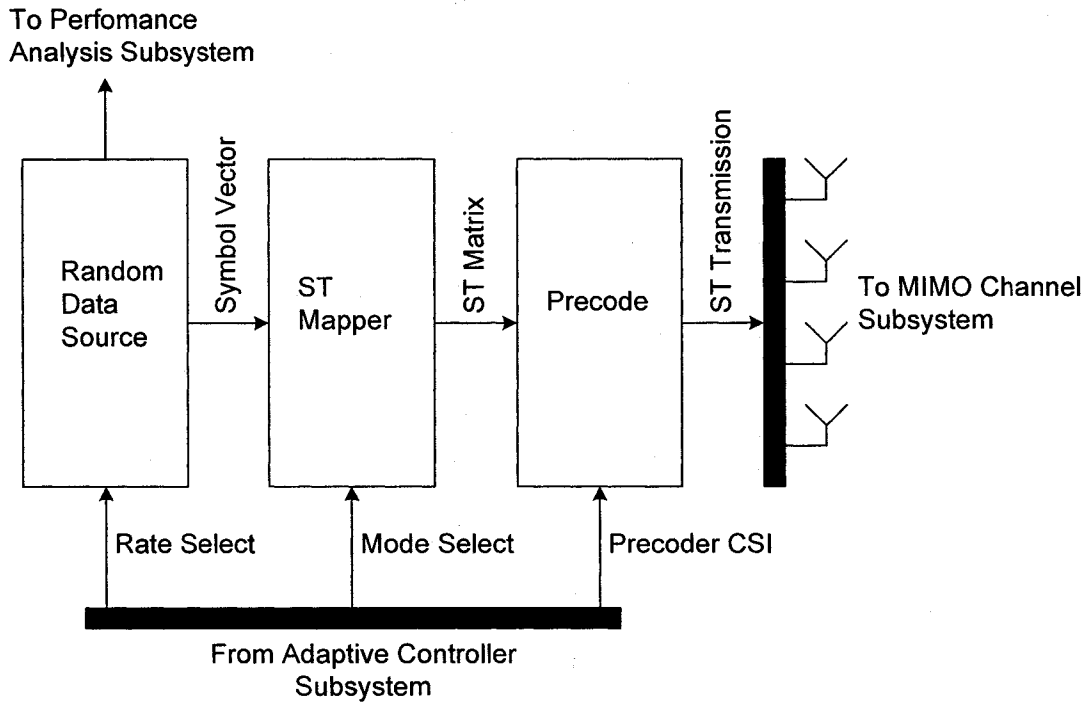


Figure 3-2 ST Transmitter Subsystem

The STS interfaces to the Adaptive Controller Subsystem (ACS), as well as the MIMO Channel and Performance Analysis Subsystems. The ST transmitter is managed by the ACS. The ACS controls the mode of operation and desired data rate. As well, the ACS provides the necessary transmitter precoding prior to ST transmission over the simulated MIMO channel.

3.2.1.1 Random Data Source

The Random Data Source, illustrated in Figure 3-3, provides uniformly distributed random data during simulation. The ACS, through the Rate Select input signal, conveys necessary symbol rate and modulation level information. The supported digital modulation is MPSK with $M \in [2, 4, 8, 16, 32]$.

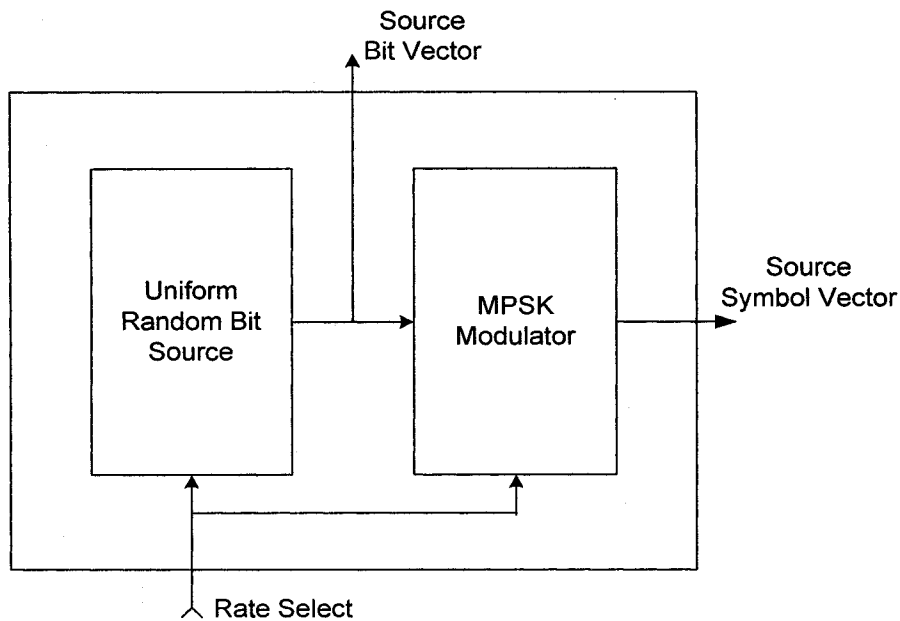


Figure 3-3 Random Data Source

The random data source forwards as reference the source bit vector to the Performance Analysis Subsystem. The source MPSK vector is forwarded to the ST Mapper module for ST processing prior to transmission.

3.2.1.2 ST Mapper

The ST Mapper module is responsible for queuing and mapping an input symbol vector across space (i.e. the transmit antenna array) and time (i.e. across symbol periods) according to a given ST processing method. The ACS instructs the ST Mapper module through the Mode Select input as to the ST mapping function to use. Supported ST mapping functions include:

ST Mapping Function	Description
G2 OSTBC	<p>2 x 2 OSTBC defined and introduced in [6]. Achieves a code rate of 1 and a diversity order of 2N:</p> $s_2 \quad s_1 \Leftrightarrow \begin{matrix} s_1 & -s_2^* \\ s_2 & s_1^* \end{matrix}$ <p>Utilized in the SMWE during training transmission for the purpose of channel estimation.</p>

G3 OSTBC	<p>3 x 8 OSTBC defined and introduced in [18]. Achieves code rate of $\frac{1}{2}$ and maximum diversity order of $3N$:</p> $\begin{matrix} & & & & s_1 & -s_2 & -s_3 & -s_4 & s_1^* & -s_2^* & -s_3^* & -s_4^* \\ s_4 & s_3 & s_2 & s_1 & \Leftrightarrow & s_2 & s_1 & s_4 & -s_3 & s_2^* & s_1^* & s_4^* & -s_3^* \\ & & & & & s_3 & -s_4 & s_1 & s_2 & s_3^* & -s_4^* & s_1^* & s_2^* \end{matrix}$ <p>Utilized in the SMWE during training transmission for the purpose of channel estimation.</p>
G4 OSTBC	<p>4 x 8 OSTBC defined and introduced in [18]. Achieves code rate of $\frac{1}{2}$ and maximum diversity order of $4N$:</p> $\begin{matrix} & & & & s_1 & -s_2 & -s_3 & -s_4 & s_1^* & -s_2^* & -s_3^* & -s_4^* \\ s_4 & s_3 & s_2 & s_1 & \Leftrightarrow & s_2 & s_1 & s_4 & -s_3 & s_2^* & s_1^* & s_4^* & -s_3^* \\ & & & & & s_3 & -s_4 & s_1 & s_2 & s_3^* & -s_4^* & s_1^* & s_2^* \\ & & & & & s_4 & s_3 & -s_2 & s_1 & s_4^* & s_3^* & -s_2^* & s_1^* \end{matrix}$ <p>Utilized in the SMWE during training transmission for the purpose of channel estimation.</p>
G5 OSTBC	<p>5 x 16 OSTBC defined and introduced in [18]. Achieves code rate of $\frac{1}{2}$ and maximum diversity order of $5N$:</p> $s_8 \quad s_7 \quad s_6 \quad \dots \quad s_1 \Leftrightarrow [\mathbf{Z}_5 \quad \mathbf{Z}_5^*] \Rightarrow$ $\mathbf{Z}_5 = \begin{matrix} s_1 & -s_2 & -s_3 & -s_4 & -s_5 & -s_6 & -s_7 & -s_8 \\ s_2 & s_1 & -s_4 & s_3 & -s_6 & s_5 & s_8 & -s_7 \\ s_3 & s_4 & s_1 & -s_2 & -s_7 & -s_8 & s_5 & s_6 \\ s_4 & -s_3 & s_2 & s_1 & -s_8 & s_7 & -s_6 & s_5 \\ s_5 & s_6 & s_7 & s_8 & s_1 & -s_2 & -s_3 & -s_4 \end{matrix}$ <p>Utilized in the SMWE during training transmission for the purpose of channel estimation.</p>
G6 OSTBC	<p>6 x 16 OSTBC defined and introduced in [18]. Achieves code rate of $\frac{1}{2}$ and maximum diversity order of $6N$:</p>

	$s_8 \ s_7 \ s_6 \ \dots \ s_1 \Leftrightarrow [\mathbf{Z}_6 \ \mathbf{Z}_6^*] \Rightarrow$ $\mathbf{Z}_6 = \begin{bmatrix} s_1 & -s_2 & -s_3 & -s_4 & -s_5 & -s_6 & -s_7 & -s_8 \\ s_2 & s_1 & -s_4 & s_3 & -s_6 & s_5 & s_8 & -s_7 \\ s_3 & s_4 & s_1 & -s_2 & -s_7 & -s_8 & s_5 & s_6 \\ s_4 & -s_3 & s_2 & s_1 & -s_8 & s_7 & -s_6 & s_5 \\ s_5 & s_6 & s_7 & s_8 & s_1 & -s_2 & -s_3 & -s_4 \\ s_6 & -s_5 & s_8 & -s_7 & s_2 & s_1 & s_4 & -s_3 \end{bmatrix}$ <p>Utilized in the SMWE during training transmission for the purpose of channel estimation.</p>
G7 OSTBC	<p>7 x 16 OSTBC defined and introduced in [18]. Achieves code rate of $\frac{1}{2}$ and maximum diversity order of $7N$:</p> $s_8 \ s_7 \ s_6 \ \dots \ s_1 \Leftrightarrow [\mathbf{Z}_7 \ \mathbf{Z}_7^*] \Rightarrow$ $\mathbf{Z}_7 = \begin{bmatrix} s_1 & -s_2 & -s_3 & -s_4 & -s_5 & -s_6 & -s_7 & -s_8 \\ s_2 & s_1 & -s_4 & s_3 & -s_6 & s_5 & s_8 & -s_7 \\ s_3 & s_4 & s_1 & -s_2 & -s_7 & -s_8 & s_5 & s_6 \\ s_4 & -s_3 & s_2 & s_1 & -s_8 & s_7 & -s_6 & s_5 \\ s_5 & s_6 & s_7 & s_8 & s_1 & -s_2 & -s_3 & -s_4 \\ s_6 & -s_5 & s_8 & -s_7 & s_2 & s_1 & s_4 & -s_3 \\ s_7 & -s_8 & -s_5 & s_6 & s_3 & -s_4 & s_1 & s_2 \end{bmatrix}$ <p>Utilized in the SMWE during training transmission for the purpose of channel estimation.</p>
G8 OSTBC	<p>8 x 16 OSTBC defined and introduced in [18]. Achieves code rate of $\frac{1}{2}$ and maximum diversity order of $8N$:</p>

	$s_8 \ s_7 \ s_6 \ \dots \ s_1 \Leftrightarrow [Z_8 \ Z_8^*] \Rightarrow$ $Z_8 = \begin{bmatrix} s_1 & -s_2 & -s_3 & -s_4 & -s_5 & -s_6 & -s_7 & -s_8 \\ s_2 & s_1 & -s_4 & s_3 & -s_6 & s_5 & s_8 & -s_7 \\ s_3 & s_4 & s_1 & -s_2 & -s_7 & -s_8 & s_5 & s_6 \\ s_4 & -s_3 & s_2 & s_1 & -s_8 & s_7 & -s_6 & s_5 \\ s_5 & s_6 & s_7 & s_8 & s_1 & -s_2 & -s_3 & -s_4 \\ s_6 & -s_5 & s_8 & -s_7 & s_2 & s_1 & s_4 & -s_3 \\ s_7 & -s_8 & -s_5 & s_6 & s_3 & -s_4 & s_1 & s_2 \\ s_8 & s_7 & -s_6 & -s_5 & s_4 & s_3 & -s_2 & s_1 \end{bmatrix}$ <p>Utilized in the SMWE during training transmission for the purpose of channel estimation.</p>
A2-BLAST [1..2]	2 x 2 A-BLAST, refer to Appendix B – Supplementary A-BLAST Mode Summary Data.
A3-BLAST [1..3]	3 x 3 A-BLAST, refer to Appendix B – Supplementary A-BLAST Mode Summary Data.
A4-BLAST [1..4]	4 x 4 A-BLAST, refer to Appendix B – Supplementary A-BLAST Mode Summary Data.
A5-BLAST [1..5]	5 x 5 A-BLAST, refer to Appendix B – Supplementary A-BLAST Mode Summary Data.
A6-BLAST [1..6]	6 x 6 A-BLAST, refer to Appendix B – Supplementary A-BLAST Mode Summary Data.
A7-BLAST [1..7]	7 x 7 A-BLAST, refer to Appendix B – Supplementary A-BLAST Mode Summary Data.
A8-BLAST [1..8]	8 x 8 A-BLAST, refer to Appendix B – Supplementary A-BLAST Mode Summary Data.
ALAMOUTI OSTBC	Same as G2 OSTBC.

Table 3-2 ST Mapping Functions

3.2.1.3 Precoder

The Precoder module is responsible for precoding the ST Mapper output prior to forwarding to the transmit antenna array for transmission across the simulated MIMO wireless channel. The ACS instructs the Precoder module through the Precoder CSI input as to the precoding function to use. The precoding function is application specific and dependent on the ST mapping function employed. The following table summarizes the supported ST transmitter precoder functions:

ST Mapping Mode	ST Transmitter Precoder Function	Dimension	Description
G2 OSTBC	\mathbf{I}_2	2 x 2 (integer)	Precoding disabled. Function invokes an identity system.
G3 OSTBC	\mathbf{I}_3	3 x 3 (integer)	Precoding disabled. Function invokes an identity system.
G4 OSTBC	\mathbf{I}_4	4 x 4 (integer)	Precoding disabled. Function invokes an identity system.
G5 OSTBC	\mathbf{I}_5	5 x 5 (integer)	Precoding disabled. Function invokes an identity system.
G6 OSTBC	\mathbf{I}_6	6 x 6 (integer)	Precoding disabled. Function invokes an identity system.
G7 OSTBC	\mathbf{I}_7	7 x 7 (integer)	Precoding disabled. Function invokes an identity system.
G8 OSTBC	\mathbf{I}_8	8 x 8 (integer)	Precoding disabled. Function invokes an identity system.
A-BLAST[1..8]	\mathbf{Q}_p^H	M x M (complex)	Function invokes the A-BLAST codec ST transmission precoding. Precoding is the Hermitian transpose of \mathbf{Q}_p , arising from a unitary QR factorization of the row

			permuted channel realization matrix H_p . Refer to §5.1.1 for details related to the A-BLAST codec.
ALAMOUTI OSTBC	I_2	2 x 2 (integer)	Precoding disabled. Function invokes an identity system.

Table 3-3 ST Transmitter Precoding Functions

3.2.2 Space-Time Receiver Subsystem (SRS)

The ST Receiver Subsystem (SRS) is illustrated in Figure 3-4. There are three modules which implement ST receiver functionality, the Precoder, the ST Demapper, and the Random Data Sink module:

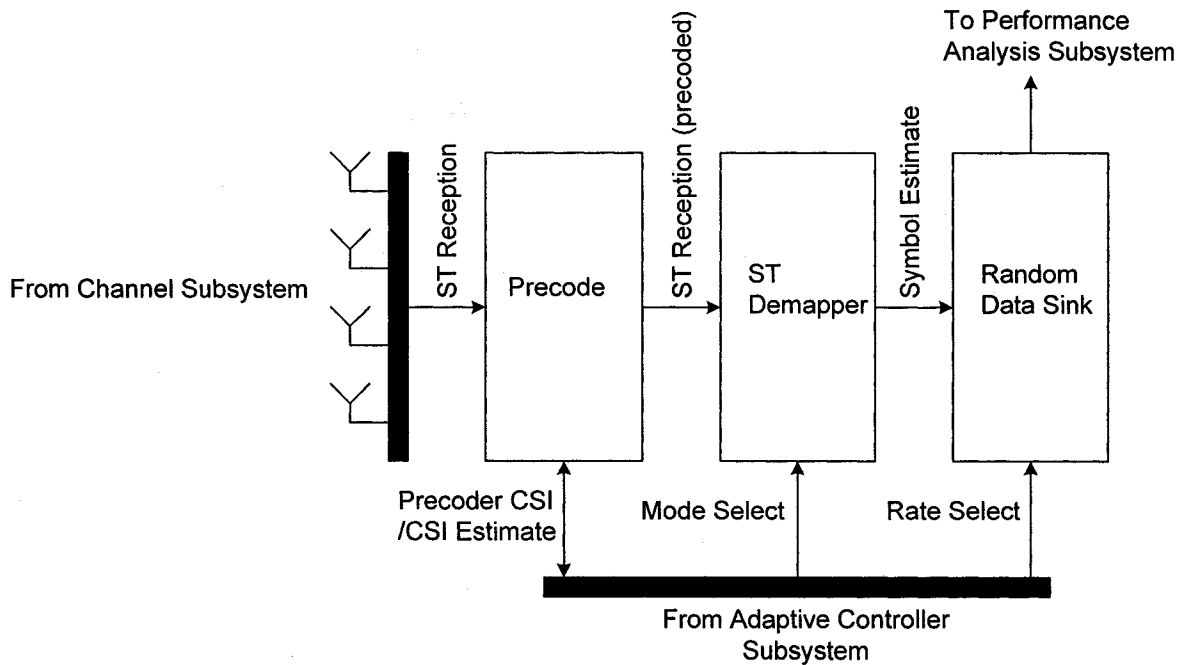


Figure 3-4 ST Receiver Subsystem

The ST receiver interfaces to the ACS, as well as the MIMO Channel and Performance Analysis Subsystems. The ST receiver is managed by the ACS. The ACS controls the mode of operation and desired data rate. As well, the ACS provides receiver precoding necessary for codeword reception and symbol decoding from the simulated MIMO channel.

3.2.2.1 Precoder

The Precoder module is responsible for precoding the ST codeword received from the simulated MIMO wireless channel via the receive antenna array. The ACS instructs the Precoder module through the Precoder CSI input as to the precoding function to use. As with the ST transmitter precoding function, the receiver precoding function is application specific and dependent on the ST mapping function employed. The following table summarizes the supported ST receiver precoder functions:

ST Mapping Mode	ST Receiver Precoder Function	Dimension	Description
G2 OSTBC	\mathbf{I}_2	2 x 2 (integer)	Precoding disabled. Function invokes an identity system.
G3 OSTBC	\mathbf{I}_3	3 x 3 (integer)	Precoding disabled. Function invokes an identity system.
G4 OSTBC	\mathbf{I}_4	4 x 4 (integer)	Precoding disabled. Function invokes an identity system.
G5 OSTBC	\mathbf{I}_5	5 x 5 (integer)	Precoding disabled. Function invokes an identity system.
G6 OSTBC	\mathbf{I}_6	6 x 6 (integer)	Precoding disabled. Function invokes an identity system.
G7 OSTBC	\mathbf{I}_7	7 x 7 (integer)	Precoding disabled. Function invokes an identity system.
G8 OSTBC	\mathbf{I}_8	8 x 8 (integer)	Precoding disabled. Function invokes an identity system.
A-BLAST[1..8]	\mathbf{P}	N x N (integer)	Function invokes the A-BLAST codec ST receiver precoding. Precoding is the row permutation \mathbf{P} , required to obtain the row permuted channel realization matrix \mathbf{H}_p .

			Refer to §5.1.1 for details related to the A-BLAST codec.
ALAMOUTI OSTBC	I_2	2 x 2 (integer)	Precoding disabled. Function invokes an identity system.

Table 3-4 ST Receiver Precoding Functions

3.2.2.2 ST Demapper

The ST Demapper module is responsible for demapping a received ST transmission to an output MPSK symbol vector estimate according to a given ST processing method. As with the ST Mapper, the ACS instructs the ST Demapper module through the `Mode Select` input as to the ST demapping function to use. The demapping is as described earlier in Table 3-2.

3.2.2.3 Random Data Sink

The Random Data Sink, illustrated in Figure 3-5, demodulates the receive symbol vector estimate and forwards the associated bit vector estimate to the Performance Analysis Subsystem for performance monitoring. The ACS, through the `Rate Select` input signal, conveys necessary symbol rate and modulation level information. The supported digital modulation is MPSK with $M \in [2, 4, 8, 16, 32]$.

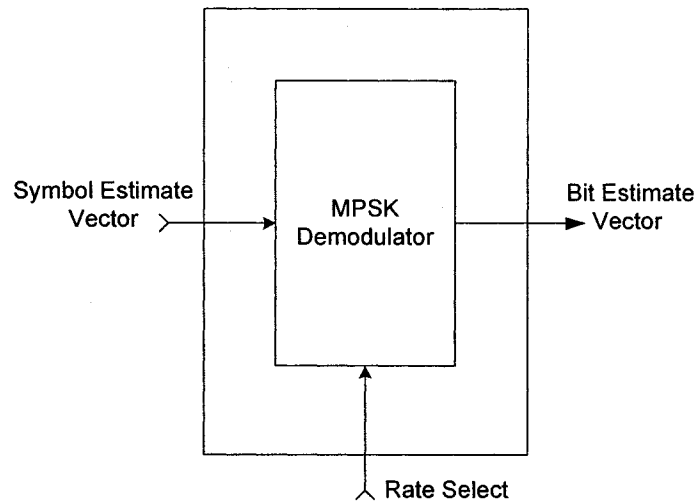


Figure 3-5 Random Data Sink

3.2.3 MIMO Channel Subsystem (MCS)

The MIMO Channel Subsystem (MCS) of Figure 3-6 simulates a narrowband frequency flat fading MIMO wireless channel. Interfaces are provided between the ST Transmitter and ST Receiver Subsystems. In addition, for test purposes, an interface is provided to the ACS for the provisioning of CSI, when the training type has been selected as PERFECT_CSI (see Table 3-1).

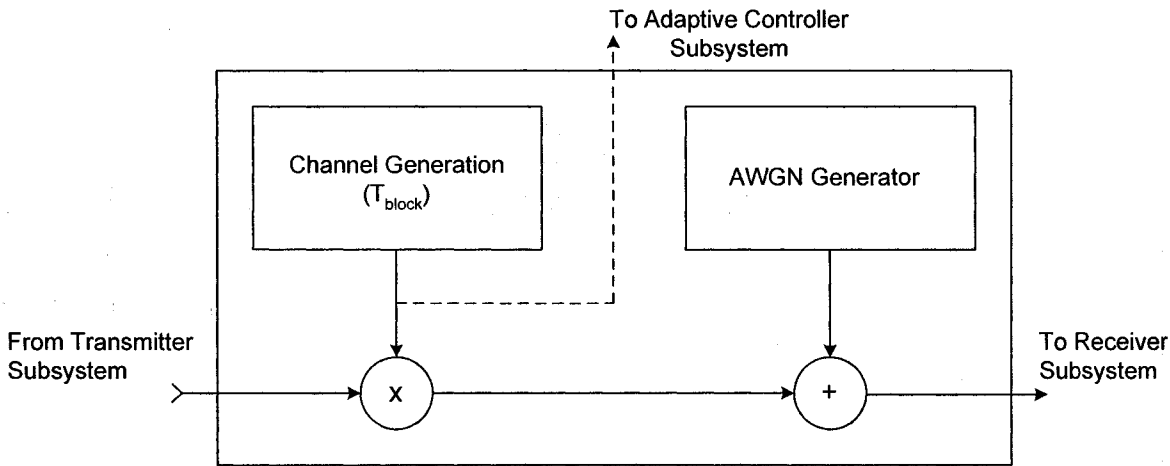


Figure 3-6 MIMO Channel Subsystem

The MCS simulates signal impairments perturbing wireless transmission. Signal impairments simulated include i) channel fading both, Raleigh (\mathbf{H}_{iid}) and Ricean (K, \mathbf{H}_r), ii) MSI, iii) antenna correlation ($\mathbf{R}_{rr}, \mathbf{R}_{tt}$), iv) antenna cross-polarization discrimination (\mathbf{X}_p), and v) AWGN. Support for block fading with programmable coherence time (T_c), and time-correlated continuous fading, with programmable temporal correlation coefficient (α), environments are available through the SMWE parameterized interface (see Table 3-1). Figure 3-7 illustrates the MIMO channel realization generation [9][31]:

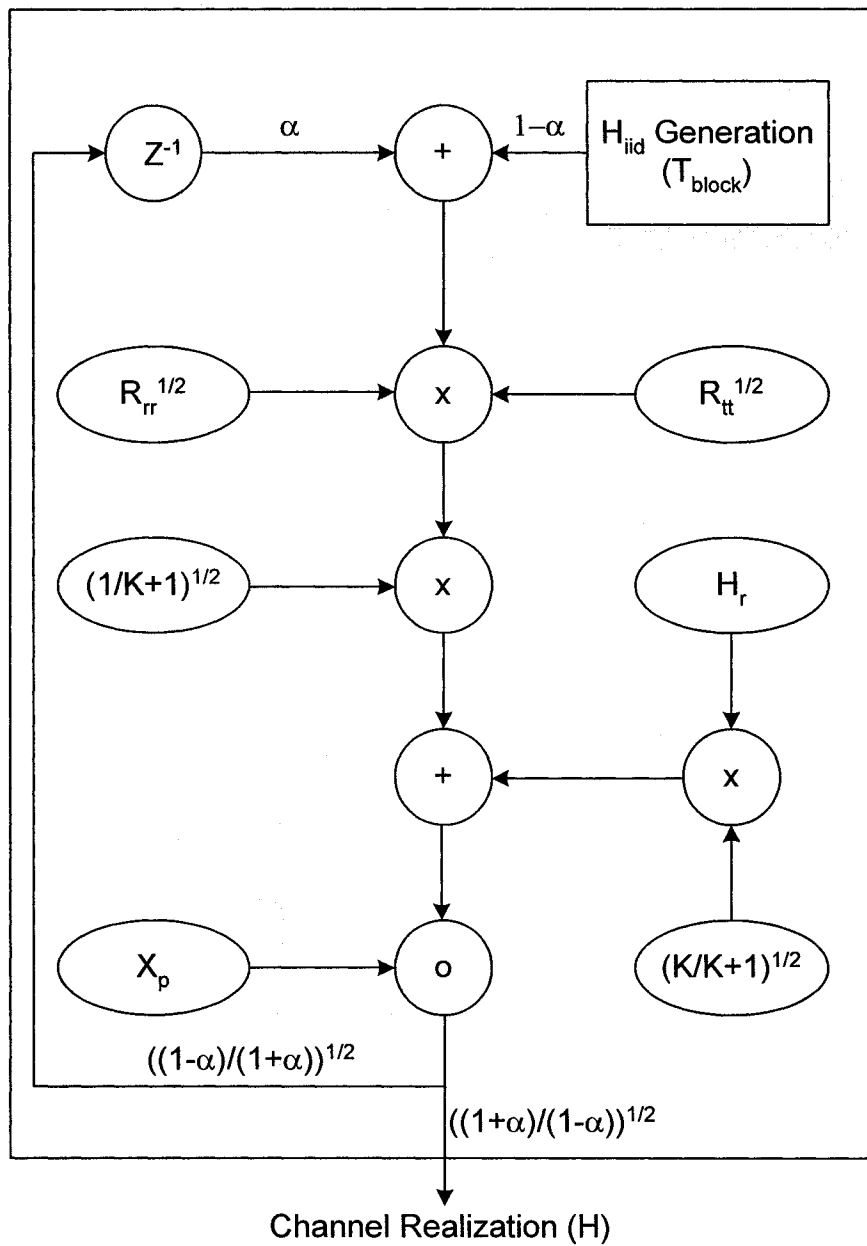


Figure 3-7 MIMO Channel Realization Generation

3.2.3.1 Block Fading MIMO Channel

In block fading environments, each channel realization is held constant for the coherence time provided to the SMWE. At the expiration of the coherence time, a new channel realization is generated according to Figure 3-7. In block fading environments, the temporal correlation coefficient would typically be zero, but not necessarily, with each MIMO channel realization being statistically independent of past realizations.

3.2.3.2 Time-Correlated Continuous Fading MIMO Channel

In time-correlated continuous fading environments, the simulated MIMO channel realization is continuously changing from one symbol interval to the next. The correlation across symbol intervals is controlled through the temporal correlation factor (α) provided to the SMWE through input parameter `T_CORR_FACT_UT` (see Table 3-1). The temporal correlation is modeled as a single pole infinite impulse response (IIR) low-pass filter applied to the real and imaginary components of the channel fading coefficients ($h_{ij} = \sigma_{ij} + j\beta_{ij}$) [31]:

$$y(n) = \alpha y(n-1) + (1-\alpha)x(n) \quad (21)$$

In this mode, the coherence time (T_c) would typically be one, but not necessarily, as the channel realization is continuously variable in time.

3.2.3.3 Spatial Correlation

In practical MIMO wireless systems with limited antenna element spacing or with significant separation between transmitter and receiver antenna arrays, angular spread of transmission becomes small and subsequently, multi-path propagation delay spread across the channel is reduced. As a result, spatial fading across antenna array elements becomes correlated. Spatial correlation acts to reduce the effective channel rank (r) as discussed in §2.2.2 and lower the achievable MIMO link capacity of (9). Spatial correlation is simulated through the SMWE with transmitter and receiver positive semi-definite Hermitian spatial covariance matrices $\mathbf{R}_{tt} \in \mathbb{C}^{M \times M}$ and $\mathbf{R}_{rr} \in \mathbb{C}^{N \times N}$ respectively (see Table 3-1). Spatial correlation is imposed on the Rayleigh channel realization through:

$$\mathbf{H}_1 = \mathbf{R}_{rr}^{1/2} \mathbf{H}_{iid} \mathbf{R}_{tt}^{1/2} \quad (22)$$

The j^{th} column of \mathbf{R}_{tt} defines the spatial correlation from all $k \neq j$ transmit antennas with the transmission path of the j^{th} antenna, as seen at a particular receive antenna element. Similarly, the i^{th} row of \mathbf{R}_{rr} defines the spatial correlation to all $l \neq i$ receive antennas with the transmission path to the i^{th} receive antenna, as seen from a particular transmit antenna element.

3.2.3.4 Line-of-Sight (LOS) Signal Propagation

In propagation environments with little local scattering or with true line-of-sight (LOS) transmission as modeled through (6), channel propagation becomes less scattered and more coherent. The existence of a LOS path acts to spatially correlate channel fading, where signal transmission is best modeled as plane

wave propagation with fading characteristics primarily a function of the direction-of-arrival (DOA), path length (R), and antenna array geometry. The LOS or Ricean channel component of each channel realization is imposed through:

$$\mathbf{H}_2 = \sqrt{\frac{1}{K+1}}\mathbf{H}_1 + \sqrt{\frac{K}{K+1}}\mathbf{H}_r \quad (23)$$

Here, \mathbf{H}_1 comes from (14), K is the Ricean power factor and $\mathbf{H}_r \in \mathbb{C}^{N \times M}$ the Ricean channel provided as inputs `K_RICEAN_UT` and `H_RICEAN_UT` respectively to the SMWE (see Table 3-1). The reader is referred to [9][32] for a discussion of how to form \mathbf{H}_r as a function of DOA, array steering vectors, antenna element separation, etc.

3.2.3.5 Antenna Cross-Polarization Discrimination

Antenna polarization diversity is one method sometimes employed to achieve a diversity gain when available space limitations dictate antenna array size or geometry. The SMWE supports antenna cross-polarization discrimination through the input parameter `X_POL_UT`. As illustrated in Figure 3-7, the cross-polarization is defined through the matrix $\mathbf{X}_p \in \mathbb{C}^{N \times M}$ which is applied through a matrix Hadamard product with the channel realization \mathbf{H}_2 of (15):

$$\mathbf{H} = \mathbf{X}_p \circ \mathbf{H}_2 \quad (24)$$

3.2.4 Adaptive Controller Subsystem (ACS)

The ACS is responsible for managing the operation of the transmitter and receiver subsystems in response to simulated environmental changes introduced through the MCS. The primary responsibilities of the ACS include:

- 1) Initiating periodic training to facilitate CSI estimation.
- 2) Analysis of channel rank and gain, receiver SNR, and residual BER.
- 3) Data mode selection for the adaptive ST transceiver.
- 4) Generation of required transmitter and receiver precoder CSI.

SMWE state information is maintained in the ACS database. The ACS database is described in Table 3-5:

Database Entry (Ctrl.)	Description																					
BitRate	Selected bit rate per M-PSK symbol (i.e. $\log_2(\text{ModLevel})$).																					
CodeRate	Selected code rate per channel use.																					
Mode	<p>Mode of operation. Supported modes include:</p> <table border="1" data-bbox="457 613 1261 1862"> <thead> <tr> <th data-bbox="457 613 824 657">Mode</th> <th data-bbox="824 613 1261 657">Description</th> </tr> </thead> <tbody> <tr> <td data-bbox="457 657 824 766">MODE_ABLAST1</td> <td data-bbox="824 657 1261 766">MxN ABLAST mode of operation. Code rate M, (M = N, M > 1).</td> </tr> <tr> <td data-bbox="457 766 824 919">MODE_ABLAST2</td> <td data-bbox="824 766 1261 919">MxN ABLAST mode of operation. Code rate M-1, (M = N, M > 1).</td> </tr> <tr> <td data-bbox="457 919 824 1072">MODE_ABLAST3</td> <td data-bbox="824 919 1261 1072">MxN ABLAST mode of operation. Code rate M-2, (M = N, M > 2).</td> </tr> <tr> <td data-bbox="457 1072 824 1225">MODE_ABLAST4</td> <td data-bbox="824 1072 1261 1225">MxN ABLAST mode of operation. Code rate M-3, (M = N, M > 3).</td> </tr> <tr> <td data-bbox="457 1225 824 1378">MODE_ABLAST5</td> <td data-bbox="824 1225 1261 1378">MxN ABLAST mode of operation. Code rate M-4, (M = N, M > 4).</td> </tr> <tr> <td data-bbox="457 1378 824 1530">MODE_ABLAST6</td> <td data-bbox="824 1378 1261 1530">MxN ABLAST mode of operation. Code rate M-5, (M = N, M > 5).</td> </tr> <tr> <td data-bbox="457 1530 824 1683">MODE_ABLAST7</td> <td data-bbox="824 1530 1261 1683">MxN ABLAST mode of operation. Code rate M-6, (M = N, M > 6).</td> </tr> <tr> <td data-bbox="457 1683 824 1836">MODE_ABLAST8</td> <td data-bbox="824 1683 1261 1836">MxN ABLAST mode of operation. Code rate M-7, (M = N, M > 7).</td> </tr> <tr> <td data-bbox="457 1836 824 1862">MODE_ALAMOUTI</td> <td data-bbox="824 1836 1261 1862">2xN Alamouti mode of</td> </tr> </tbody> </table>		Mode	Description	MODE_ABLAST1	MxN ABLAST mode of operation. Code rate M, (M = N, M > 1).	MODE_ABLAST2	MxN ABLAST mode of operation. Code rate M-1, (M = N, M > 1).	MODE_ABLAST3	MxN ABLAST mode of operation. Code rate M-2, (M = N, M > 2).	MODE_ABLAST4	MxN ABLAST mode of operation. Code rate M-3, (M = N, M > 3).	MODE_ABLAST5	MxN ABLAST mode of operation. Code rate M-4, (M = N, M > 4).	MODE_ABLAST6	MxN ABLAST mode of operation. Code rate M-5, (M = N, M > 5).	MODE_ABLAST7	MxN ABLAST mode of operation. Code rate M-6, (M = N, M > 6).	MODE_ABLAST8	MxN ABLAST mode of operation. Code rate M-7, (M = N, M > 7).	MODE_ALAMOUTI	2xN Alamouti mode of
Mode	Description																					
MODE_ABLAST1	MxN ABLAST mode of operation. Code rate M, (M = N, M > 1).																					
MODE_ABLAST2	MxN ABLAST mode of operation. Code rate M-1, (M = N, M > 1).																					
MODE_ABLAST3	MxN ABLAST mode of operation. Code rate M-2, (M = N, M > 2).																					
MODE_ABLAST4	MxN ABLAST mode of operation. Code rate M-3, (M = N, M > 3).																					
MODE_ABLAST5	MxN ABLAST mode of operation. Code rate M-4, (M = N, M > 4).																					
MODE_ABLAST6	MxN ABLAST mode of operation. Code rate M-5, (M = N, M > 5).																					
MODE_ABLAST7	MxN ABLAST mode of operation. Code rate M-6, (M = N, M > 6).																					
MODE_ABLAST8	MxN ABLAST mode of operation. Code rate M-7, (M = N, M > 7).																					
MODE_ALAMOUTI	2xN Alamouti mode of																					

		operation.								
	MODE_TRAIN_G2	Training mode using G2 OSTBC.								
	MODE_TRAIN_G3	Training mode using G3 OSTBC.								
	MODE_TRAIN_G4	Training mode using G4 OSTBC.								
	MODE_TRAIN_G5	Training mode using G5 OSTBC.								
	MODE_TRAIN_G6	Training mode using G6 OSTBC.								
	MODE_TRAIN_G7	Training mode using G7 OSTBC.								
	MODE_TRAIN_G8	Training mode using G8 OSTBC.								
ModLevel	Selected M-PSK modulation level. Supported modulation levels include 2, 4, 8, 16, and 32.									
RxPrec[1..3]	ST receiver first/second/third precoder information.									
TBlock	Selected ST-Block length in symbol periods.									
TrainType	Selected training type. Supported training modes are:									
	<table border="1"> <thead> <tr> <th>Mode</th> <th>Description</th> </tr> </thead> <tbody> <tr> <td>PERFECT_CSI</td> <td>CSI is perfect.</td> </tr> <tr> <td>LSE_CSI</td> <td>CSI is obtained through preamble training employing OSTBC and LS estimation. [18]</td> </tr> <tr> <td>MMSE_CSI</td> <td>CSI is obtained through preamble training employing OSTBC and MMSE estimation. [18]</td> </tr> </tbody> </table>	Mode	Description	PERFECT_CSI	CSI is perfect.	LSE_CSI	CSI is obtained through preamble training employing OSTBC and LS estimation. [18]	MMSE_CSI	CSI is obtained through preamble training employing OSTBC and MMSE estimation. [18]	
Mode	Description									
PERFECT_CSI	CSI is perfect.									
LSE_CSI	CSI is obtained through preamble training employing OSTBC and LS estimation. [18]									
MMSE_CSI	CSI is obtained through preamble training employing OSTBC and MMSE estimation. [18]									
TxPrec	ST transmitter precoder information.									

Table 3-5 ACS Database

The following pseudo code describes the ACS operation:

```

ACS(Hest,           // Current MIMO channel estimate
  Snr,              // Receiver average SNR (dB)
  PwrThresh,       // Percent power threshold for channel rank estimation
  BERThresh,       // Maximum BER target threshold
  Ctrl[],          // ACS database

```

```

)
// If training completed, setup for data transfers
if Ctrl.Mode == {MODE_TRAIN_G2/3/4/5/6/7/8}

    // Generate required Tx/Rx precoding based on channel estimate
    [Ctrl.TxPrec,
     Ctrl.RxPrec1,
     Ctrl.RxPrec2,
     Ctrl.RxPrec3] = Generate_Precoding(Ctrl.Mode, Hest)

    // Select mode of operation for upcoming data transfer
    [Ctrl.Mode,
     Ctrl.CodeRate,
     Ctrl.BitRate,
     Ctrl.ModLevel,
     Ctrl.TBlock] = Mode_Select(Ctrl.Mode, Hest, Snr, PwrThresh, BERThresh)

    // Select diversity combiner weighting
    Ctrl.RxPrec3 = Select_Diversity_Weights(Ctrl.Mode, Ctrl.RxPrec3)

    // Reset the training timer
    Ctrl.TTrain = Reset_Timer(Ctrl.Mode)

// Otherwise data transfer completed
else
    // Test if training timer expired
    if Ctrl.TTrain <= 0
        [Ctrl.Mode,
         Ctrl.CodeRate,
         Ctrl.BitRate,
         Ctrl.ModLevel,
         Ctrl.TBlock,
         Ctrl.TxPrec,
         Ctrl.RxPrec1,
         Ctrl.RxPrec2,
         Ctrl.RxPrec3] = Initialize_Training(Ctrl.Mode)
    endif
endif

```

Figure 3-8 ACS Pseudo Code

The generation of precoding information as well as adaptive mode selection is codec specific and is described with additional detail in §5.

3.2.5 Performance Analysis Subsystem (PAS)

The Performance Analysis Subsystem (PAS) of Figure 3-1 monitors BER performance of data transfer throughout a simulation.

State information for performance monitoring is maintained in the PAS database. The PAS database is described in Table 3-6:

Database Entry (Perf.)	Description
AveEigen[1..min(N,M)]	Tracks average MIMO channel eigenvalues. The length of AveEigen is dependent on the spatial dimensions of the MIMO channel.
AveGain	Tracks average MIMO channel power gain in ratio.
AveHErr	Tracks average channel estimation error.
AveQRErr	Tracks average QR factorization error.
AveRank	Tracks average MIMO channel rank.
AveSnr	Tracks average receiver SNR in dB.
BitBins[1..M]	Tracks bits transmitted across modes 1 to M.
BitErrBins[1..M]	Tracks bit errors transmitted across modes 1 to M.
RateBins[1..M]	Tracks the ST-Blocks transmitted across modes 1 to M.
RankBins[1..min(M,N)]	MIMO channel rank histogram. The length of RankBins is dependent on the spatial dimensions of the MIMO channel.
SnrOutageTbl[]	Tracks outage statistics based on BER threshold parameter and average receiver SNR levels.
SymBins[1..M]	Tracks symbols transmitted across modes 1 to M.
SymErrs[1..M]	Tracks symbol errors transmitted across modes 1 to M.

Table 3-6 PAS Database

At the completion of each simulation, summary data, including the SMWE parameters, as defined in AMIMOSimDef.m (see Appendix A – SMWE Source File Listing), as well as performance results, are logged to file for analysis. The following illustrates typical log file formatting:

```
Log File, /home/jlee/matlab/AMIMO/sim/20050513_ber/amimo-k0-20050513T215418.txt
Start Time, 13-May-2005
Stop Time, 13-May-2005
Ellapsed Time(min), 3.908366e+02
Simulation Length (ST Blocks), 1000000
Simulation Length (Data Blocks), 950000
Simulation Length (Training Blocks), 50000
Simulation Mode, ABLAST1
Tx Antennas, 4
Rx Antennas, 4
Average SNR (dB), 30
Average Rank, 3.54
Average Gain (ratio), 16.00
BER Threshold, 1.000000e-01
Channel Rank Power Threshold (ratio), 0.99
Coherence Time, 80
CSI, LS Estimation
Receiver Spatial Correlation:
  1.00, 0.00, 0.00, 0.00
  0.00, 1.00, 0.00, 0.00
  0.00, 0.00, 1.00, 0.00
  0.00, 0.00, 0.00, 1.00
Transmitter Spatial Correlation:
  1.00, 0.00, 0.00, 0.00
  0.00, 1.00, 0.00, 0.00
  0.00, 0.00, 1.00, 0.00
  0.00, 0.00, 0.00, 1.00
Ricean Power Factor, 0.00
Ricean Channel:
  0.71+j0.71, 0.71+j0.71, 0.71+j0.71, 0.71+j0.71
  0.71+j0.71, 0.71+j0.71, 0.71+j0.71, 0.71+j0.71
  0.71+j0.71, 0.71+j0.71, 0.71+j0.71, 0.71+j0.71
  0.71+j0.71, 0.71+j0.71, 0.71+j0.71, 0.71+j0.71
Cross Polarization Discrimination:
  1.00, 1.00, 1.00, 1.00
  1.00, 1.00, 1.00, 1.00
  1.00, 1.00, 1.00, 1.00
  1.00, 1.00, 1.00, 1.00

ABLAST1 Mode:
Percentage Utilization, 100.00
Symbol Error Rate, 2.346974e-03
Goodput (SER), 3.99
Bit Error Rate, 1.293257e-03
Goodput (BER), 7.99
```

```

ABLAST2 Mode:
Percentage Utilization, 0.00
Symbol Error Rate, 0.000000e+00
Goodput (SER), 0.00
Bit Error Rate, 0.000000e+00
Goodput (BER), 0.00

ABLAST3 Mode:
Percentage Utilization, 0.00
Symbol Error Rate, 0.000000e+00
Goodput (SER), 0.00
Bit Error Rate, 0.000000e+00
Goodput (BER), 0.00

ABLAST4 Mode:
Percentage Utilization, 0.00
Symbol Error Rate, 0.000000e+00
Goodput (SER), 0.00
Bit Error Rate, 0.000000e+00
Goodput (BER), 0.00

Total Symbols, 15200000
Total Symbol Error, 35674
Average Symbol Error Rate, 2.346974e-03
Average Symbol Rate, 4.00
Goodput (Symbols), 3.99

Total Bits, 30400000
Total Bit Error, 39315
Average Bit Error Rate, 1.293257e-03
Average Bit Rate, 8.00
Goodput (Bits), 7.99

Goodput (BER(1.000000e-01)), 7.99
Residual BER, 1.293282e-03

```

Figure 3-9 Performance Monitor Log File (Sample)

3.3 Summary

This chapter provides for the reader a description of a simulation environment, called the SMWE, developed in Matlab[®], as part of the research described herein, to facilitate performance benchmarking and adaptive space-time algorithm development. The performance results provided in the remainder of this document have been generated using the SMWE. The reader is referred to Appendix A – SMWE Source File Listing for related source code and archive information. The correctness of simulation implementation has been verified through a combination of source code inspection, subsystem functionality testing using known test vectors as well as performance monitoring of random data

transfers under perfect CSI conditions and imperfect CSI. All implemented ST mapping and demapping functions have been tested for correctness. Performance results have been compared with similar results documented in literature [18].

4 Layered Space-Time (LST) Processing Performance Benchmarks

The following sections document the non-adaptive layered space-time (LST) processing methods used as comparative performance benchmarks throughout the research described hereafter. For consistency, performance data for all methods was obtained through simulation using the SMWE. Simulation duration is 10^6 space-time codeword transfers over a narrowband, block fading (coherence time of 20 space-time codewords), independent identically distributed (i.i.d.) simulated MIMO channel. CSI was obtained through preamble training using OSTBC codeword transfers and Least Squares (LS) based channel estimation [18]. Side channel feedback of CSI is without delay. All methods employ Binary Coded Decimal (BCD) encoded QPSK modulation, OSUC based decoding, and minimum mean squared error (MMSE) symbol detection.

4.1 LST Spatial Multiplexing Methods

This section documents the non-adaptive LST spatial multiplexing performance benchmarks.

For MIMO systems operating in full rank (i.e. $r = \min(N, M)$) Raleigh fading environments, the V-BLAST LST encoding is known to provide maximum spatial multiplexing gain [18][20][26]. §4.1.1-§4.1.3 provides BER versus average SNR [dB] curves, obtained through the SMWE, for V-BLAST transmission. In addition, spatial fading correlation is controlled through the Ricean Power Factor (K), as per §3.2.3.4, such that the average rank over all MIMO channel realizations may be varied from the limits of full rank Raleigh fading, indicative of many indoor propagation environments, toward the fully rank deficient MIMO channel, typical of many outdoor LOS propagation environments.

In addition to receiver SNR dependency, the BER performance of V-BLAST transmission is highly dependent on the existence of uncorrelated Raleigh fading. As fading becomes spatially correlated, and the MIMO channel becomes rank deficient (i.e. $r < \min(N, M)$), the ability of V-BLAST to spatial multiplex independent data streams is reduced as MSI levels increase. This is illustrated through the horizontal shift in the BER curves. As well, at low SNR levels, BER performance is further degraded due to CSI errors introduced through channel estimation.

4.1.1 V-BLAST (M = N = 2)

For the system described, the V-BLAST LST encoding provides a maximum spatial multiplexing gain of 2, a diversity order of 2, and throughput of 2 [s/cu].

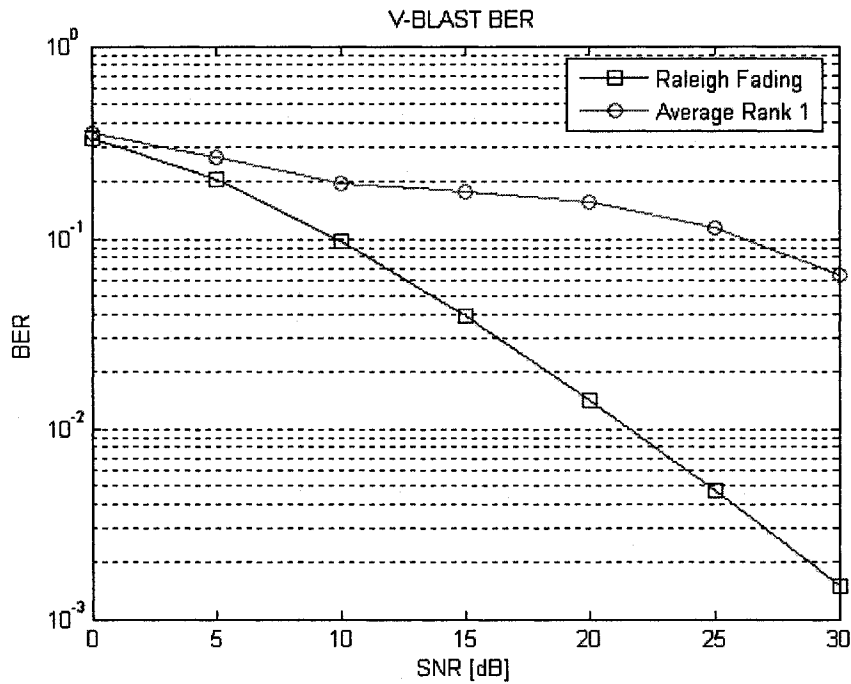


Figure 4-1 V-BLAST BER vs. SNR (M=N=2, QPSK)

4.1.2 V-BLAST (M = N = 4)

For the system described, the V-BLAST LST encoding provides a maximum spatial multiplexing gain of 4, a diversity order of 4, and throughput of 4 [s/cu].

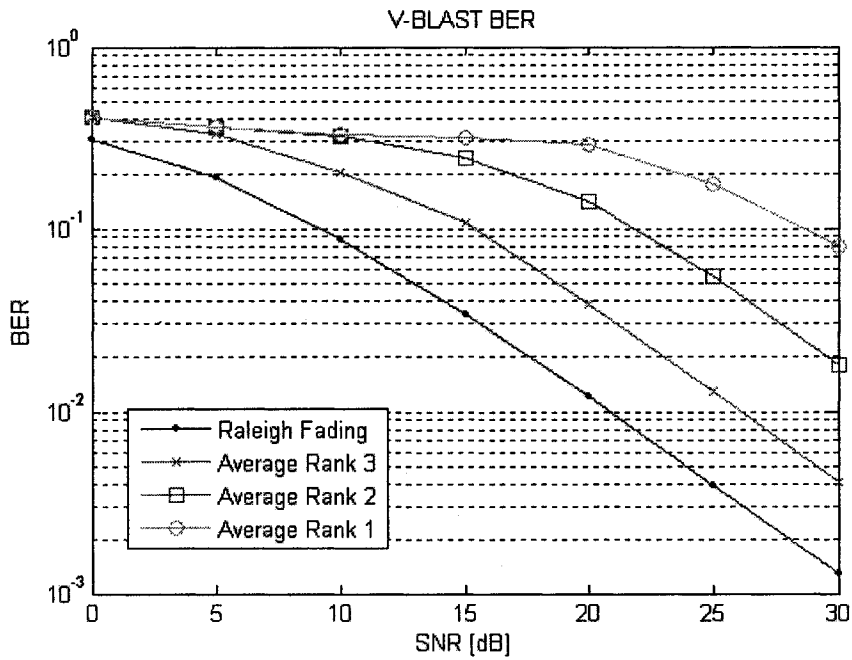


Figure 4-2 V-BLAST BER vs. SNR ($M=N=4$, QPSK)

4.1.3 V-BLAST ($M = N = 8$)

For the system described, the V-BLAST LST encoding provides a maximum spatial multiplexing gain of 8, a diversity order of 8, and throughput of 8 [s/cu].

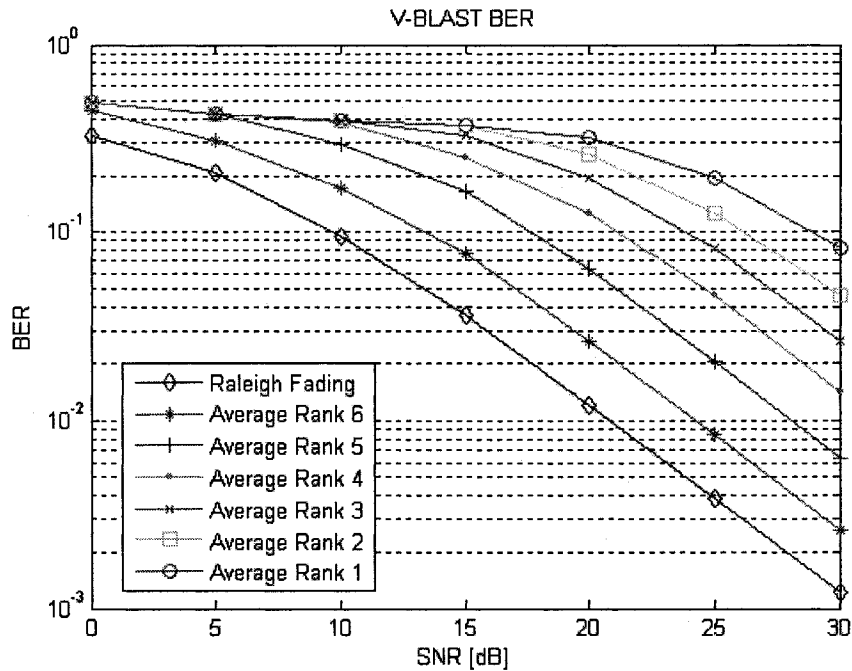


Figure 4-3 V-BLAST BER vs. SNR ($M=N=8$, QPSK)

4.2 LST Diversity Methods

This section documents the non-adaptive LST diversity performance benchmarks.

The D-BLAST LST encoding provides maximum diversity order (i.e. MN) while achieving unity code rate in symbol per channel use [s/cu] [18]. At low SNR or highly rank deficient environments, the error performance of spatial multiplexing alone can become prohibitively high due to CSI errors and absence of spatial eigenmodes respectively. Symbol diversity across space and time can aid in symbol detection through the coherent diversity combining of redundant streams, lowering the average probability of symbol detection error [22][23]. §4.2.1-§4.2.3 provide BER versus average SNR [dB] curves, obtained through the SMWE, for D-BLAST transmission. In addition, spatial fading correlation is controlled through the Ricean Power Factor (K), as per §3.2.3.4, such that the average rank over all MIMO channel realizations may be varied from the limits of full rank Rayleigh fading, indicative of many indoor propagation environments, toward the fully rank deficient MIMO channel, typical of many outdoor LOS propagation environments.

The BER performance of D-BLAST transmission is superior to that of V-BLAST. The increased slope of the BER versus SNR curves is a measure of the additional diversity provided through D-BLAST LST encoding. It is also clear from the curves that the error performance of D-BLAST is far less dependent on the existence of uncorrelated Rayleigh fading. As fading becomes spatially correlated, and the MIMO channel becomes rank deficient (i.e. $r < \min(N, M)$), the negative effects of MSI on symbol detection does not exist as D-BLAST does not attempt to spatially multiplex independent data streams. As well, although spatial correlation tends to reduce diversity gain by correlating microscopic fading across antenna elements, the D-BLAST LST is still able to exploit array gain (see §2.3.1) through the coherent combining of redundant data streams. As with V-BLAST, at low SNR levels, the BER performance is degraded due to CSI errors introduced through channel estimation.

4.2.1 D-BLAST (M = N = 2)

For the system described, the D-BLAST LST encoding provides a no spatial multiplexing gain, a maximum diversity order of 4, and throughput of 1 [s/cu].

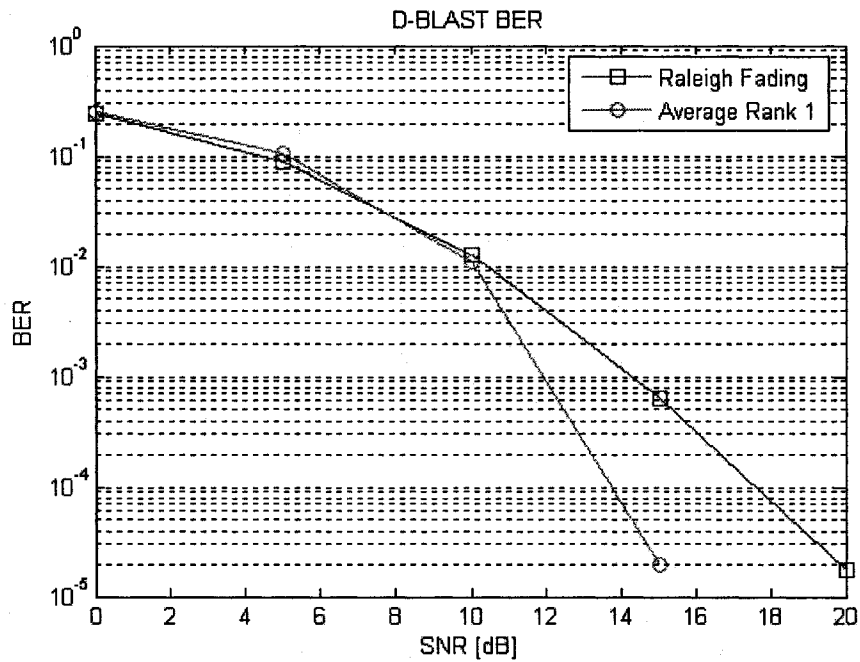


Figure 4-4 D-BLAST BER vs. SNR (M=N=2, QPSK)

4.2.2 D-BLAST (M = N = 4)

For the system described, the D-BLAST LST encoding provides a no spatial multiplexing gain, a maximum diversity order of 16, and throughput of 1 [s/cu].

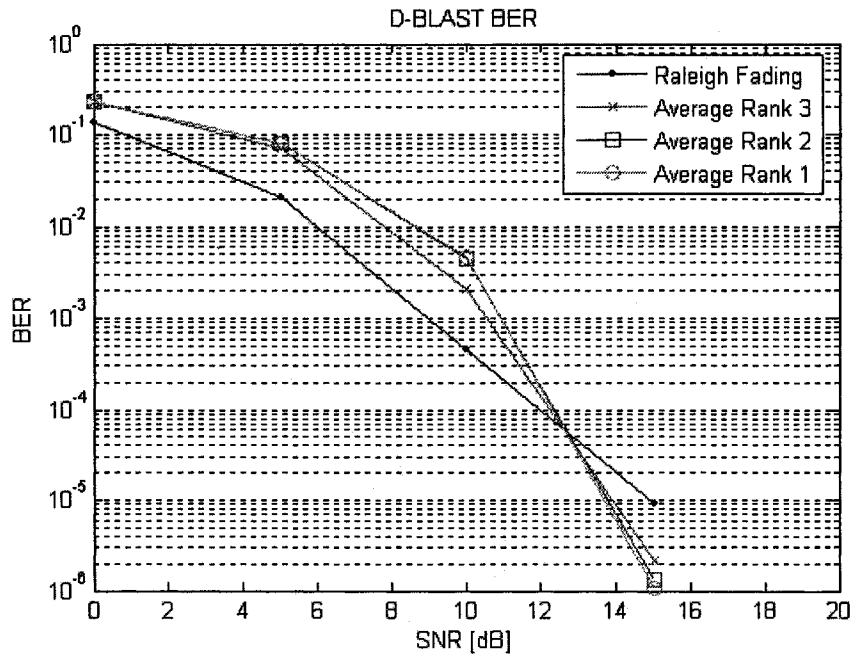


Figure 4-5 D-BLAST BER vs. SNR ($M=N=4$, QPSK)

4.2.3 D-BLAST ($M = N = 8$)

For the system described, the D-BLAST LST encoding provides a no spatial multiplexing gain, a maximum diversity order of 64, and throughput of 1 [s/cu].

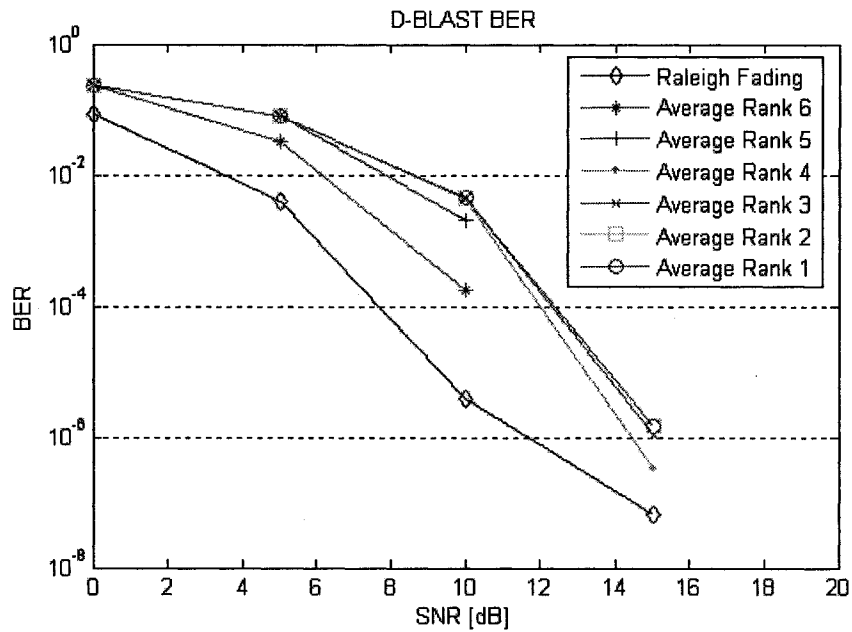


Figure 4-6 D-BLAST BER vs. SNR ($M=N=8$, QPSK)

4.3 Summary

This chapter provides the non-adaptive spatial multiplexing and diversity encoding performance benchmarks, provided by V-BLAST and D-BLAST respectively, used throughout the research described hereafter. For consistency, performance data for all methods, both non-adaptive and otherwise, is obtained through simulation using the SMWE.

Considerable efforts have been made to ensure the correctness of simulation implementation and accuracy of recorded results.

5 Adaptive MIMO Space-Time Processing Research

As outlined in §1.1, the research described herein is motivated toward developing a new and novel adaptive MIMO space-time processing algorithm which is fully self-conforming, of realizable complexity, and able to automatically adapt to a time varying MIMO wireless channel. The ideal adaptation converging toward the correct balance of reliability (i.e. residual BER) and capacity (i.e. spectral efficiency) necessary for superior wireless link performance (i.e. link *goodput*).

5.1 Adaptive BLAST (A-BLAST)

The Adaptive BLAST (A-BLAST) method was developed following the completion of a literature review in the areas of diversity and spatial multiplexing space-time processing [1-12][18-23][26-28], multi-user MIMO coding techniques [18][33], matrix computations [19], as well as networking background in the areas of sub-rate data multiplexing.

As with non-adaptive BLAST systems, the A-BLAST method is applicable to any MIMO deployment environment with equally sized antenna arrays provisioned such that $M = N$. In the case of $M < N$, the receiver would select an optimal subset of N_M receive antennas for symmetric ($M = N_M$) communication [34][35]. In a similar manner, in the case of $M > N$, the transmitter would select an optimal subset of M_N transmit antennas for symmetric ($M_N = N$) communication.

Implementations using two, four, and eight element antenna arrays were selected for evaluation because of their expected immediate practicability in WLAN and BWA markets.

5.1.1 Space-Time Codec Description

The A-BLAST space-time codec is illustrated in block diagram in Figure 5-1:

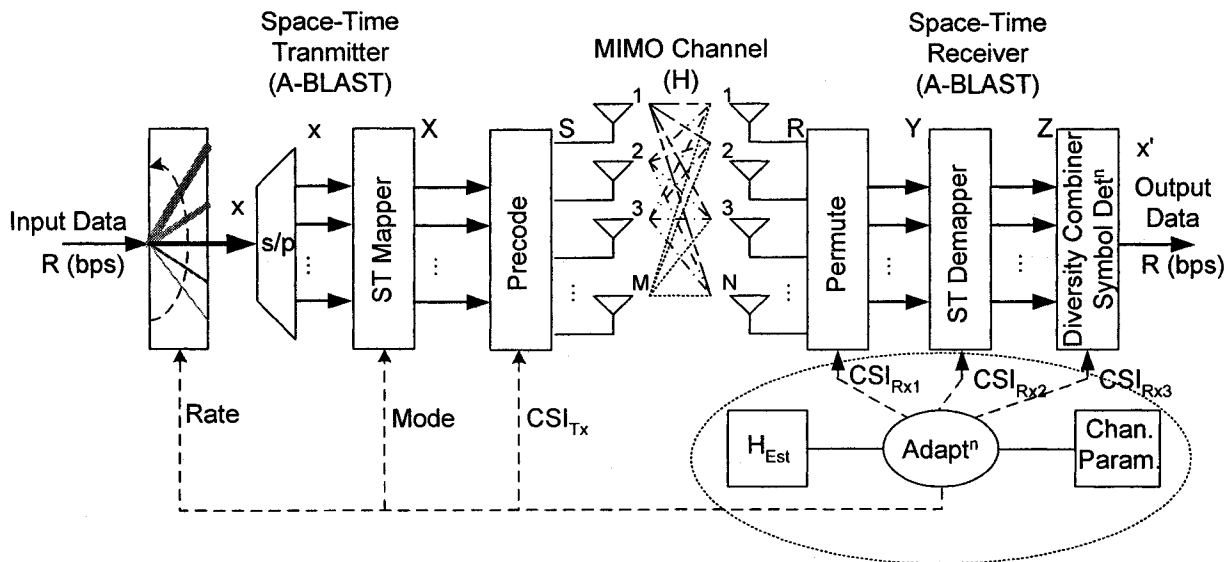


Figure 5-1 A-BLAST Block Diagram

Through preamble or pilot training, the system obtains an estimate of the MIMO channel (\mathbf{H}_{Est}). The A-BLAST codec, with knowledge of the MIMO channel, and estimates of channel rank and average receiver SNR, selects a mode which maximizes the code rate (R) given the current channel realization and target BER threshold.

The input symbol vector $\mathbf{x} \in C^{Q \times 1}$ belongs to an M-ary complex symbol constellation such as M-PSK. The space-time mapping converts the input symbol vector to an A-BLAST space-time codeword $\mathbf{S} \in C^{M \times M}$ based on the operating mode (see Table 3-2). The Q input symbols are mapped across space (i.e. M transmit antennas) and time (i.e. M symbol periods). The degree of diversity order versus spatial multiplexing gain is dependent on the mode selected through adaptation. The A-BLAST codec increases diversity order, or equivalently reduces spatial multiplexing capability, from the bottom up in the space-time codeword. The codec through space-time signal processing attempts to partition the MIMO channel in a similar manner, that is to say ordered from lowest to highest available composite receive channel gain (3). When error performance dictates, the codec begins to add diversity to the receive channels of lowest quality and retain spatial multiplexing gain, when spatial eigenmodes exists, over receive antennas of higher composite receive channel gain.

Neglecting errors in channel estimation (i.e. $\mathbf{H}_{\text{Est}} = \mathbf{H}$), receive channels (i.e. rows) from the MIMO channel estimate are analyzed and permuted in order of decreasing receive channel gain:

$$\mathbf{H}_p = \mathbf{P}\mathbf{H} \Leftrightarrow \mathbf{H} = \mathbf{P}^T \mathbf{H}_p \quad (25)$$

Here $\mathbf{P} \in I^{M \times M}$ is the required row permutation matrix ($\mathbf{P}\mathbf{P}^T = \mathbf{I}_M \in I^{M \times M}$) necessary to obtain an equivalent but row permuted channel realization \mathbf{H}_p . The Hermitian transpose of the row permuted channel matrix \mathbf{H}_p is decomposed through a unitary QR transformation as:

$$\mathbf{QR} = \mathbf{H}_p^H \Rightarrow \quad (26)$$

$$(\mathbf{QR})^H = \mathbf{H}_p \Leftrightarrow \mathbf{L}_p \mathbf{Q}_p \quad (27)$$

In (27), $\mathbf{L}_p = \mathbf{R}^H \in C^{M \times M}$ and $\mathbf{Q}_p = \mathbf{Q}^H \in C^{M \times M}$. Through the QR transformation, \mathbf{Q}_p is unitary with $\mathbf{Q}_p \mathbf{Q}_p^H = \mathbf{Q}_p^H \mathbf{Q}_p = \mathbf{I}_M$. The matrix \mathbf{L}_p is lower triangular and preserves the total MIMO channel power $\|\mathbf{H}_p\|_F^2$ and equivalently $\|\mathbf{H}\|_F^2$. Similarly, for $i \in [1..M]$, the i^{th} receive channel gain of \mathbf{H} is preserved through the channel permutation and QR decomposition:

$$\|\tilde{\mathbf{h}}_{p,p(i)}^T\|_2^2 = \|\tilde{\mathbf{l}}_{p,p(i)}^T\|_2^2 \Leftrightarrow \|\tilde{\mathbf{h}}_i^T\|_2^2 \quad (28)$$

In (28), $p(i)$ is the permutation mapping the i^{th} row of \mathbf{H} to row $p(i)$ of \mathbf{H}_p .

Referring to Figure 5-1, selecting the transmitter precoding as $\text{CSI}_{\text{Tx}} = \mathbf{Q}_p^H$, the received space-time codeword incident on the receive antenna array may be represented as:

$$\mathbf{R} = \mathbf{H}(\mathbf{Q}_p^H \mathbf{S}) + \mathbf{N} \quad (29)$$

Here, $\mathbf{N} \in C^{M \times M}$ is the receive ZMCSCG noise matrix. At the receiver, selecting partial CSI as $\text{CSI}_{\text{Rx1}} = \mathbf{P}$, the received codeword is permuted as:

$$\begin{aligned} \mathbf{Y} &= (\mathbf{P})(\mathbf{H})(\mathbf{Q}_p^H \mathbf{S}) + \mathbf{N} \Rightarrow \\ \mathbf{Y} &= \mathbf{P}\mathbf{H}\mathbf{Q}_p^H \mathbf{S} + \mathbf{P}\mathbf{N} \end{aligned} \quad (30)$$

Substituting (27) \rightarrow (25) \rightarrow (30) we obtain:

$$\begin{aligned} \mathbf{Y} &= \mathbf{P}(\mathbf{P}^T \mathbf{H}_p)(\mathbf{Q}_p^H \mathbf{S}) + \mathbf{P}\mathbf{N} \Rightarrow \\ \mathbf{Y} &= (\mathbf{P}\mathbf{P}^T)(\mathbf{L}_p \mathbf{Q}_p)(\mathbf{Q}_p^H \mathbf{S}) + \mathbf{P}\mathbf{N} \Rightarrow \\ \mathbf{Y} &= \mathbf{L}_p \mathbf{S} + \mathbf{P}\mathbf{N} \end{aligned} \quad (31)$$

The space-time demapper, with $\text{CSI}_{\text{Rx2}} = \mathbf{L}_p$, may mitigate MSI through:

$$\begin{aligned}
\mathbf{Z} &= \mathbf{L}_p^{-1} \mathbf{Y} \Rightarrow \\
\mathbf{Z} &= \mathbf{S} + (\mathbf{L}_p^{-1} \mathbf{P}) \mathbf{N} \Rightarrow \\
\mathbf{Z} &= \mathbf{S} + \bar{\mathbf{N}}
\end{aligned} \tag{32}$$

In practice, rather than computing \mathbf{L}_p^{-1} , which may become singular in the high SNR and highly rank deficient environment, the space-time codeword (\mathbf{S}) is decoded using OSUC linear processing in order of decreasing SINR [18]. The uppermost layer of the transmission matrix \mathbf{S} is decoded first. This layer, because of the permutation performed through precoding, experiences maximum composite receive gain, no MSI, and in the absence of external radio frequency interference (RFI), is perturbed only by receiver noise ($\bar{\mathbf{N}}$). Once decoded, utilizing receiver CSI (\mathbf{L}_p), MSI associated with the decoded symbols is removed from the lower layers of the space-time codeword and decoding continues iteratively on the remaining layers in order of decreasing SINR.

5.1.2 Adaptation (Mode Selection)

At the heart of the A-BLAST method is the adaptation algorithm used to adapt the space-time mapping of codeword (\mathbf{S}) for the maximization of wireless link goodput, given a target maximum allowable residual BER. Based on estimates of receive signal quality and available spatial degrees of freedom, dictated by the average receiver SNR (S_{nr}) and MIMO channel realization (H_{est}) column rank (H_{rank}) respectively, the A-BLAST adaptation is intended to select a mode of operation ($Ctrl.Mode$) which provides the optimum or near optimum balance between code rate ($Ctrl.CodeRate$) and diversity order such that throughput is maximized while link residual BER remains below a tolerable maximum threshold (BER_{Thresh}):

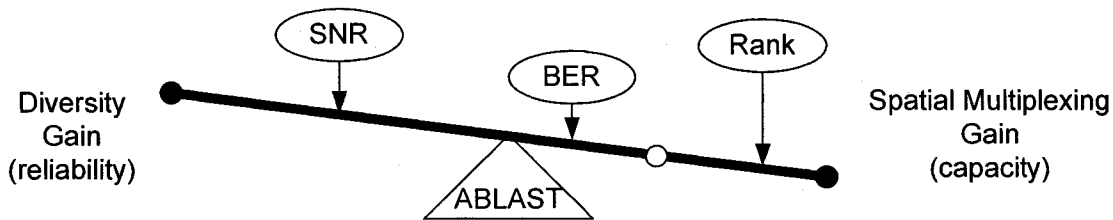


Figure 5-2 A-BLAST Diversity vs. Spatial Multiplexing Balancing

The following pseudo code describes the adaptation algorithm:

```

[           Ctrl.Mode,           // A-BLAST mode of operation (on exit)
           Ctrl.CodeRate,        // A-BLAST code rate [sym/channel use]
           Ctrl.BitRate,         // A-BLAST bit rate [bit/channel use]

```

```

        Ctrl.ModLevel,    // A-BLAST modulation order
        Ctrl.TBlock      // A-BLAST ST codeword length [symbol periods]
] =
Mode_Select(
    Ctrl.Mode,           // A-BLAST mode of operation (on entry)
    Hest,              // Estimate of MIMO channel realization
    AveSnr,             // Receiver average SNR
    PwrThresh,         // Power gain threshold (rank estimation)
    BERThresh          // System imposed maximum BER threshold
)
// Estimate channel rank (% of total channel power)
// Rank ~ # of eigenmodes required to achieve % of total channel power)
[M,
    N,                  // Number of Tx Antennas
    Hrank,             // Channel rank estimate
    Hgain,            // Channel power gain estimate
] = Est_Rank(Hest,    // MIMO channel estimate
            PwrThresh // Channel power gain threshold
)
// Estimate receive antenna SNR
Snr = 10log(Hgain) + AveSnr - 10log(M*N)

// Select A-BLAST mode based on rank, SNR, and BER target
// (using reference BER curves from $0)
[Ctrl.Mode,
    Ctrl.CodeRate,    // A-BLAST code rate [sym/channel use]
    Ctrl.TBlock,      // A-BLAST ST codeword length [symbol periods]
] = Stc_Sel(Ctrl.Mode, // A-BLAST mode of operation (existing)
            Hrank,     // Channel rank estimate
            Snr,       // Receiver SNR estimate
            BERThresh // Residual BER Target
)

// Set modulation to QPSK (adaptive modulation could be implemented here)
Ctrl.ModLevel = QPSK_Level
Ctrl.BitRate = Ctrl.CodeRate * QPSK_Rate

```

5.1.3 A2-BLAST Implementation ($M = N = 2$)

The following sub-sections detail the research completed using the SMWE for an A2-BLAST implementation with two antennas at the base station and subscriber terminals (i.e. $M = N = 2$). Documented are the comparative performance results of residual BER and link goodput.

As illustrated in Table 3-2, two modes are supported A2-BLAST[1..2]. The code rate in bit-per-second per Hertz [bps/Hz] using QPSK modulation and diversity order of each mode is summarized in Figure 5-3:

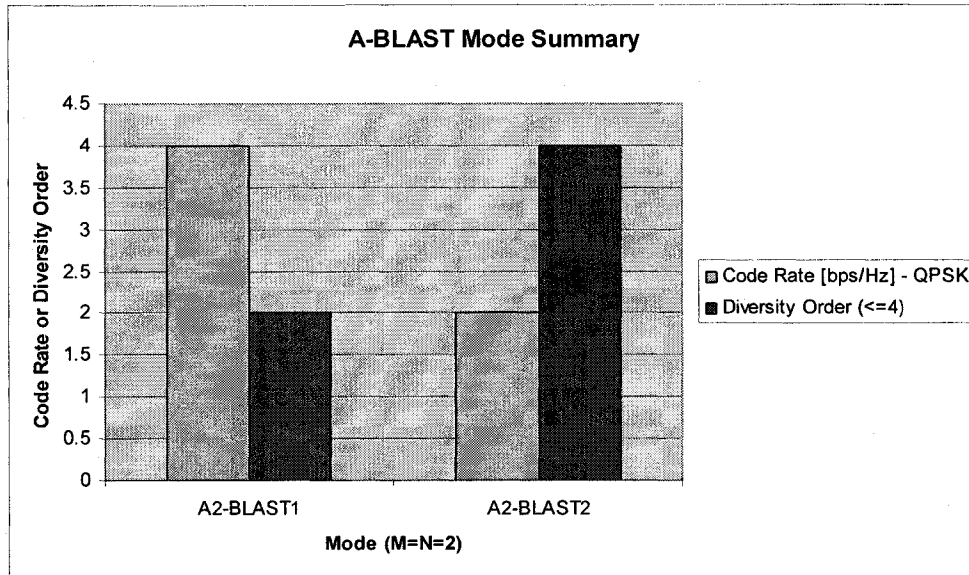


Figure 5-3 A2-BLAST Mode Summary ($M=N=2$)

The reader is referred to Appendix B – Supplementary A-BLAST Mode Summary Data for a description of the individual A2-BLAST space-time mappings functions. It should be noted that A2-BLAST1 is equivalent to V-BLAST, providing maximum code rate and minimum diversity order, while A2-BLAST2 is D-BLAST, providing minimum code rate but maximum diversity order. No intermediary modes are provided and A2-BLAST adaptation simply switches between the capacity and reliability performance benchmarks provided by V-BLAST and D-BLAST respectively.

Reference BER curves for each A2-BLAST mode was obtained using the SMWE. These curves are shown in Figure 5-4 and Figure 5-5. The average SNR (ρ) was varied from 0dB to 30dB in increments of 5dB. Additionally, the average rank (\bar{r}) of MIMO channel realizations was controlled through the Ricean Power Factor (K), see §3.2.3.4. The average MIMO channel rank was varied from full rank Rayleigh fading (i.e. $\bar{r} \approx 2$) down to fully rank deficient (i.e. $\bar{r} \approx 1$).

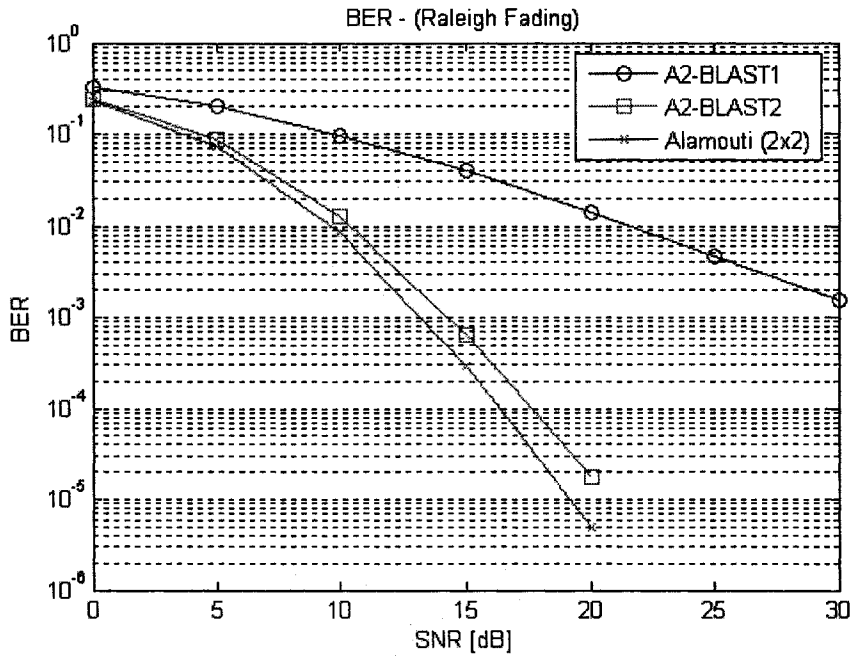


Figure 5-4 A2-BLAST Reference BER Curves (Raleigh Fading)

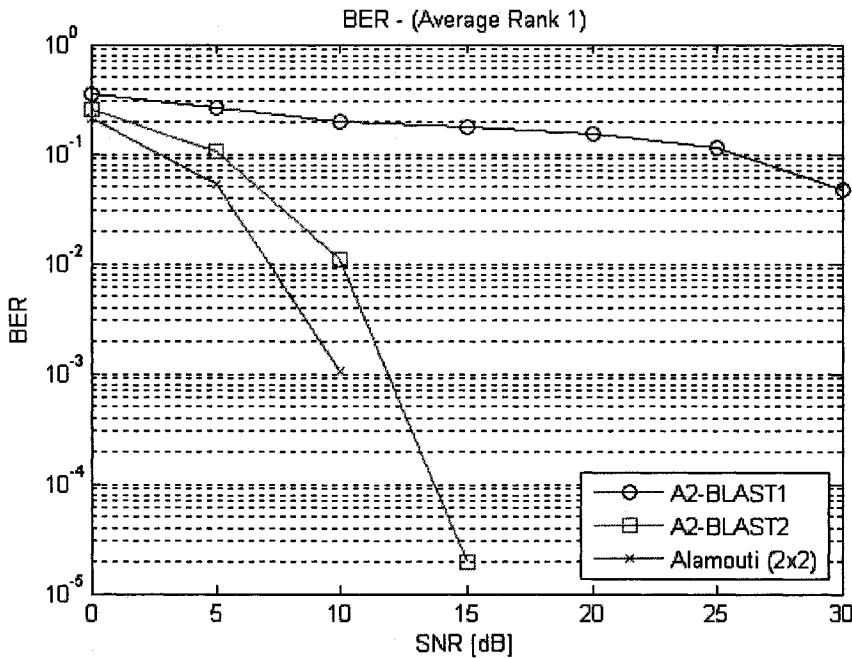


Figure 5-5 A2-BLAST Reference BER Curves (Average Rank 1)

As evident in Figure 5-4 and Figure 5-5, as fading becomes spatially correlated, error performance of A2-BLAST1 providing spatial multiplexing gain degrades more quickly than A2-BLAST2 providing only increased diversity order. These curves provide a reference by which the A2-BLAST mode may be

adapted given estimates of receive signal quality, MIMO channel rank, and system imposed BER tolerance.

In addition, applicable to the two antenna array symmetric MIMO channel, shown is the BER performance of the Alamouti OSTBC which provides, unlike all other known OSTBC methods, unity code rate [s/cu] and full diversity order improvement without the need for CSI at the transmitter [6][18][27]. Because Alamouti OSTBC, like A2-BLAST2, provides unity code rate and full diversity order improvement, its performance will be documented as comparative benchmark through §5.1.3.1.

5.1.3.1 Performance Results

The performance of A2-BLAST is compared against the non-adaptive LST processing benchmarks V-BLAST and D-BLAST, as well as Alamouti OSTBC, in Figure 5-6 to Figure 5-17. Performance is measured in terms of resulting link goodput and residual BER for target BER thresholds of 10^{-1} , 10^{-2} , and 10^{-3} respectively.

In the Rayleigh fading and high SNR environments, A2-BLAST adapts to V-BLAST providing maximum code rate given the MIMO channel's ability to accommodate spatial multiplexing and high receive signal quality. In Ricean fading and low SNR environments, A2-BLAST adapts to D-BLAST providing maximum diversity order in the absence of available spatial eigenmodes or existence of poor receive signal quality respectively. At moderate levels of receive signal quality and MIMO spatial fading correlation, A2-BLAST *switches* between V-BLAST and D-BLAST providing a superior but coarse balance between the relative weighting of diversity order and spatial multiplexing gain within the space-time codeword as conditions change across MIMO channel realizations.

5.1.3.1.1 Residual BER Threshold of 10^{-1}

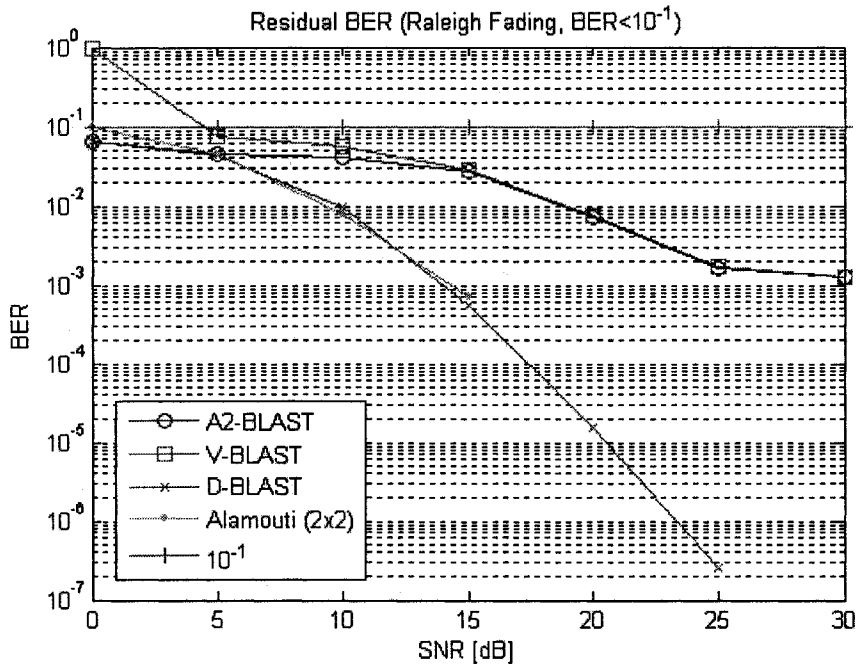


Figure 5-6 A2-BLAST Residual BER (Raleigh Fading, BER < 10^{-1})

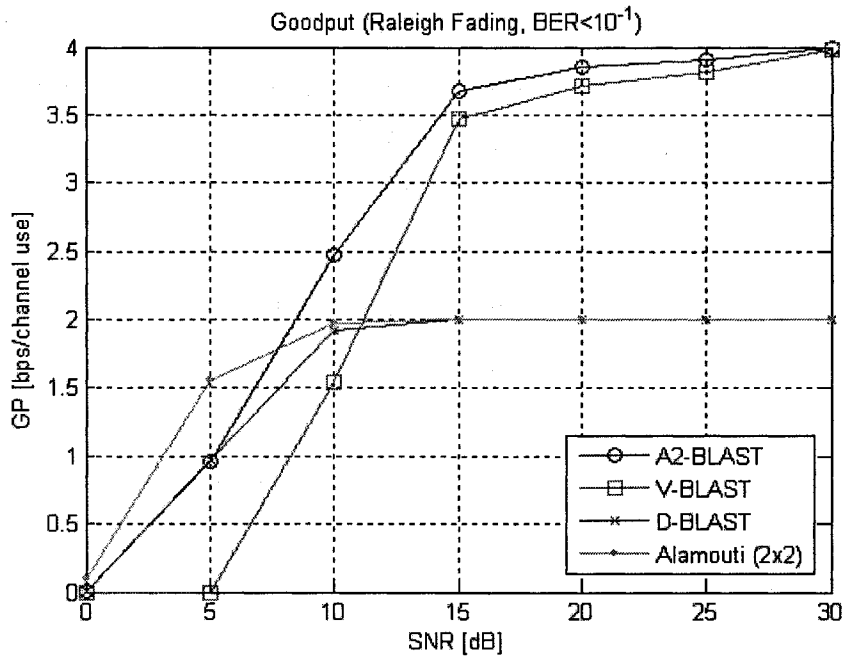


Figure 5-7 A2-BLAST Goodput (Raleigh Fading, BER < 10^{-1})

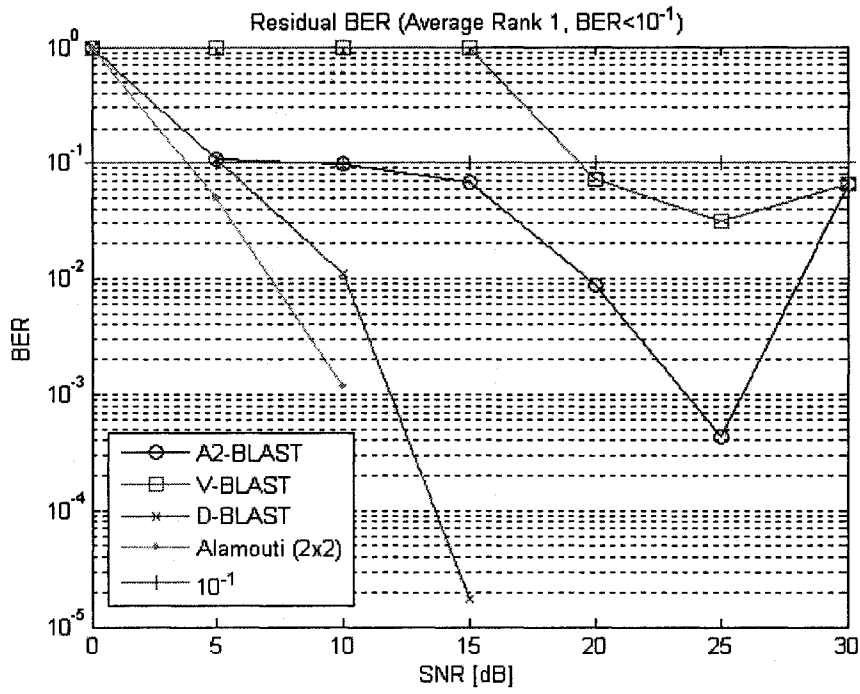


Figure 5-8 A2-BLAST Residual BER (Average Rank 1, BER < 1e-1)

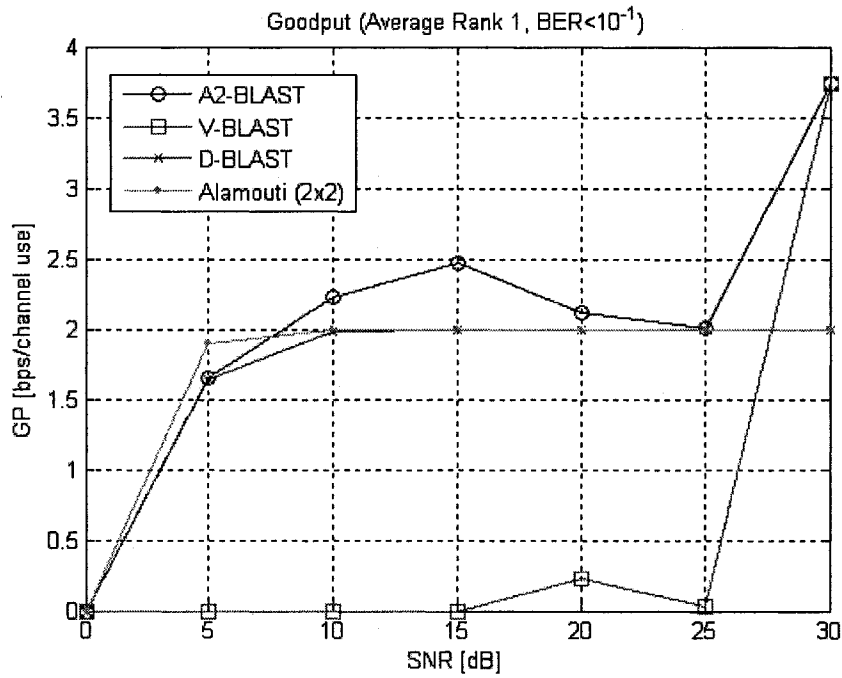


Figure 5-9 A2-BLAST Goodput (Average Rank 1, BER < 1e-1)

5.1.3.1.2 Residual BER Threshold of 10^{-2}

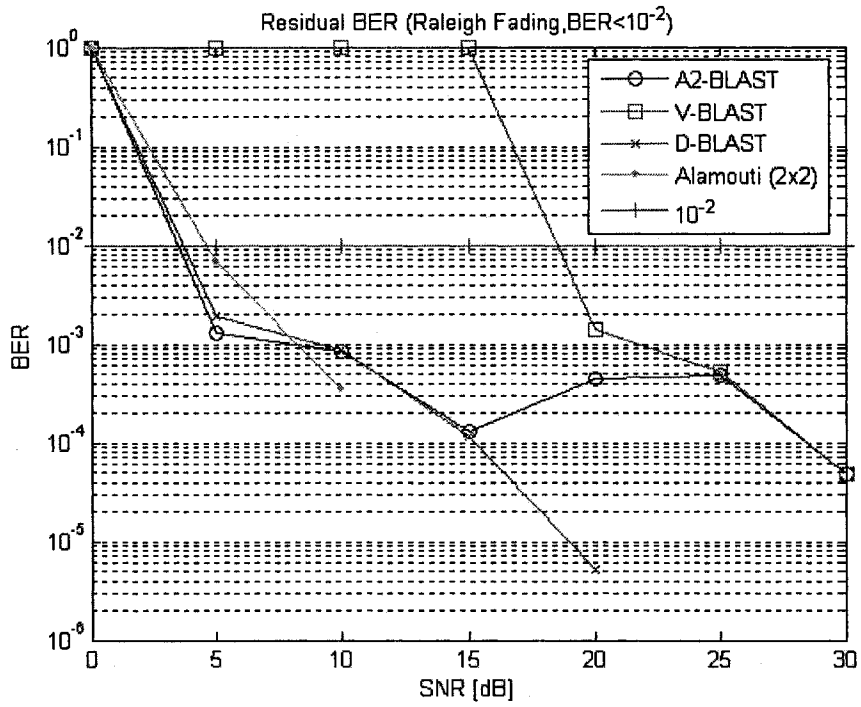


Figure 5-10 A2-BLAST Residual BER (Raleigh Fading, BER < $1e-2$)

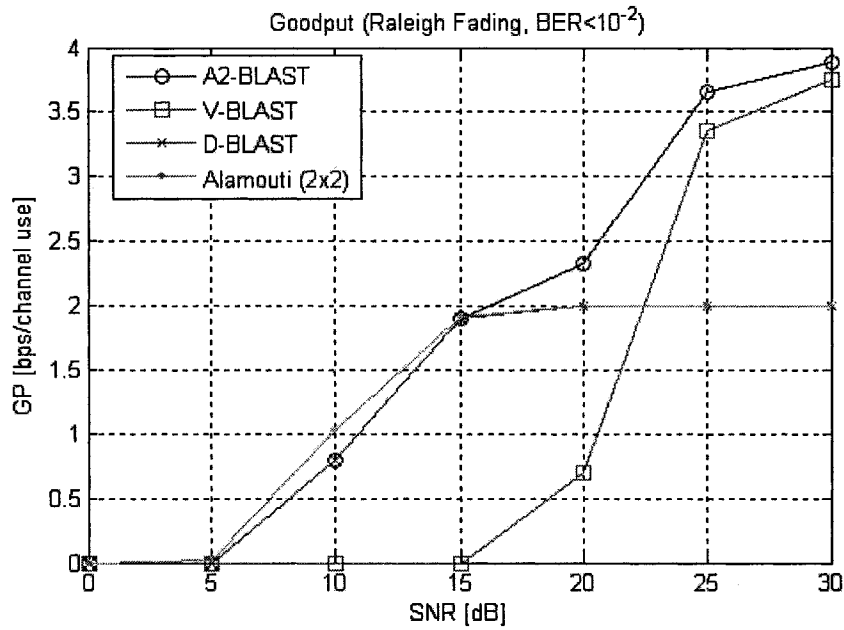


Figure 5-11 A2-BLAST Goodput (Raleigh Fading, BER < $1e-2$)

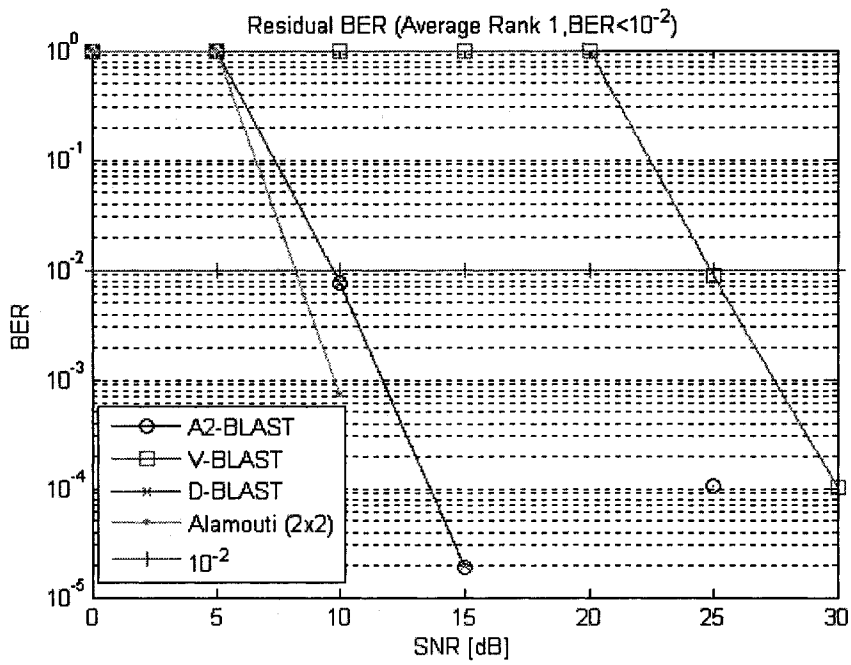


Figure 5-12 A2-BLAST Residual BER (Average Rank 1, BER < 1e-2)

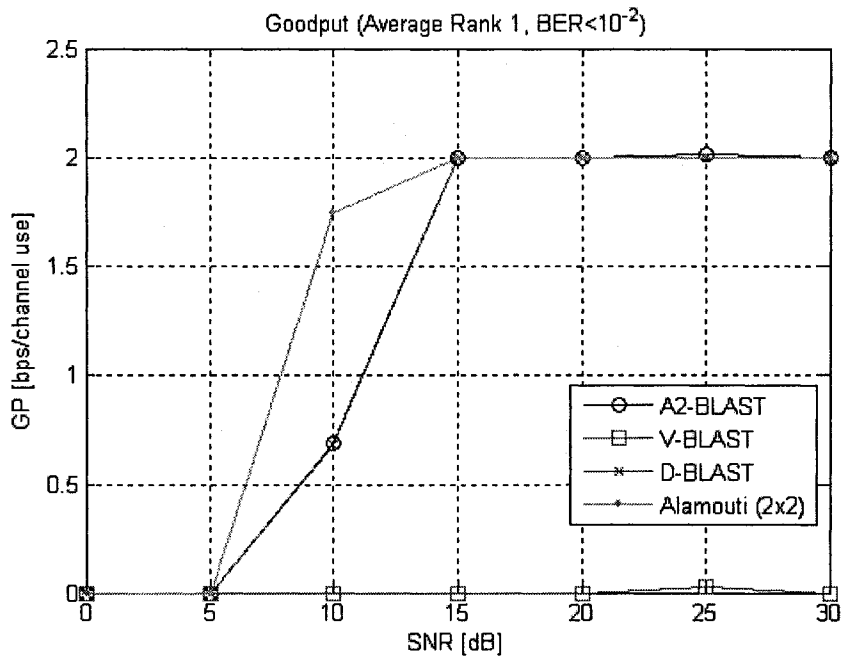


Figure 5-13 A2-BLAST Goodput (Average Rank 1, BER < 1e-2)

5.1.3.1.3 Residual BER Threshold of 10^{-3}

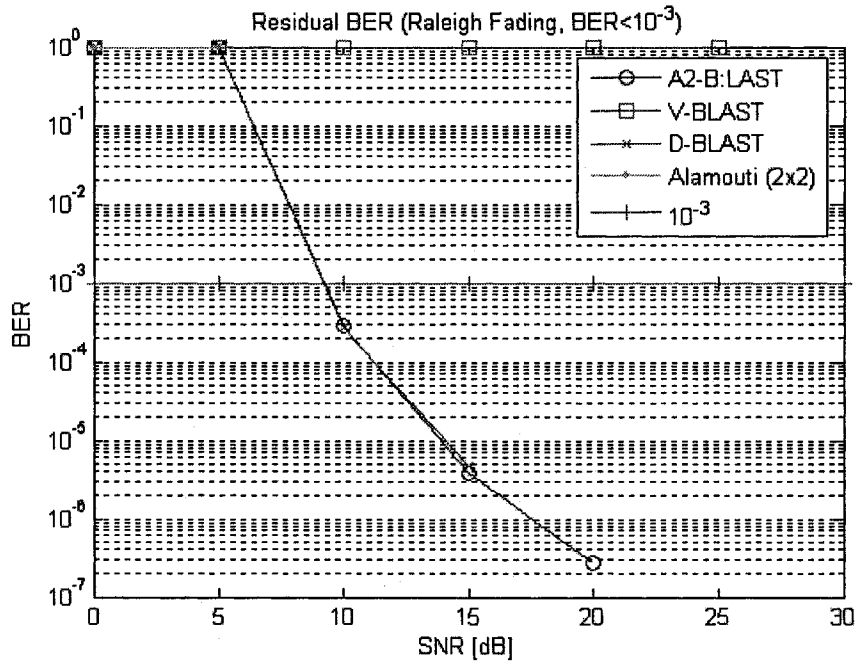


Figure 5-14 A2-BLAST Residual BER (Raleigh Fading, BER 10^{-3})

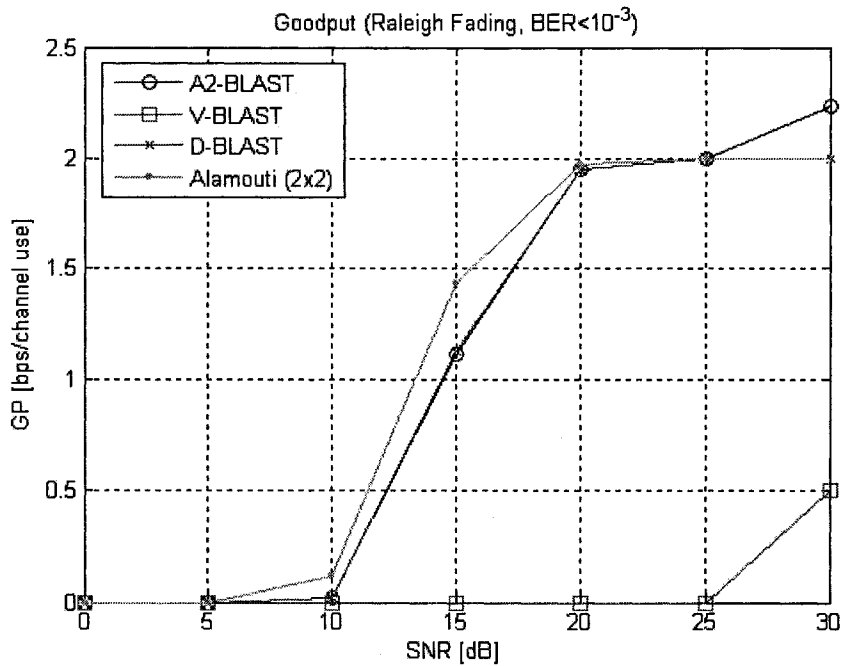


Figure 5-15 A2-BLAST Goodput (Raleigh Fading, BER 10^{-3})

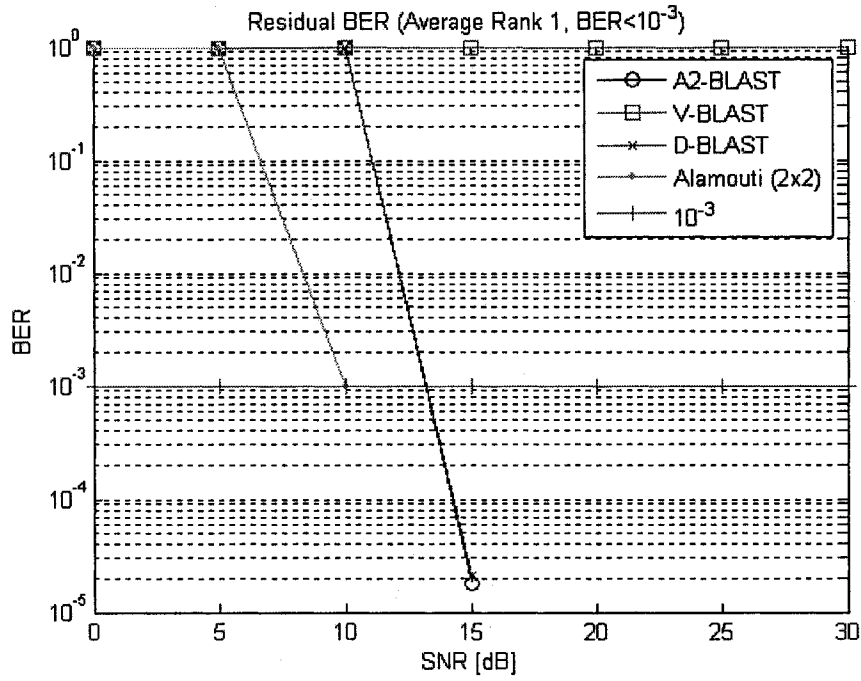


Figure 5-16 A2-BLAST Residual BER (Average Rank 1, BER < 1e-3)

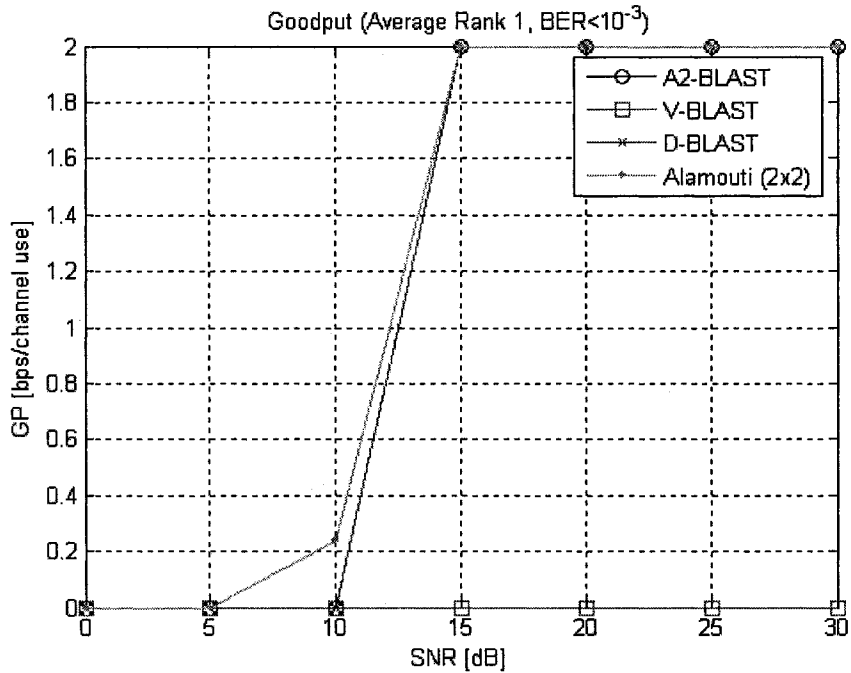


Figure 5-17 A2-BLAST Goodput (Average Rank 1, BER < 1e-3)

5.1.3.2 Summary

The A2-BLAST approach to adaptive space-time processing provides no intermediate modes in addition to A2-BLAST1 (i.e. V-BLAST) and A2-BLAST2 (i.e. D-BLAST). As such, A2-BLAST represents a

minimum limit case with respect to adaptation, providing simply a *switching* mechanism, based on MIMO channel conditions, between the spatial multiplexing and diversity encoded LST benchmarks.

In general, at high levels, A2-BLAST provides improved link goodput relative to the non-adaptive benchmarks. This is a result of high CSI quality and ability of A2-BLAST to exploit spatial multiplexing when channel conditions allow. At low SNR levels, where errors in CSI and rank estimation are greatest, Alamouti OSTBC provides superior goodput. This is due to the fact that Alamouti OSTBC, based on orthogonal designs, is a rate one code equivalent to D-BLAST, but requires no CSI precoding at the transmitter and is less susceptible to symbol estimation error propagation arising from the OSUC based symbol detection employed through A-BLAST.

At the allowable BER threshold level of 10^{-1} , correctable with a cyclic Forward Error Correction (FEC) code such as the BCH(127, 36) [36][37], V-BLAST residual BER exceeds the outage threshold at approximately 5dB SNR in Raleigh fading but this outage SNR increases to approximately 20dB in the fully rank deficient propagation environment. In contrast, through adaptive space-time processing using A2-BLAST, the channel is useable down to an average receive SNR of 5dB, even in the most highly rank deficient propagation environment. The Alamouti OSTBC is capable of operating down to approximately 4dB average SNR.

When the allowable BER threshold level is reduced to 10^{-3} , V-BLAST residual BER levels exceed the outage BER threshold at approximately 25dB SNR in Raleigh fading. As the MIMO channel becomes rank deficient due to Ricean fading, V-BLAST is unable to achieve the necessary BER performance and is continuously in an outage condition. In contrast, A2-BLAST, switching to A2-BLAST2 mode (i.e. D-BLAST), is able to operate with positive goodput levels and residual BER below the outage BER threshold of 10^{-3} down to an average receive SNR of 10dB, even in the fully rank deficient propagation environment. The Alamouti OSTBC is capable of operating down to approximately 5-10dB average SNR.

5.1.4 A4-BLAST Implementation ($M = N = 4$)

The following sub-sections detail the research completed using the SMWE for an A4-BLAST implementation with four antennas at the base station and subscriber terminals (i.e. $M = N = 4$). Documented are the comparative performance results of residual BER and link goodput.

As illustrated in Table 3-2, four modes are supported A4-BLAST[1..4]. The code rate [bps/Hz] using QPSK modulation and diversity order of each mode is summarized in Figure 5-18:

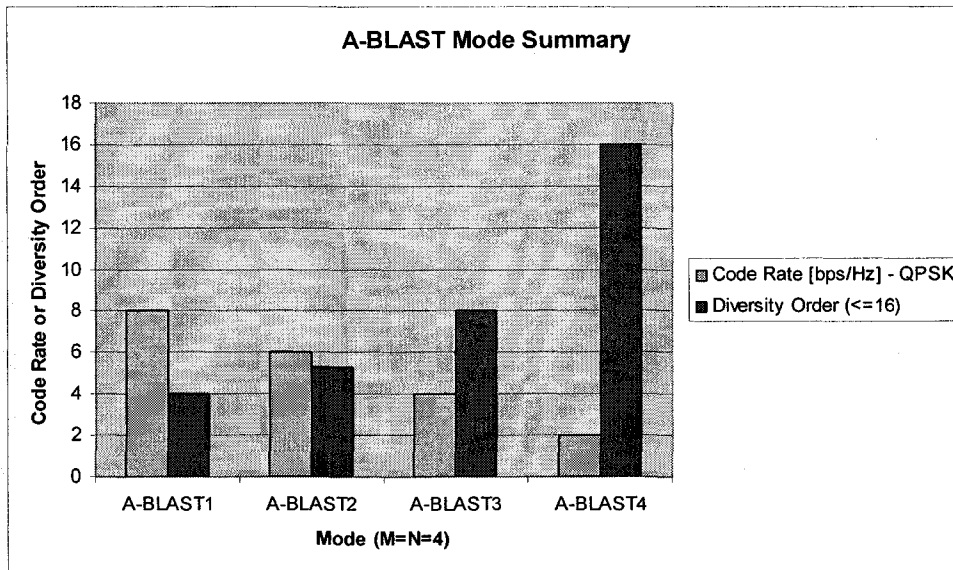


Figure 5-18 A4-BLAST Mode Summary ($M=N=4$)

The reader is referred to Appendix B – Supplementary A-BLAST Mode Summary Data for a description of the individual A4-BLAST space-time mappings functions. It should be noted that A4-BLAST1 is equivalent to V-BLAST, providing maximum code rate and minimum diversity order, while A4-BLAST4 is D-BLAST, providing minimum code rate but maximum diversity order. The intermediary modes A4-BLAST2 and A4-BLAST3 provide a useful bridging between the capacity and reliability performance benchmarks provided by V-BLAST and D-BLAST respectively.

Reference BER curves for each A4-BLAST mode was obtained using the SMWE. These curves are shown in Figure 5-19 to Figure 5-22. The average SNR (ρ) was varied from 0dB to 30dB in increments of 5dB. Additionally, the average rank (\bar{r}) of MIMO channel realizations was controlled through the Ricean Power Factor (K), see §3.2.3.4. The average MIMO channel rank was varied from full rank Rayleigh fading (i.e. $\bar{r} \approx 4$) down to fully rank deficient (i.e. $\bar{r} \approx 1$).

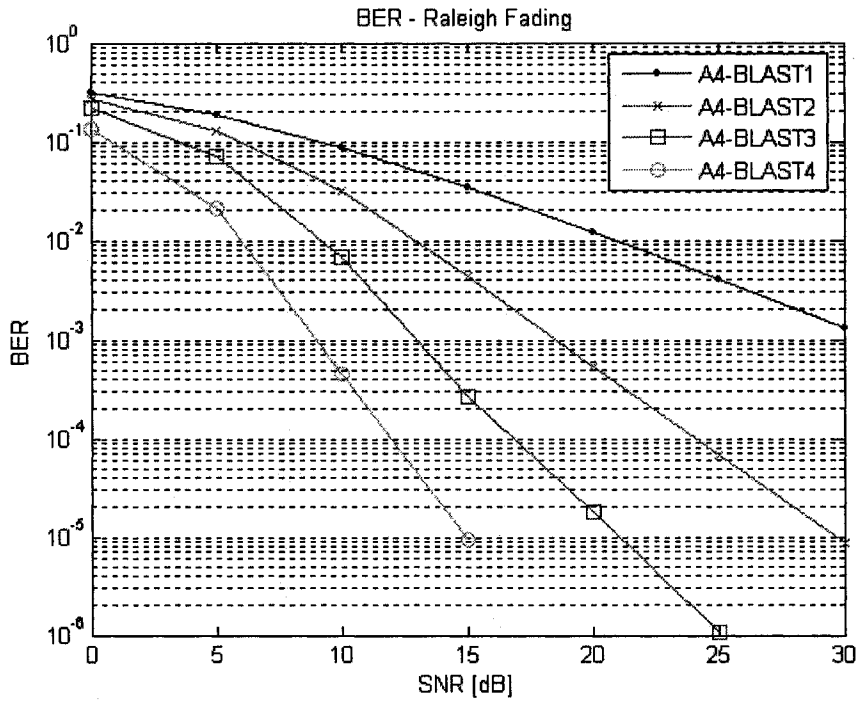


Figure 5-19 A4-BLAST Reference BER Curves (Raleigh Fading)

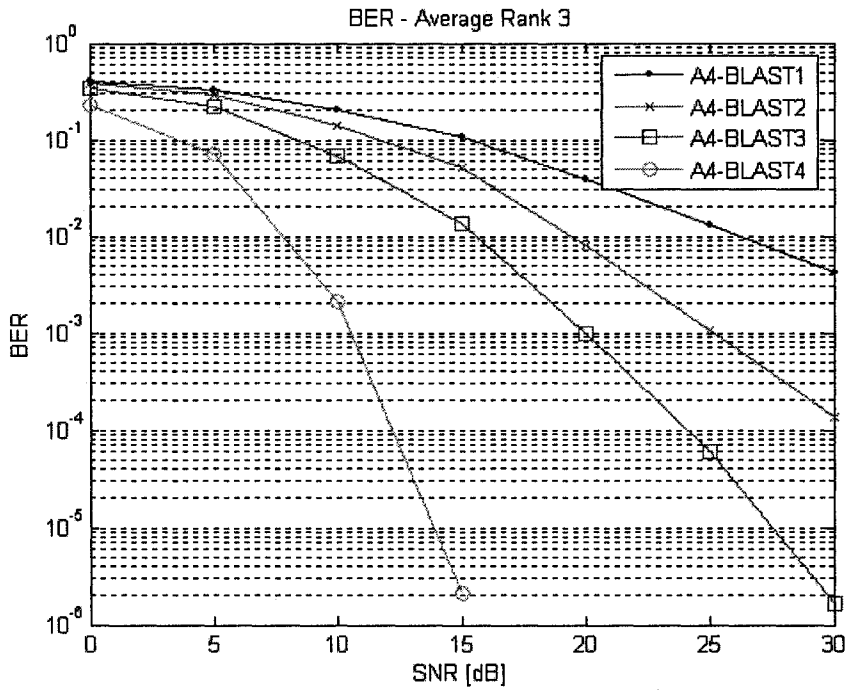


Figure 5-20 A4-BLAST Reference BER Curves (Average Rank 3)

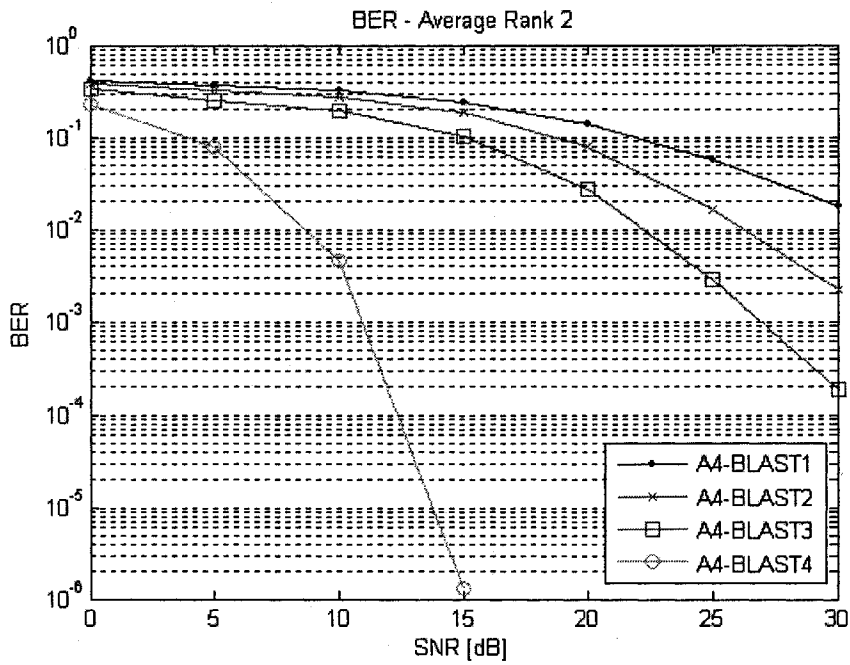


Figure 5-21 A4-BLAST Reference BER Curves (Average Rank 2)

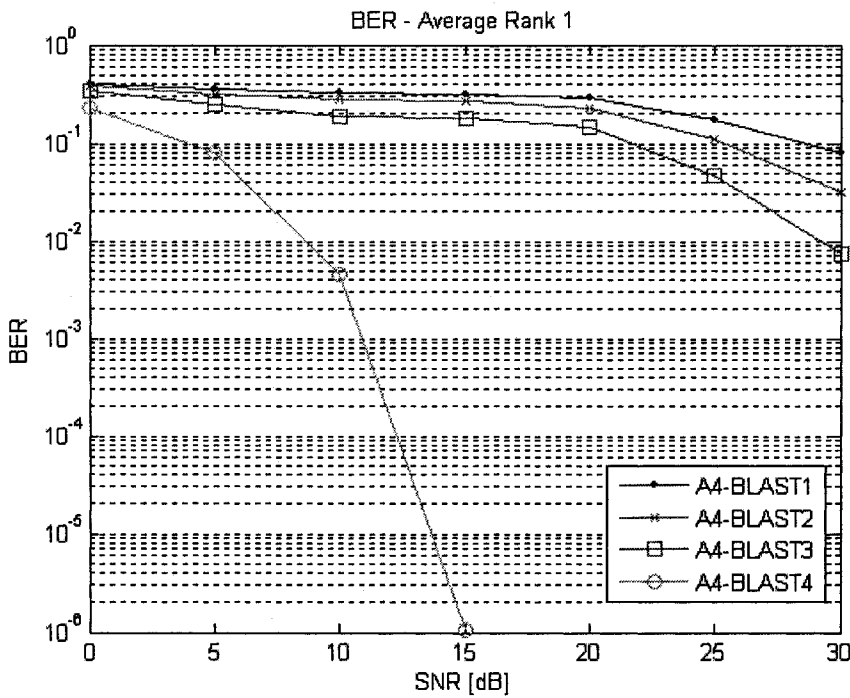


Figure 5-22 A4-BLAST Reference BER Curves (Average Rank 1)

As evident in Figure 5-19 to Figure 5-22, as fading becomes spatially correlated, error performance of A4-BLAST modes providing higher levels of spatial multiplexing degrade more quickly than modes providing less spatial multiplexing in favor of higher diversity order. These curves provide a reference

by which the A4-BLAST mode may be adapted given estimates of receive signal quality, MIMO channel rank, and system imposed BER tolerance.

5.1.4.1 Performance Results

The performance of A4-BLAST is compared against the non-adaptive LST processing benchmarks V-BLAST and D-BLAST in Figure 5-23 to Figure 5-46. Performance is measured in terms of resulting link goodput and residual BER for target BER thresholds of 10^{-1} , 10^{-2} , and 10^{-3} respectively.

In the full rank and high SNR environments, A4-BLAST adapts to V-BLAST providing maximum code rate given the MIMO channel's ability to accommodate spatial multiplexing and high receive signal quality. In the highly rank deficient or low SNR environments, A4-BLAST adapts to D-BLAST providing maximum diversity order in the absence of available spatial eigenmodes or existence of poor receive signal quality respectively. At moderate levels of receive signal quality and MIMO channel spatial rank, A4-BLAST adapts to intermediary modes A4-BLAST2 and A4-BLAST3 providing a superior balance between the relative weighting of diversity order and spatial multiplexing gain within the space-time codeword.

5.1.4.1.1 Residual BER Threshold of 10^{-1}

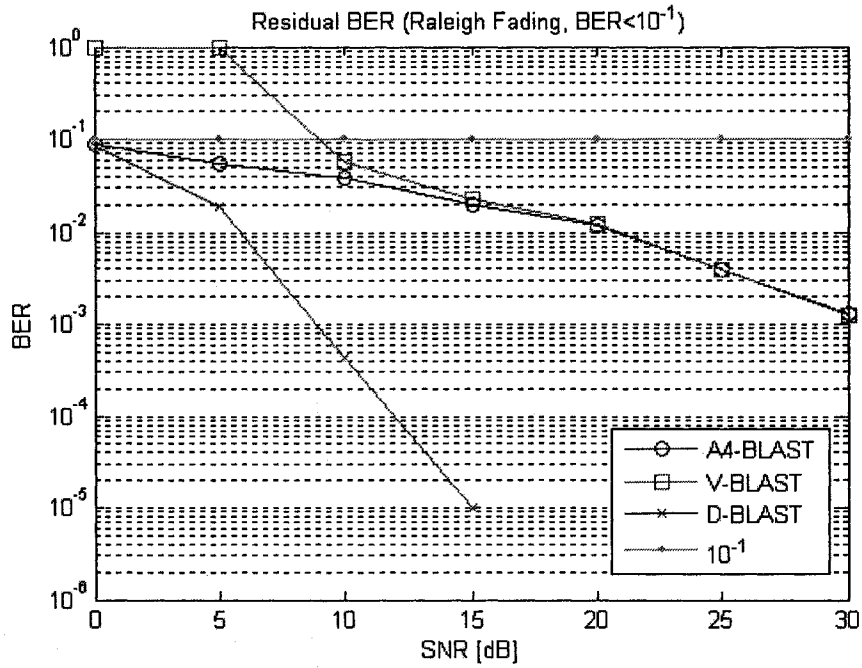


Figure 5-23 A4-BLAST Residual BER (Raleigh Fading, BER < 10^{-1})

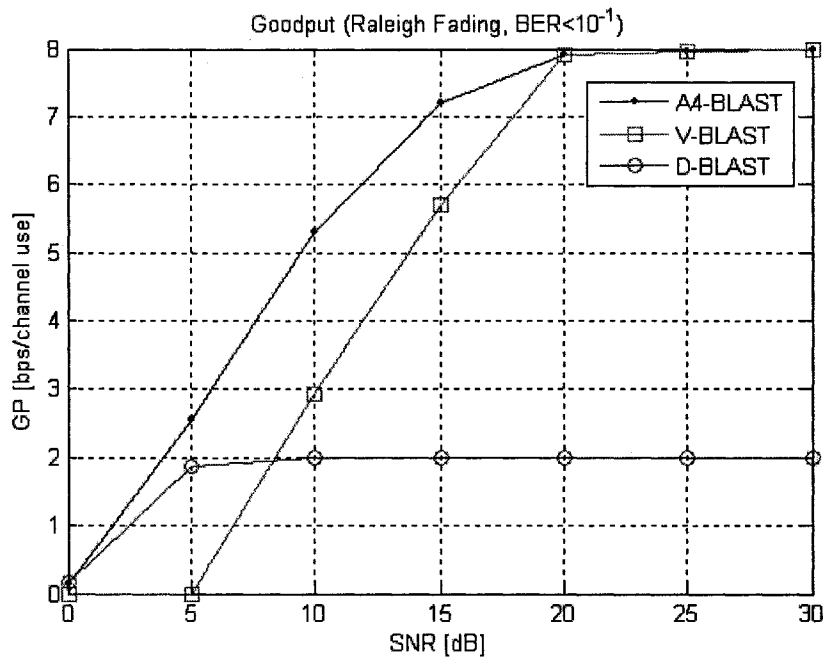


Figure 5-24 A4-BLAST Goodput (Raleigh Fading, BER < 10^{-1})

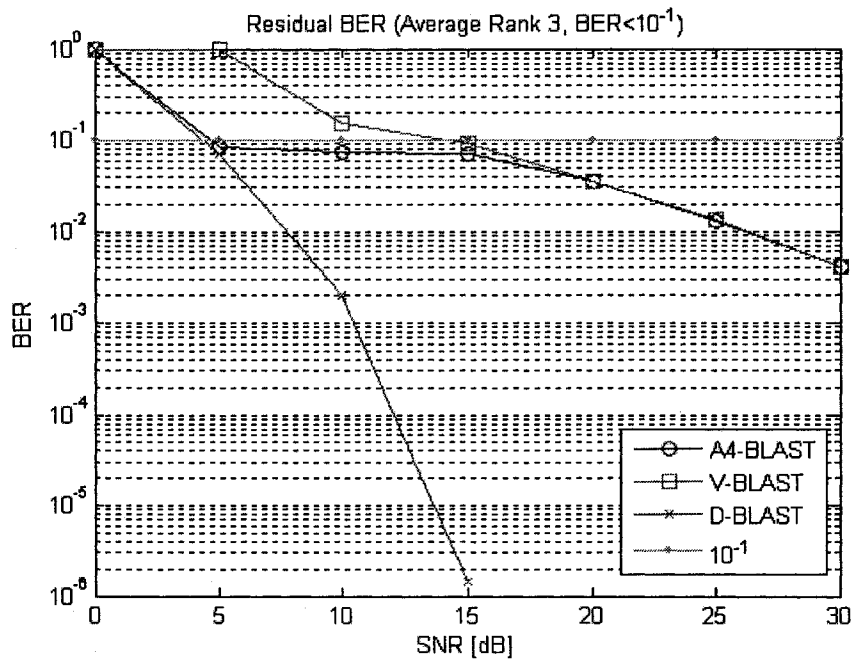


Figure 5-25 A4-BLAST Residual BER (Average Rank 3, BER < 1e-1)

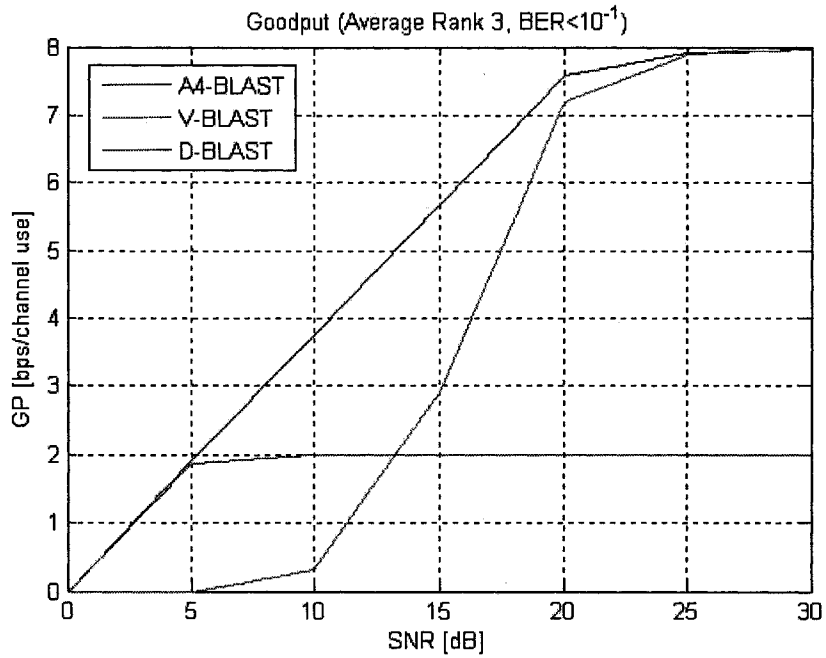


Figure 5-26 A4-BLAST Goodput (Average Rank 3, BER < 1e-1)

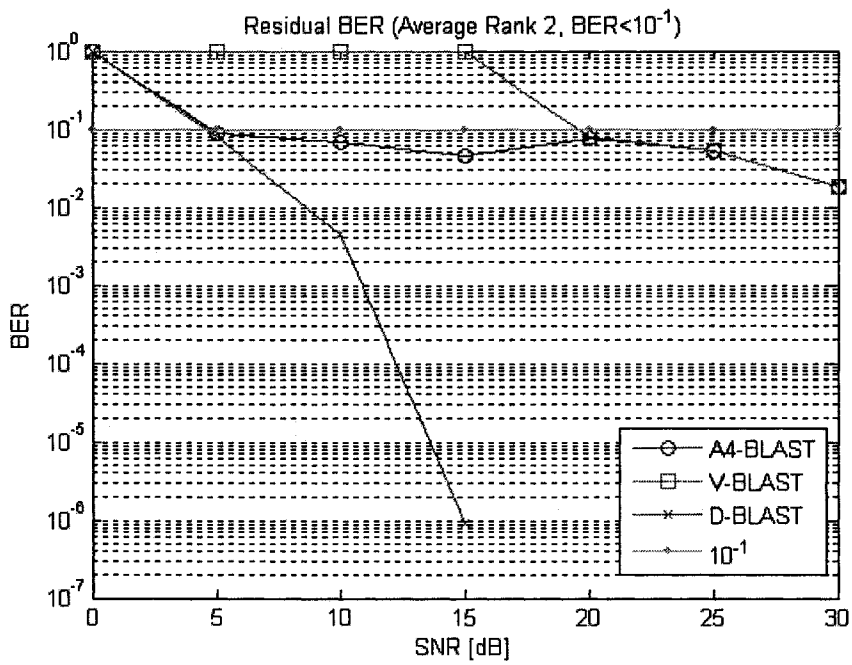


Figure 5-27 A4-BLAST Residual BER (Average Rank 2 BER < 1e-1)

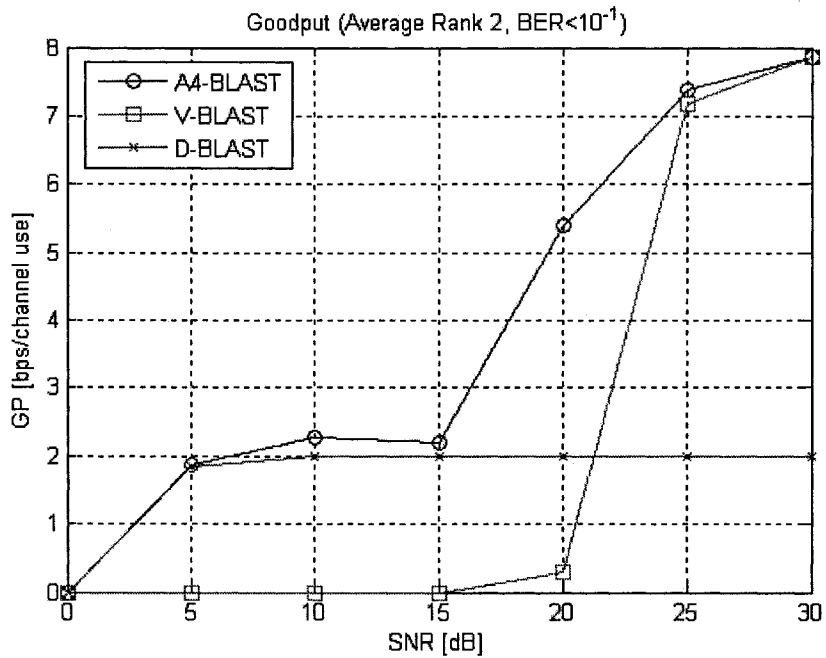


Figure 5-28 A4-BLAST Goodput (Average Rank 2 BER < 1e-1)

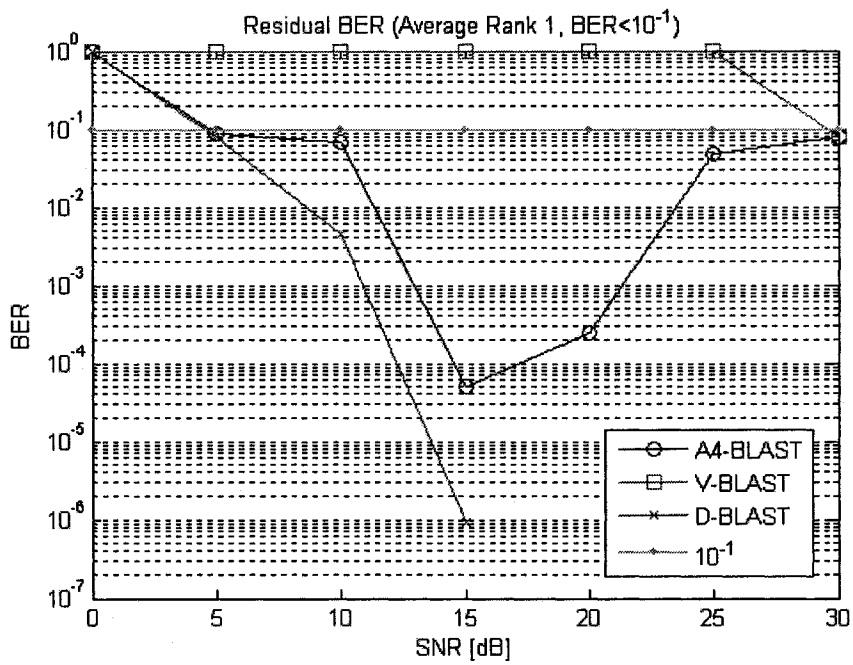


Figure 5-29 A4-BLAST Residual BER (Average Rank 1 BER < 1e-1)

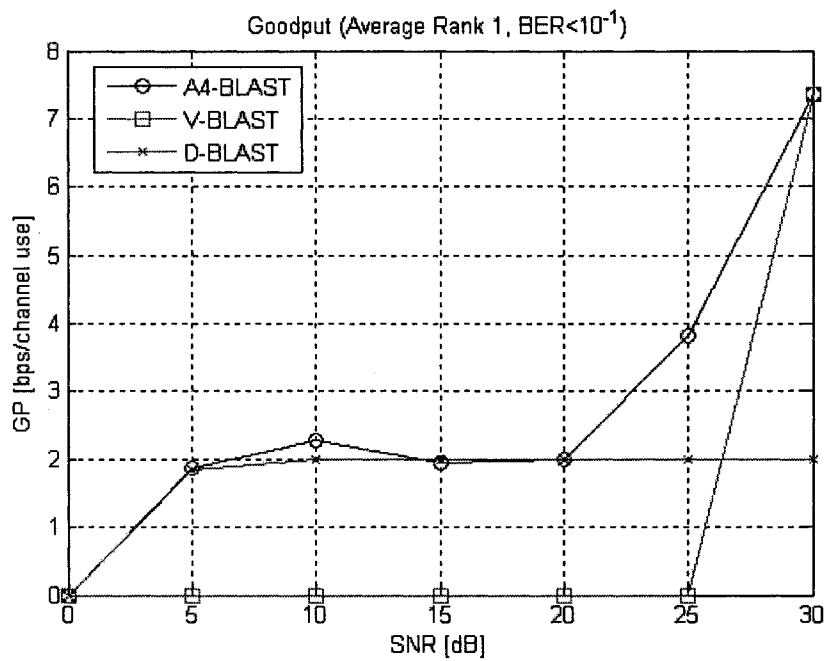


Figure 5-30 A4-BLAST Goodput (Average Rank 1 BER < 1e-1)

5.1.4.1.2 Residual BER Threshold of 10^{-2}

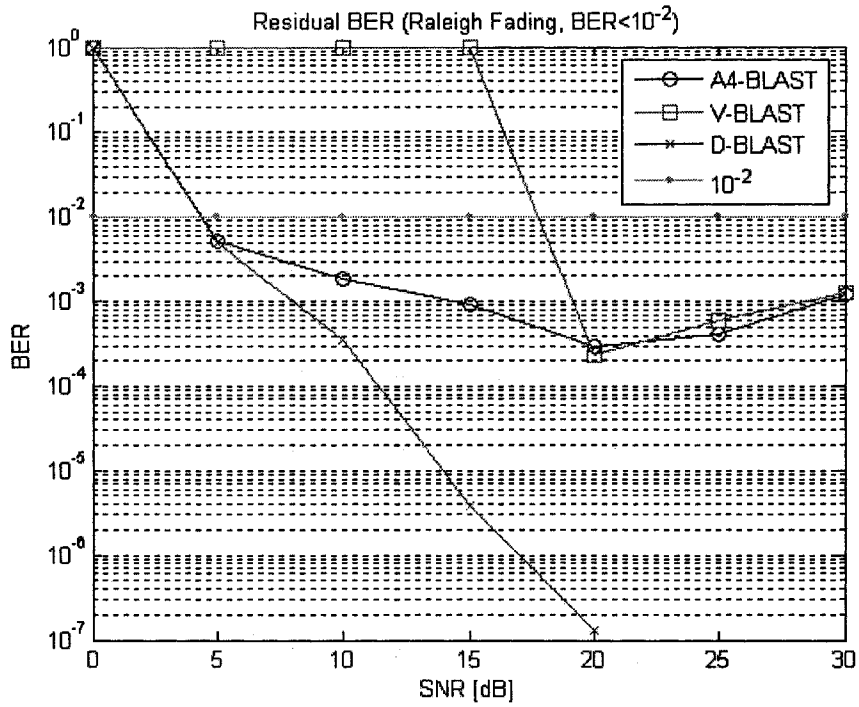


Figure 5-31 A4-BLAST Residual BER (Raleigh Fading, BER < 10^{-2})

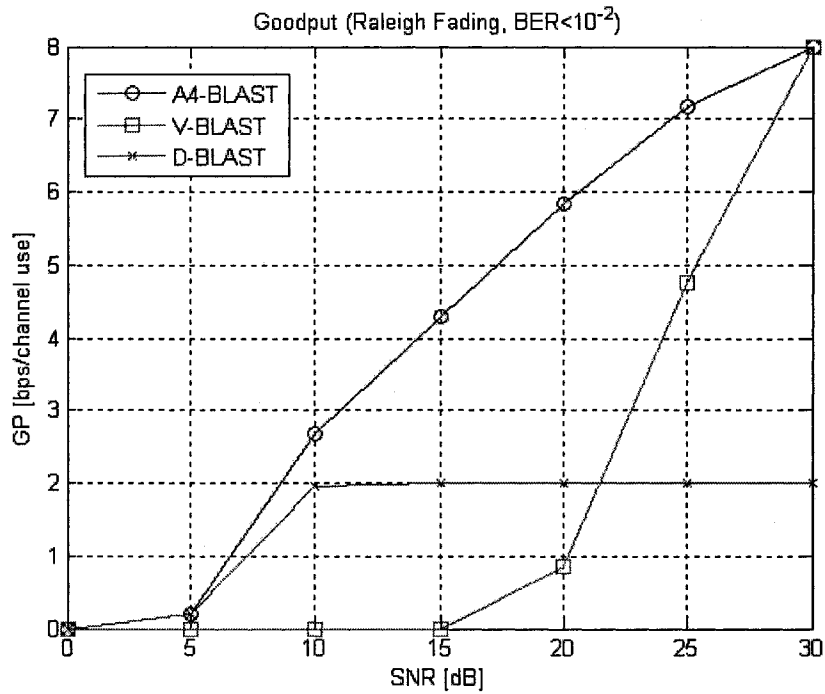


Figure 5-32 A4-BLAST Goodput (Raleigh Fading, BER < 10^{-2})

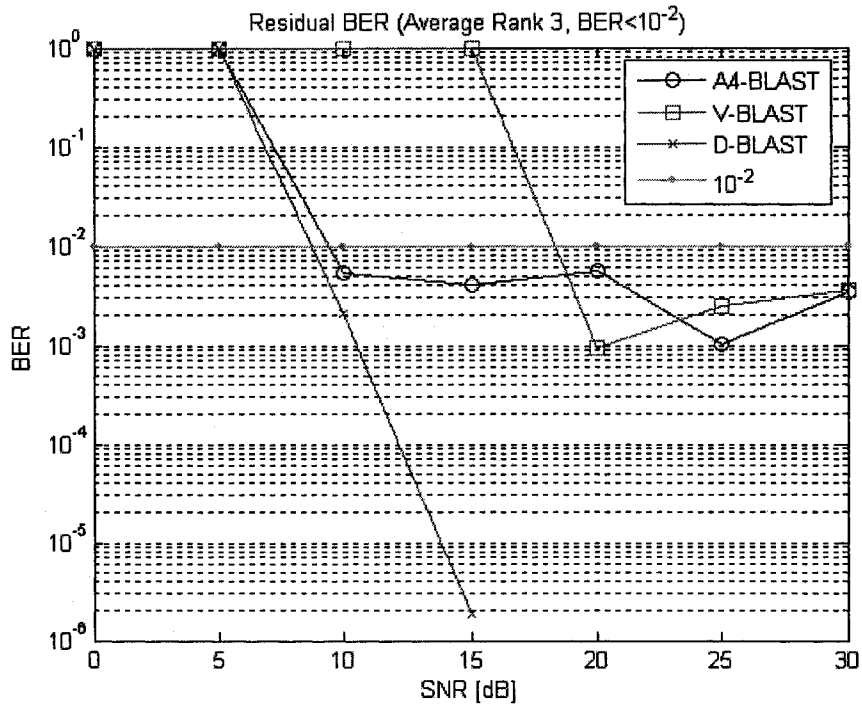


Figure 5-33 A4-BLAST Residual BER (Average Rank 3, BER < 1e-2)

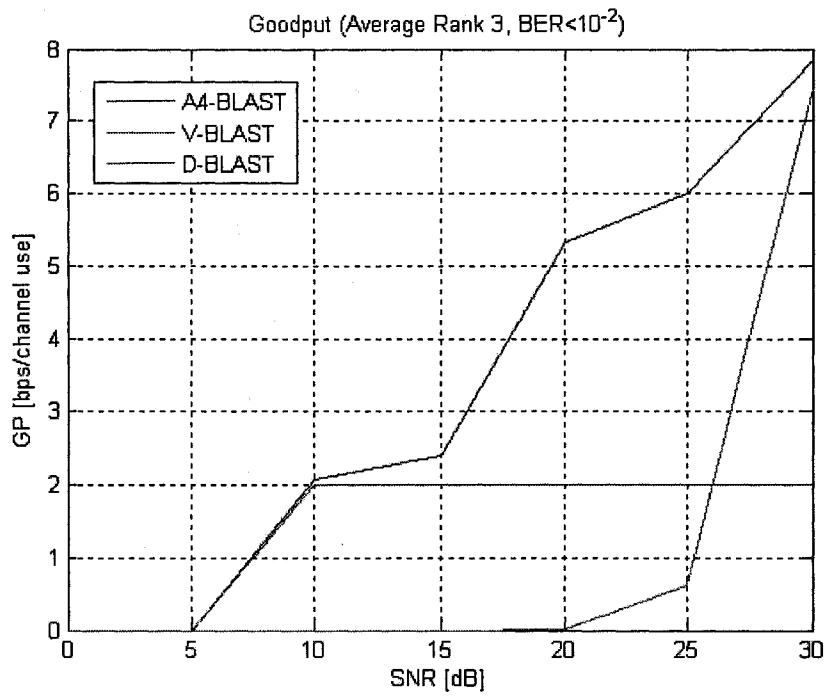


Figure 5-34 A4-BLAST Goodput (Average Rank 3, BER < 1e-2)

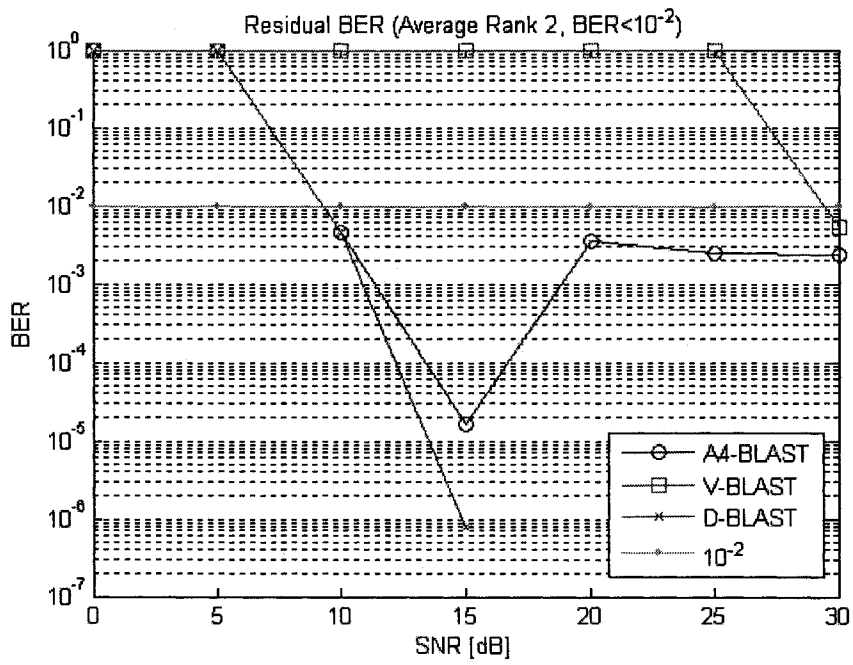


Figure 5-35 A4-BLAST Residual BER (Average Rank 2 BER < 1e-2)

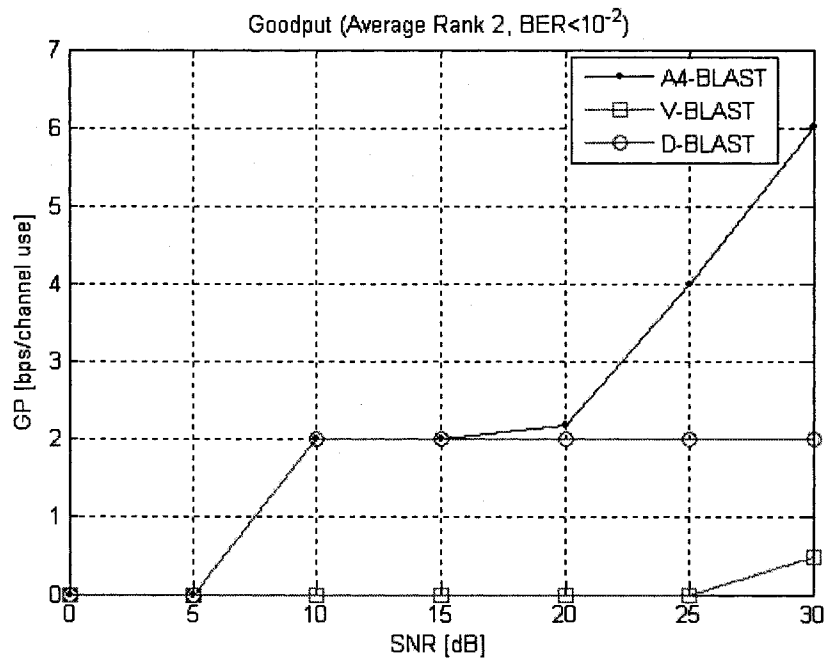


Figure 5-36 A4-BLAST Goodput (Average Rank 2, BER < 1e-2)

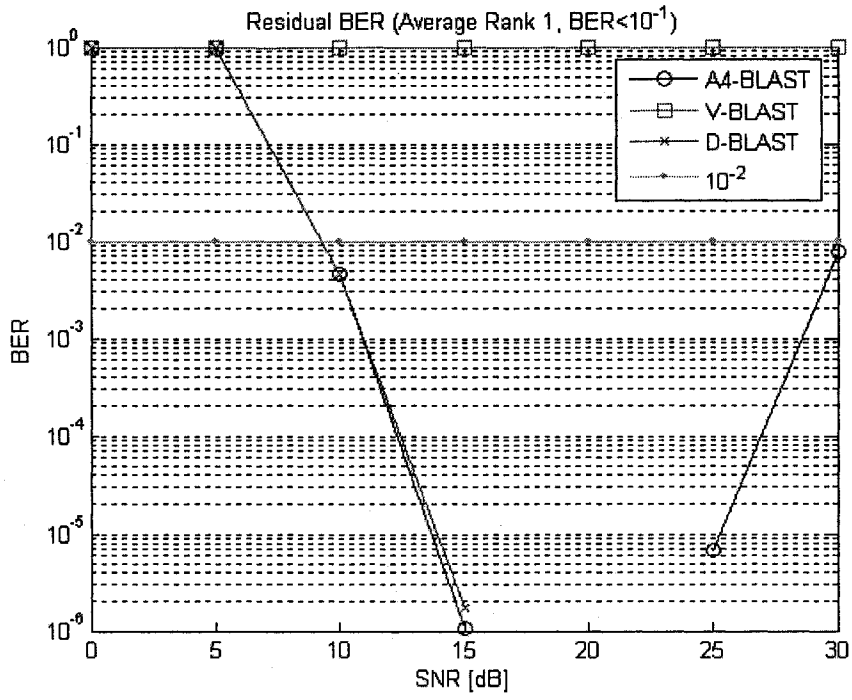


Figure 5-37 A4-BLAST Residual BER (Average Rank 1, BER < 1e-2)

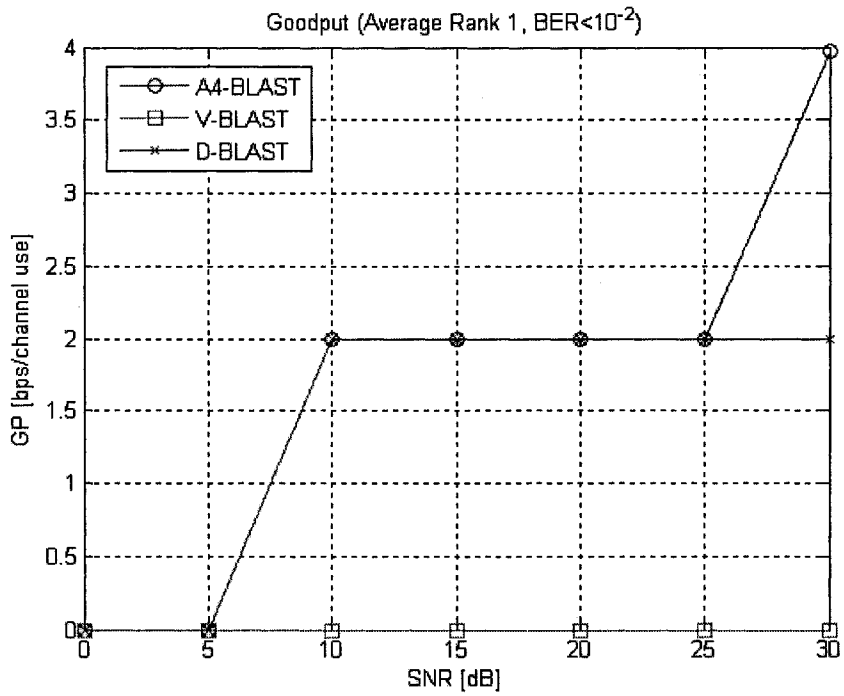


Figure 5-38 A4-BLAST Goodput (Average Rank 1, BER < 1e-2)

5.1.4.1.3 Residual BER Threshold of 10^{-3}

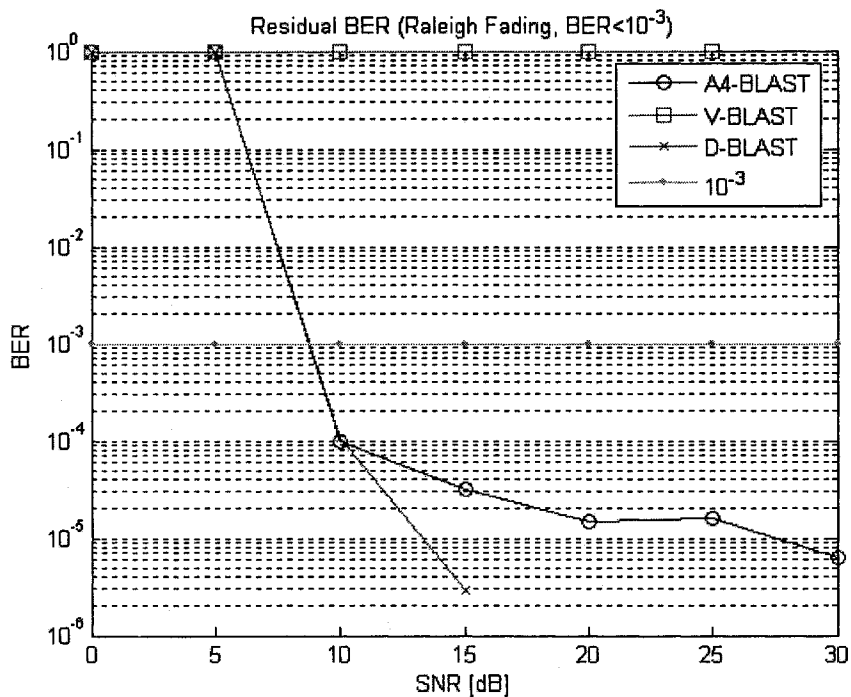


Figure 5-39 A4-BLAST Residual BER (Rayleigh Fading, BER <math><1e-3</math>)

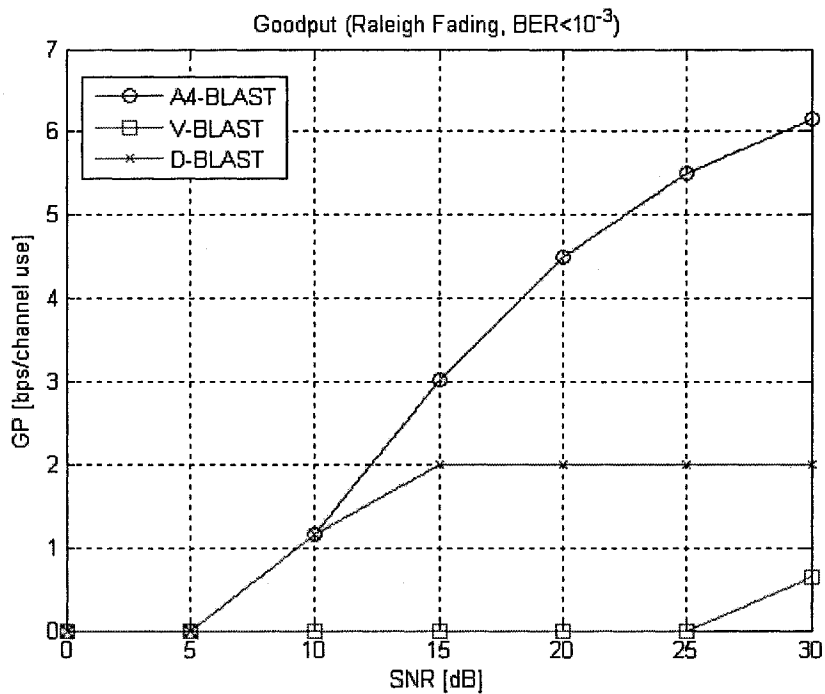


Figure 5-40 A4-BLAST Goodput (Rayleigh Fading, BER <math><1e-3</math>)

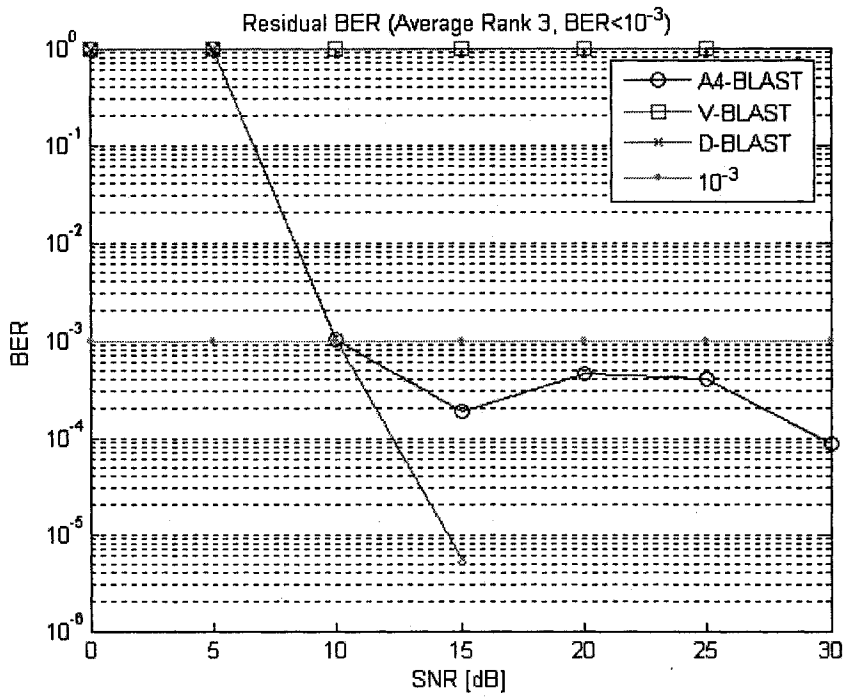


Figure 5-41 A4-BLAST Residual BER (Average Rank 3, BER < 1e-3)

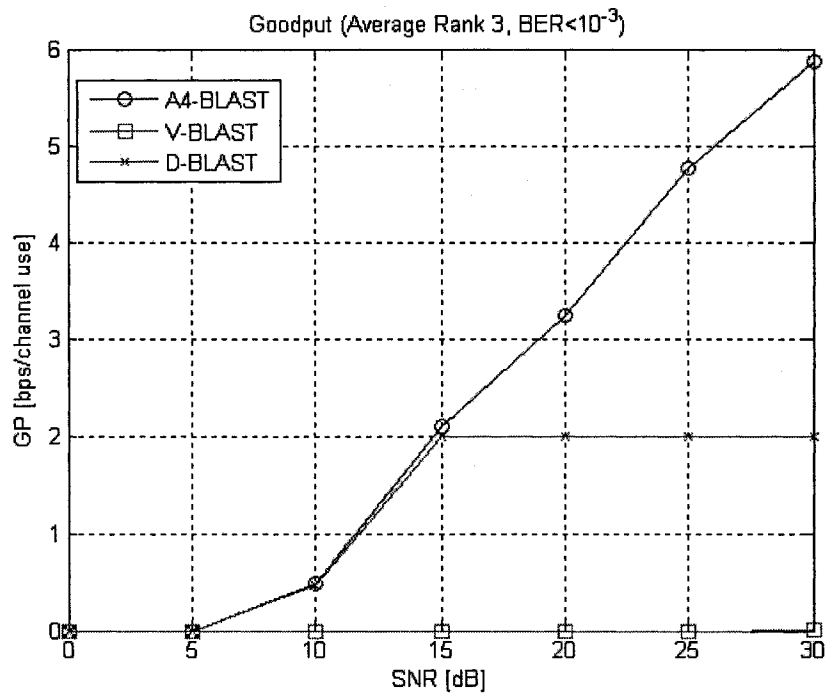


Figure 5-42 A4-BLAST Goodput (Average Rank 3, BER < 1e-3)

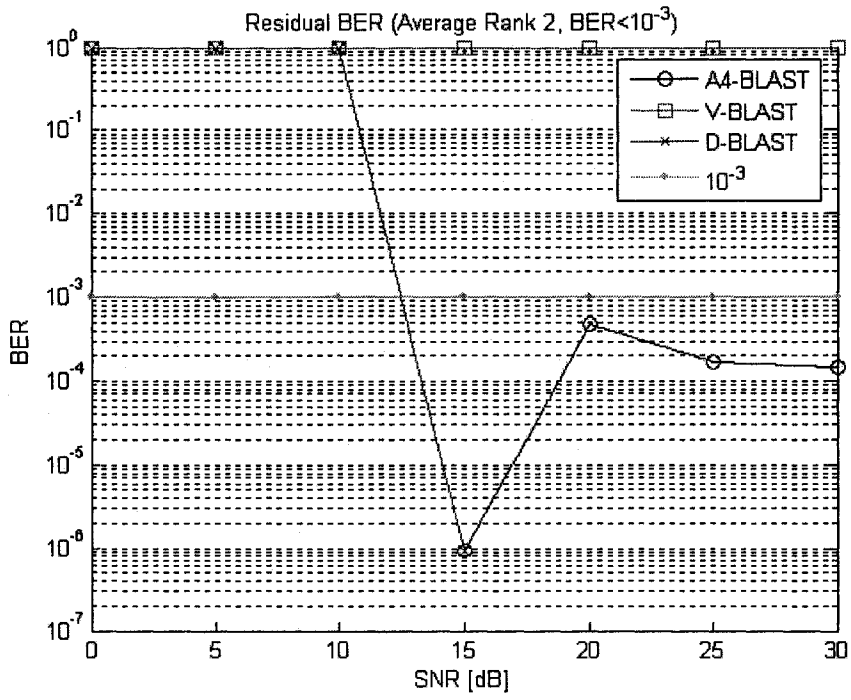


Figure 5-43 A4-BLAST Residual BER (Average Rank 2, BER < 1e-3)

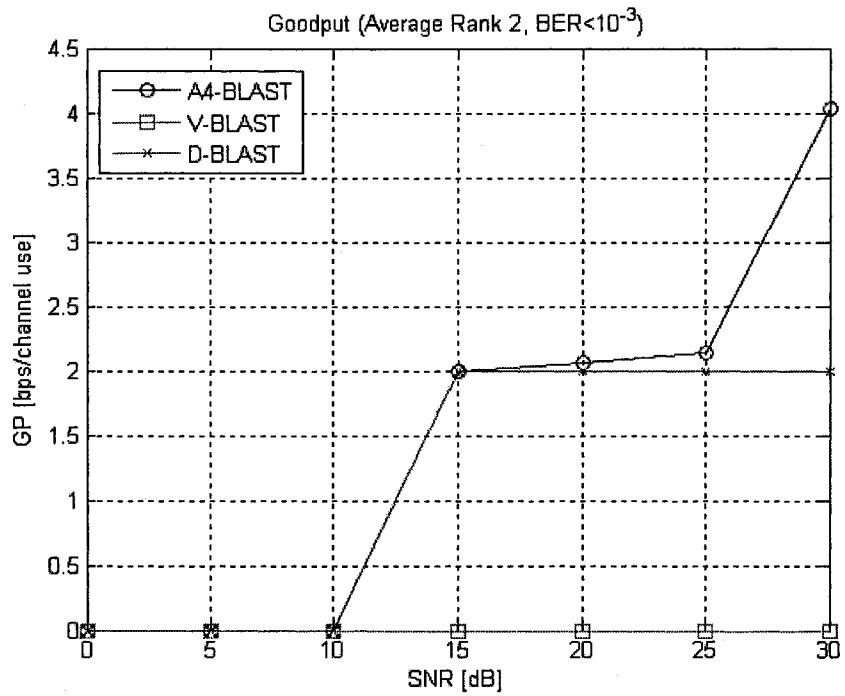


Figure 5-44 A4-BLAST Goodput (Average Rank 2, BER < 1e-3)

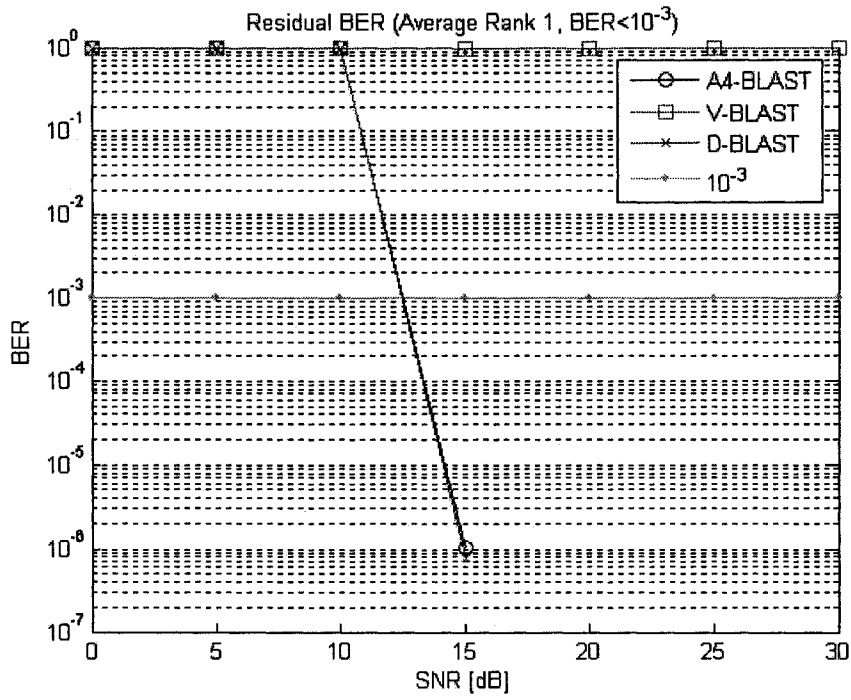


Figure 5-45 A4-BLAST Residual BER (Average Rank 1, BER < 1e-3)

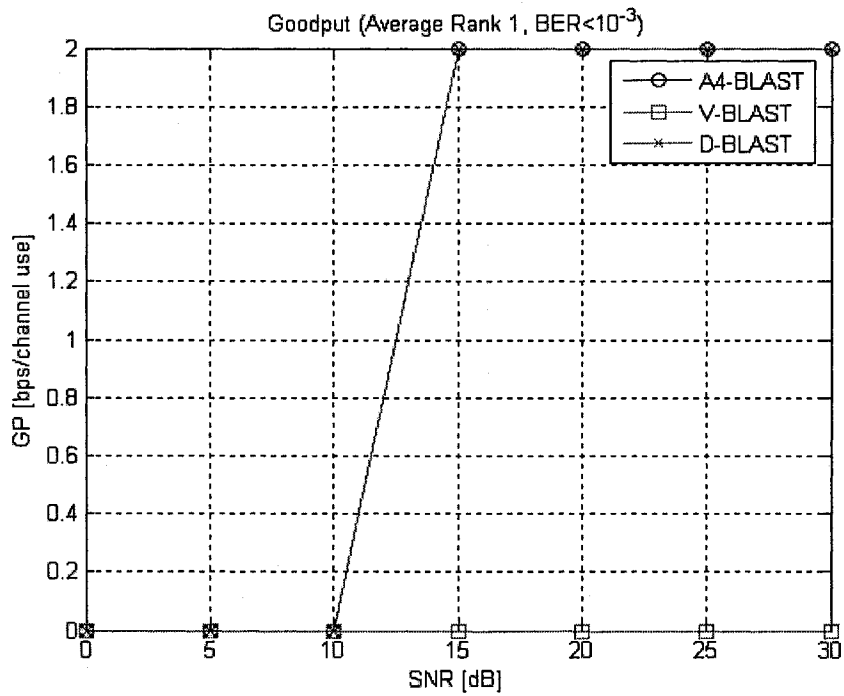


Figure 5-46 A4-BLAST Goodput (Average Rank 1, BER < 1e-3)

5.1.4.2 Summary

The A4-BLAST approach to adaptive space-time processing provides two intermediate modes for adaptation, A4-BLAST2 and A4-BLAST3, providing a superior level of granular control over codeword diversity mapping and spectral efficiency. As evident in the performance results of §5.1.4.1.1-§5.1.4.1.3, A4-BLAST provides improved link goodput relative to the non-adaptive spatial multiplexing and diversity benchmarks V-BLAST and D-BLAST respectively.

At the allowable BER threshold level of 10^{-1} , correctable with a cyclic Forward Error Correction (FEC) code such as the BCH(127, 36) [36][37], V-BLAST residual BER exceeds the outage threshold at approximately 9.2dB SNR in Raleigh fading but this outage SNR increases to 25dB in the fully rank deficient propagation environment. In contrast, through adaptive space-time processing using A4-BLAST, the channel is useable down to an average receive SNR of 5dB, even in the most highly rank deficient propagation environment.

When the allowable BER threshold level is reduced to 10^{-3} , V-BLAST residual BER levels exceed the outage BER threshold at approximately 25dB SNR in Raleigh fading. As the MIMO channel becomes rank deficient due to Ricean fading and unable to support spatial multiplexing, V-BLAST is unable to achieve the necessary BER performance and is continuously in an outage condition. In contrast, A4-BLAST, utilizing the intermediate modes defined in Figure 5-18, is able to operate at positive goodput levels with residual BER below the outage BER threshold of 10^{-3} down to an average receive SNR of 10dB, even in the fully rank deficient propagation environment.

5.1.5 A8-BLAST Implementation (M = N = 8)

The following sub-sections detail the research completed using the SMWE for an A8-BLAST implementation with eight antennas at the base station and subscriber terminals (i.e. M = N = 8). Documented are the comparative performance results of residual BER and link goodput.

As illustrated in Table 3-2, eight modes are supported A8-BLAST[1..8]. The code rate [bps/Hz] using QPSK modulation and diversity order of each mode is summarized in Figure 5-47:

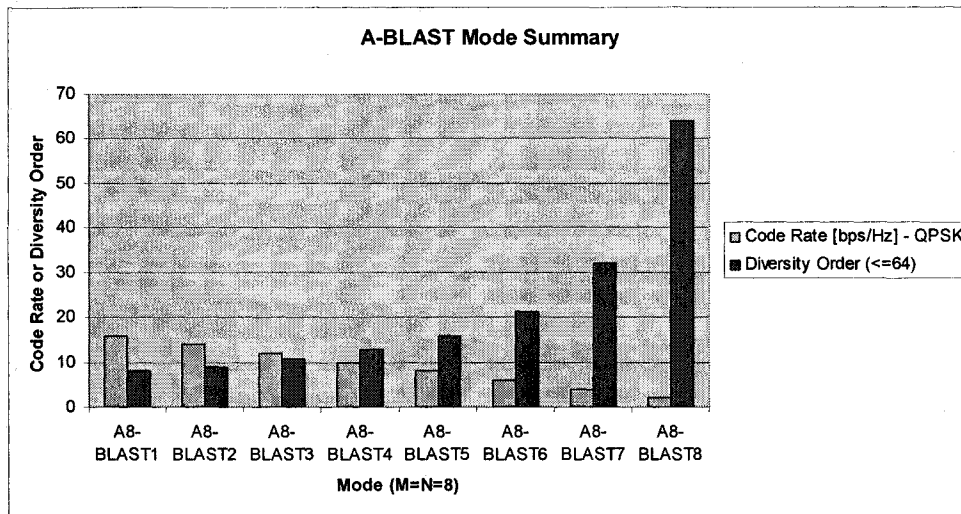


Figure 5-47 A8-BLAST Mode Summary (M=N=8)

The reader is referred to Appendix B – Supplementary A-BLAST Mode Summary Data for a description of the individual A8-BLAST space-time mappings functions. It should be noted that A8-BLAST1 is equivalent to V-BLAST, providing maximum code rate and minimum diversity order, while A8-BLAST8, equivalent to D-BLAST, provides minimum code rate but maximum diversity order. The intermediary modes A8-BLAST2 and A8-BLAST7 provide a highly granular bridging between the capacity and reliability performance benchmarks provided by V-BLAST and D-BLAST respectively.

Reference BER curves for each A8-BLAST mode was obtained using the SMWE. These curves are shown in Figure 5-48 to Figure 5-54. The average SNR (ρ) was varied from 0dB to 30dB in increments of 5dB. Additionally, the average rank (\bar{r}) of MIMO channel realizations was controlled through the Ricean Power Factor (K), see §3.2.3.4. The average MIMO channel rank was varied from full rank Rayleigh fading (i.e. $\bar{r} \approx 8$) down to fully rank deficient (i.e. $\bar{r} \approx 1$).

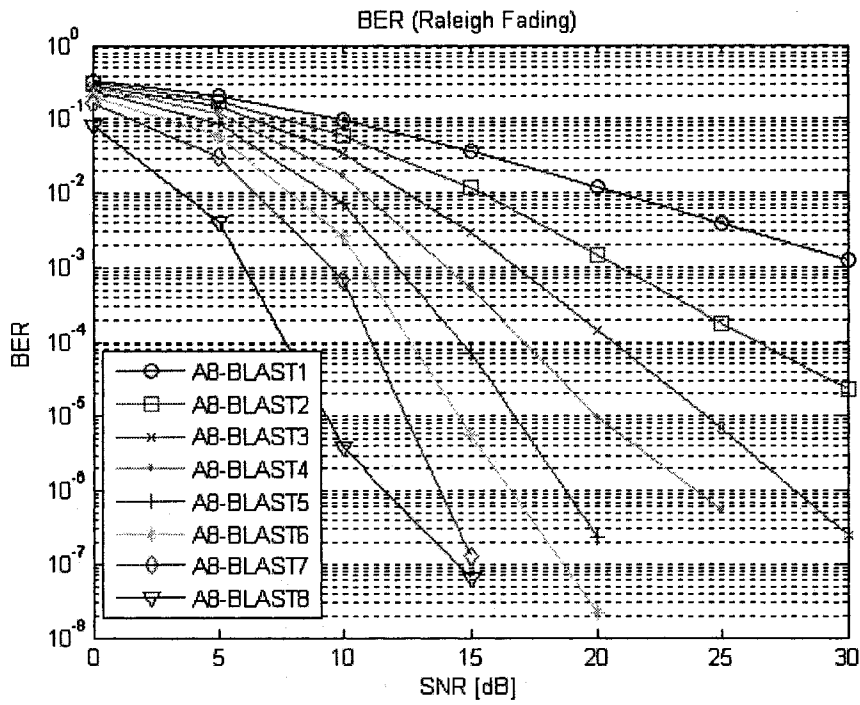


Figure 5-48 A8-BLAST Reference BER Curves (Rayleigh Fading)

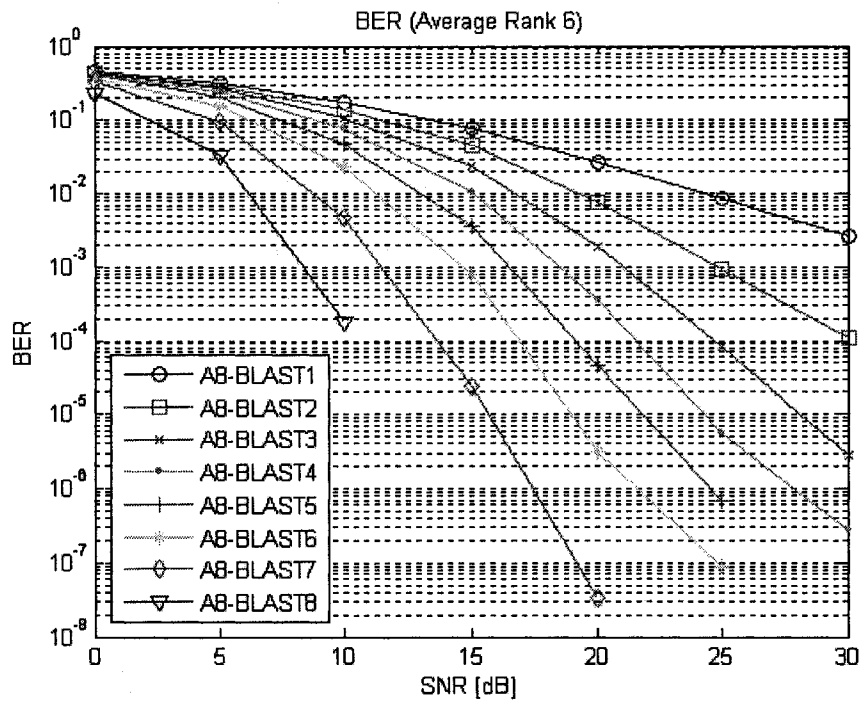


Figure 5-49 A8-BLAST Reference BER Curves (Average Rank 6)

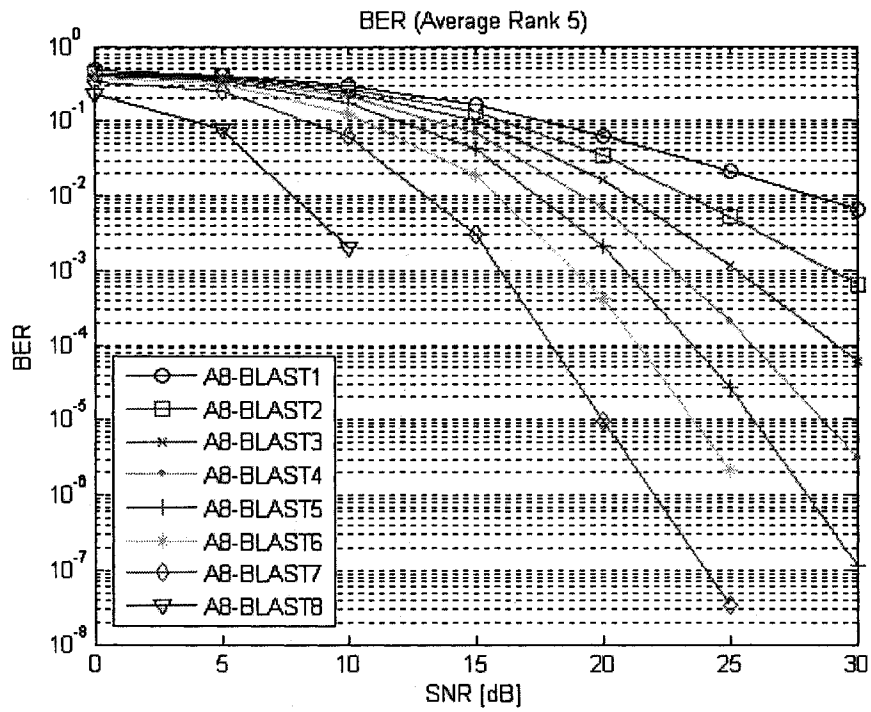


Figure 5-50 A8-BLAST Reference BER Curves (Average Rank 5)

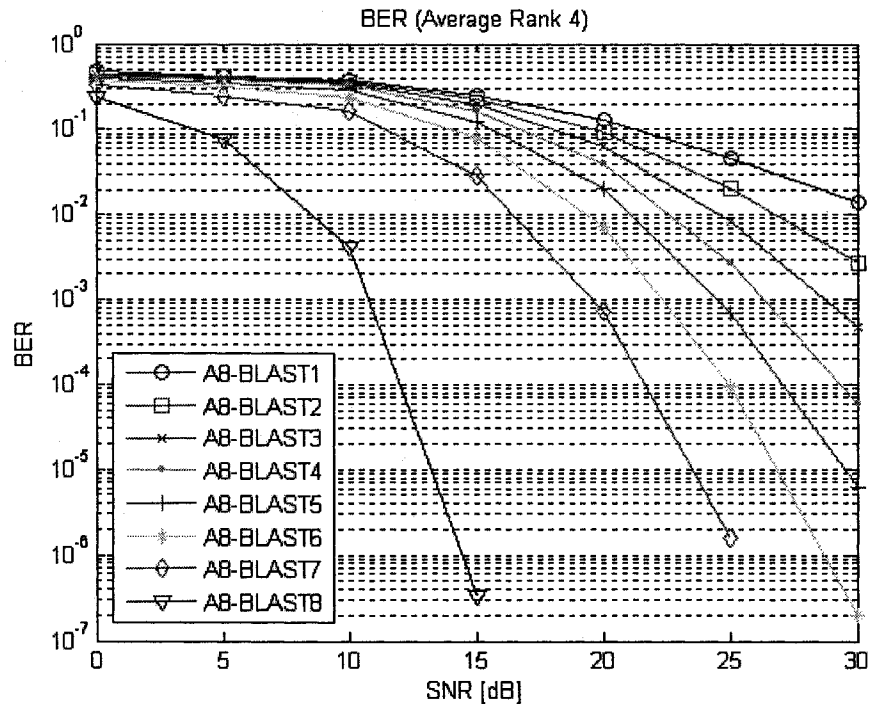


Figure 5-51 A8-BLAST Reference BER Curves (Average Rank 4)

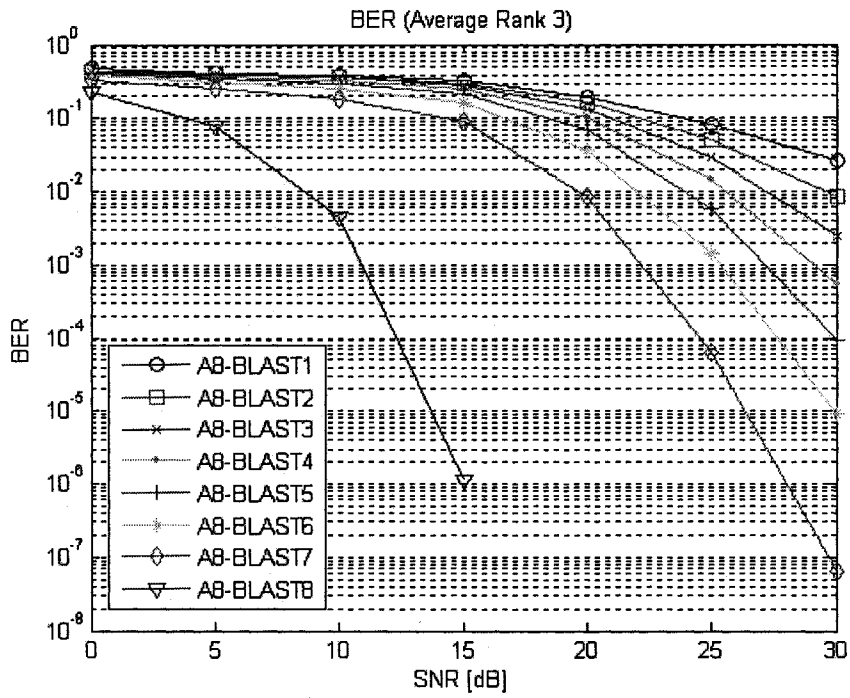


Figure 5-52 A8-BLAST Reference BER Curves (Average Rank 3)

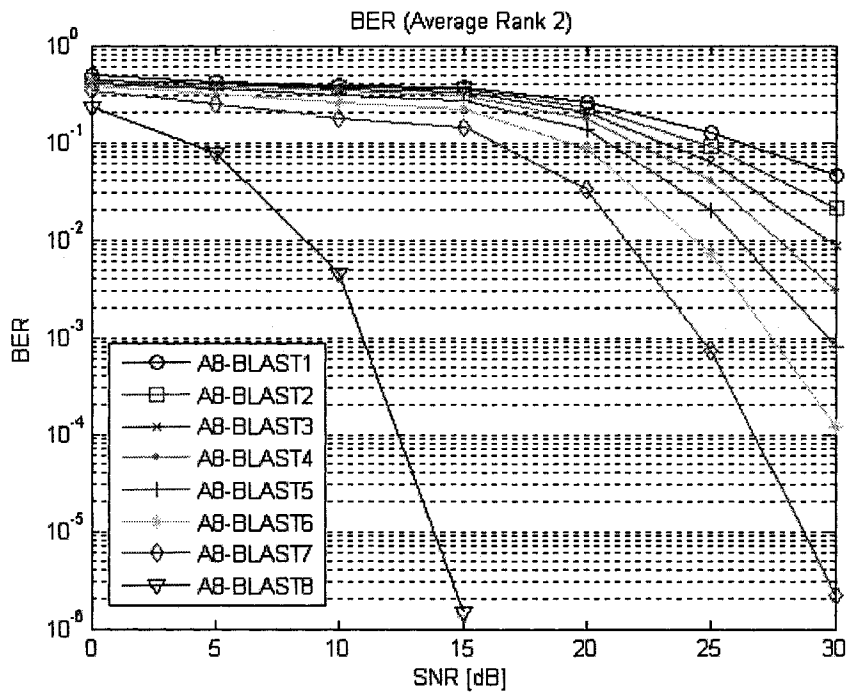


Figure 5-53 A8-BLAST Reference BER Curves (Average Rank 2)

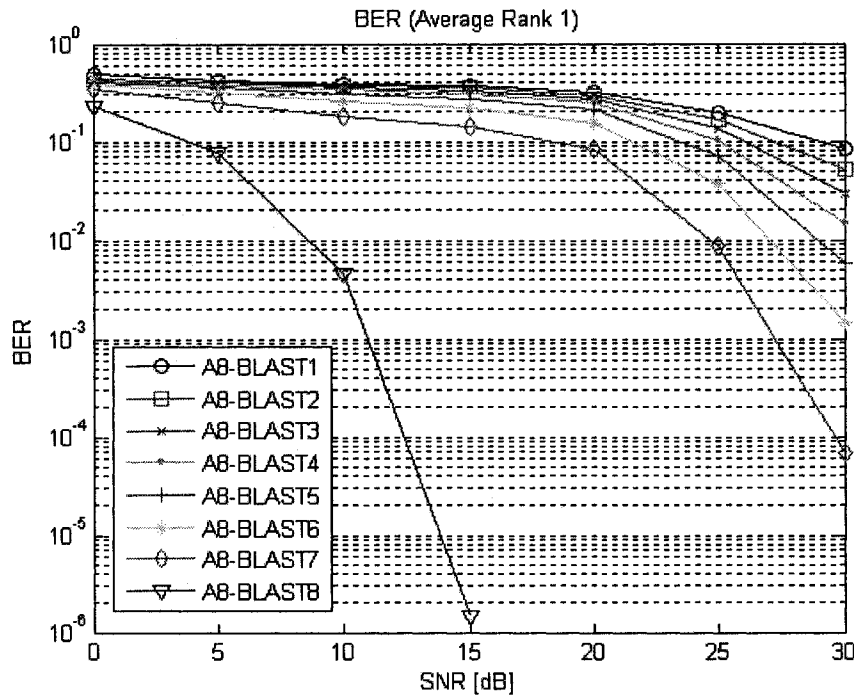


Figure 5-54 A8-BLAST Reference BER Curves (Average Rank 1)

As evident in Figure 5-48 to Figure 5-54, as fading becomes spatially correlated, error performance of A8-BLAST modes providing higher levels of spatial multiplexing degrade more quickly than modes providing less spatial multiplexing in favor of higher diversity order. These curves provide a reference by which the A8-BLAST mode may be adapted given estimates of receive signal quality, MIMO channel rank, and system imposed BER tolerance.

5.1.5.1 Performance Results

The performance of A8-BLAST is compared against the non-adaptive LST processing benchmarks in Figure 5-55 to Figure 5-72. Performance is measured in terms of resulting link goodput and residual BER for target BER thresholds of 10^{-1} , 10^{-2} , and 10^{-3} respectively.

As evident from the curves, A8-BLAST, utilizing the intermediary modes A8-BLAST2 to A8-BLAST7, is able to provide superior usable throughput, while operating below the allowable residual BER thresholds, over a wide range of operating environments.

5.1.5.1.1 Residual BER Threshold of 10^{-1}

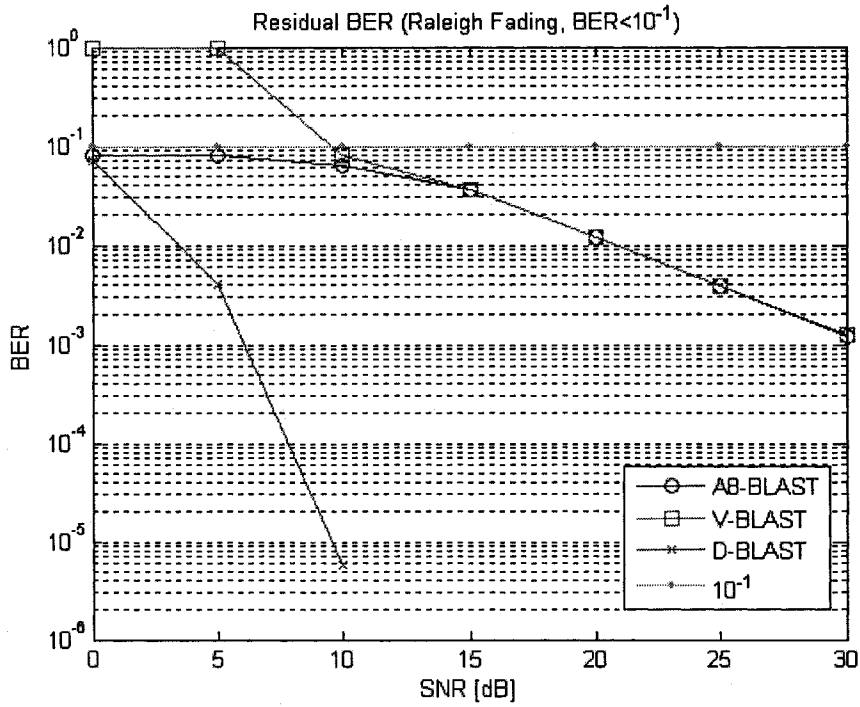


Figure 5-55 A8-BLAST Residual BER (Raleigh Fading, $BER < 1e-1$)

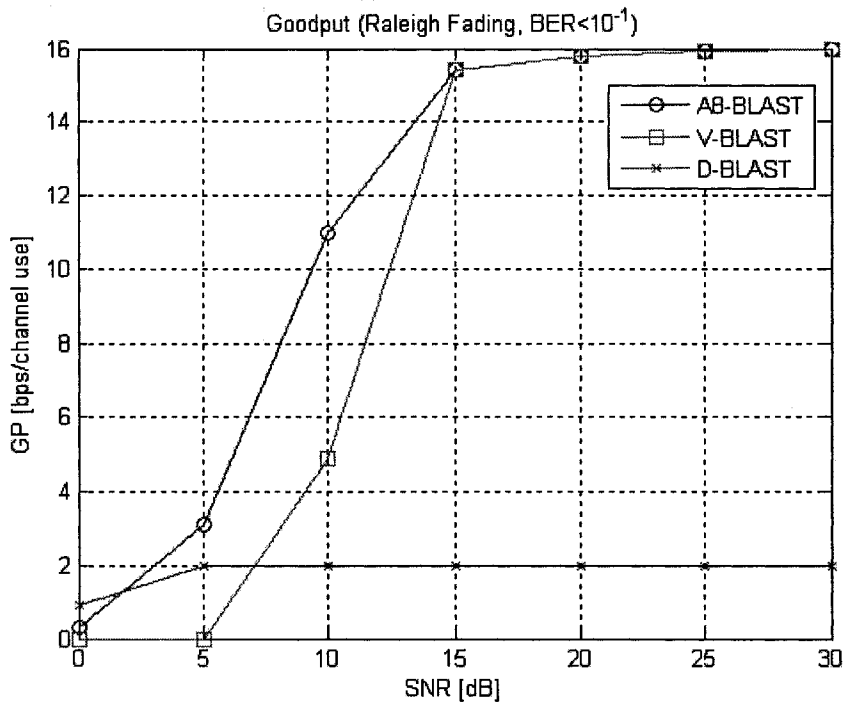


Figure 5-56 A8-BLAST Goodput (Raleigh Fading, $BER < 1e-1$)

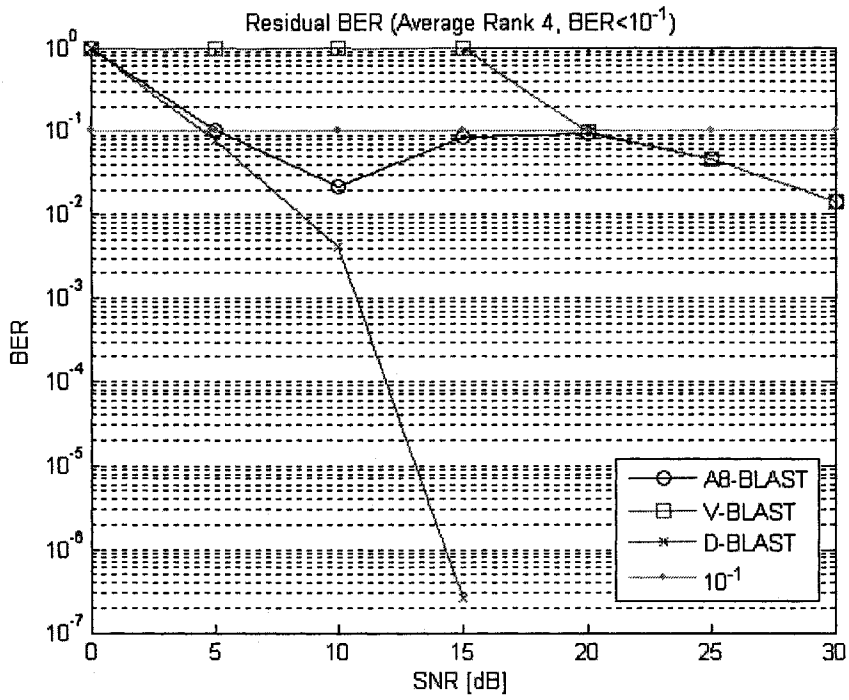


Figure 5-57 A8-BLAST Residual BER (Average Rank 4, BER < 1e-1)

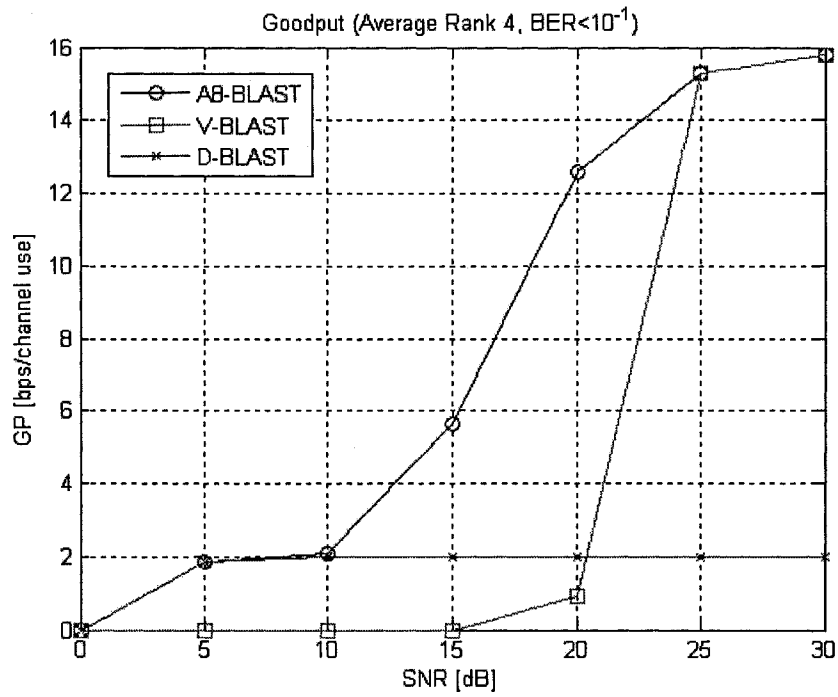


Figure 5-58 A8-BLAST Goodput (Average Rank 4, BER < 1e-1)

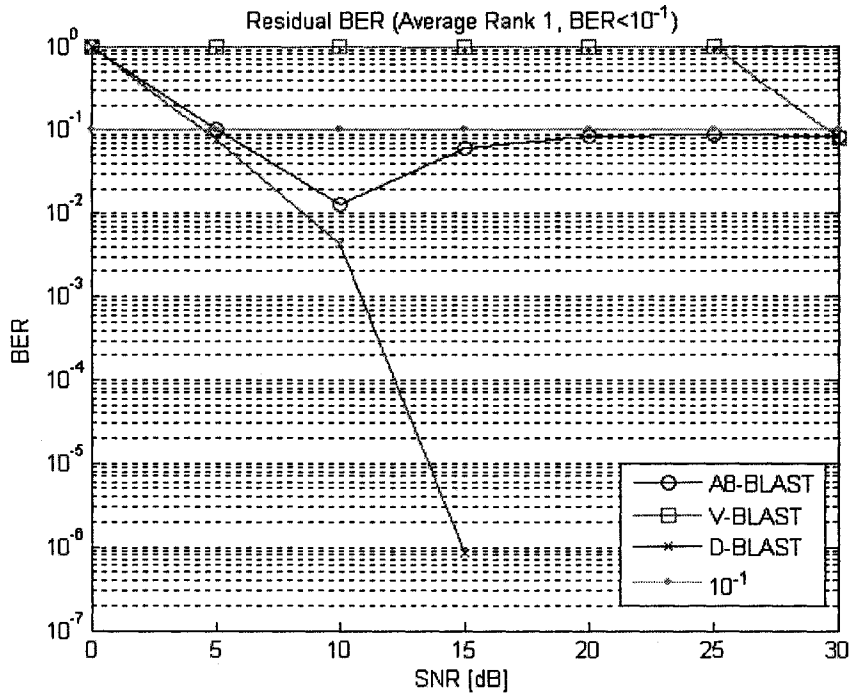


Figure 5-59 A8-BLAST Residual BER (Average Rank 1, BER < 1e-1)

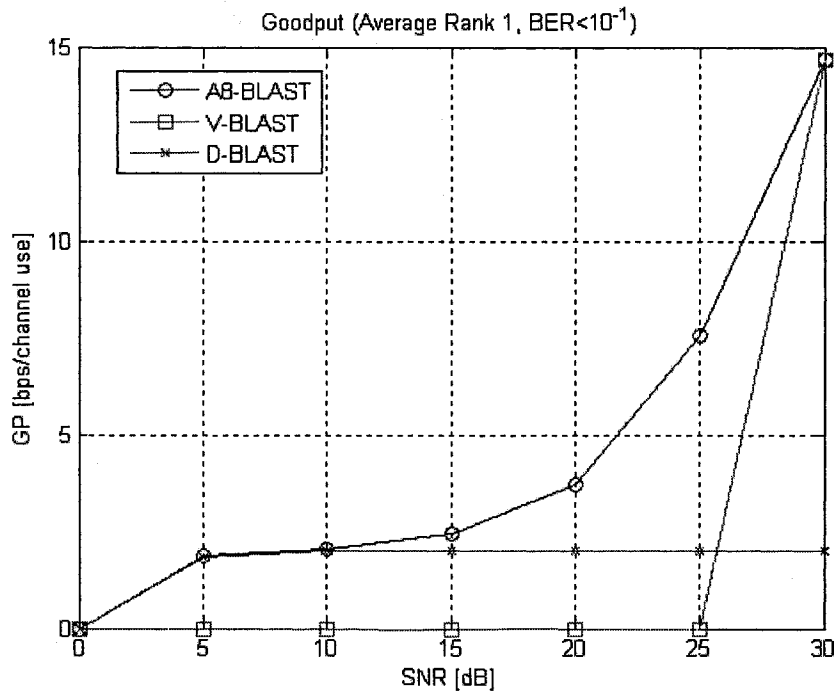


Figure 5-60 A8-BLAST Goodput (Average Rank 1, BER < 1e-1)

5.1.5.1.2 Residual BER Threshold of 10^{-2}

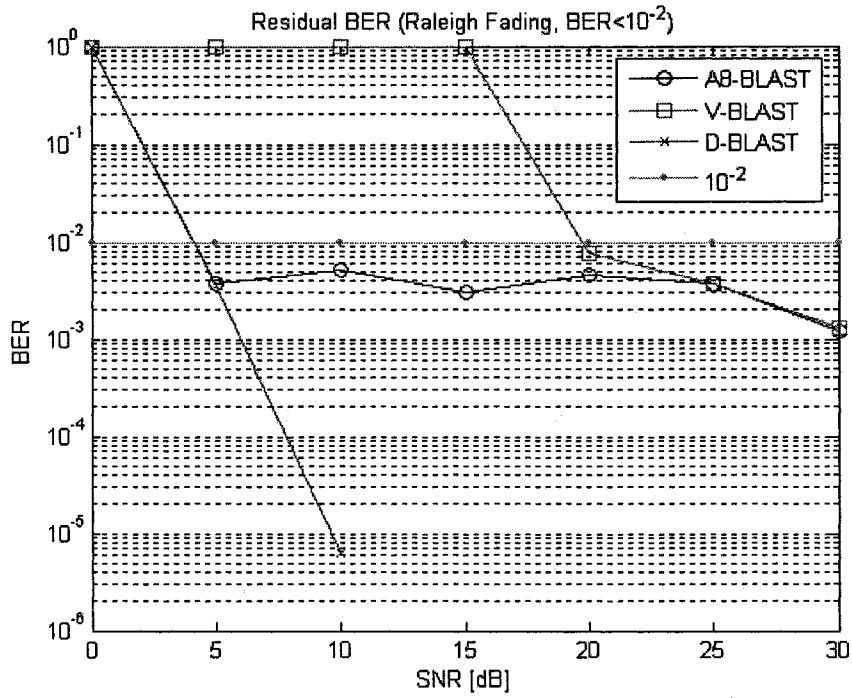


Figure 5-61 A8-BLAST Residual BER (Raleigh Fading, $BER < 1e-2$)

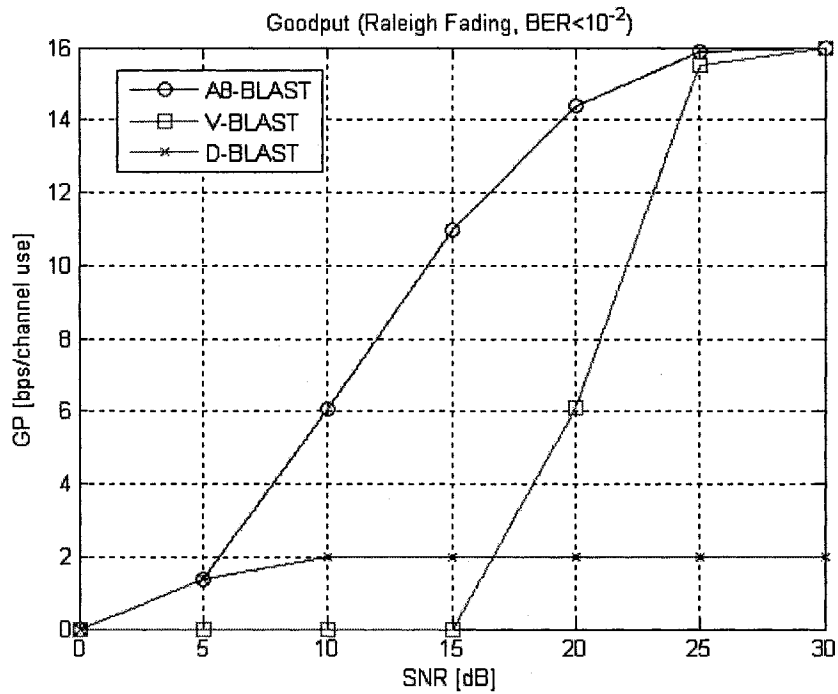


Figure 5-62 A8-BLAST Goodput (Raleigh Fading, $BER < 1e-2$)

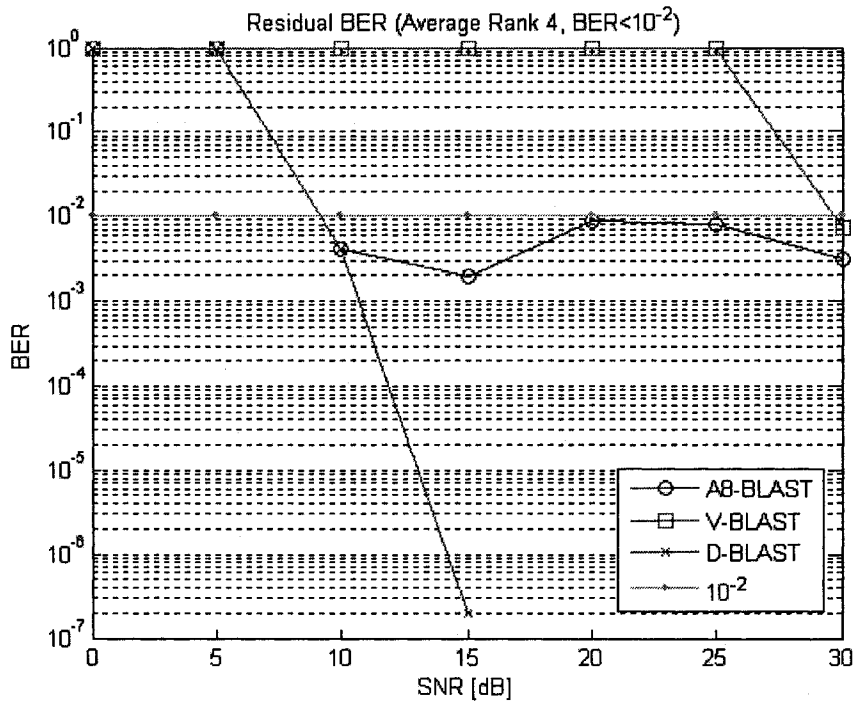


Figure 5-63 A8-BLAST Residual BER (Average Rank 4, BER < 1e-2)

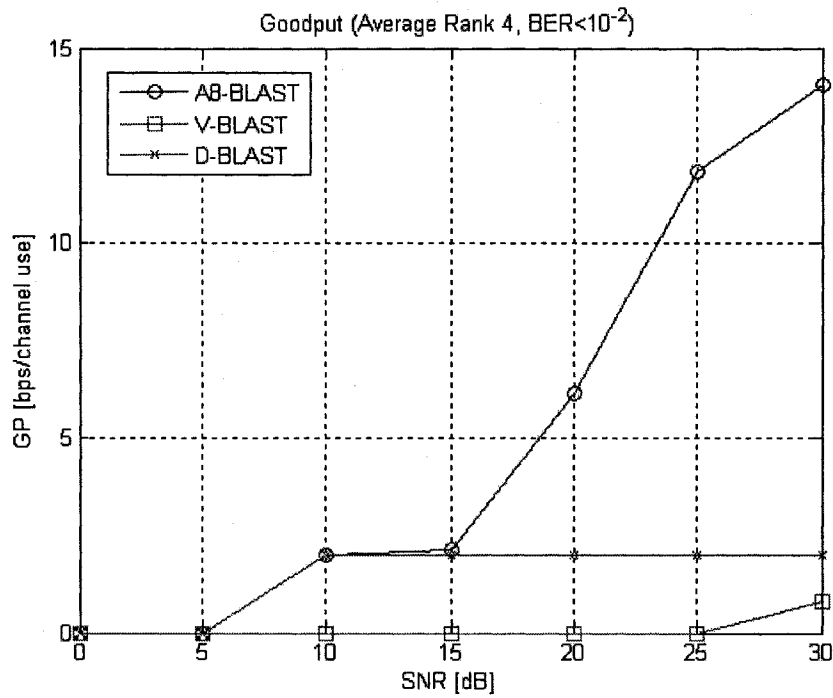


Figure 5-64 A8-BLAST Goodput (Average Rank 4, BER < 1e-2)

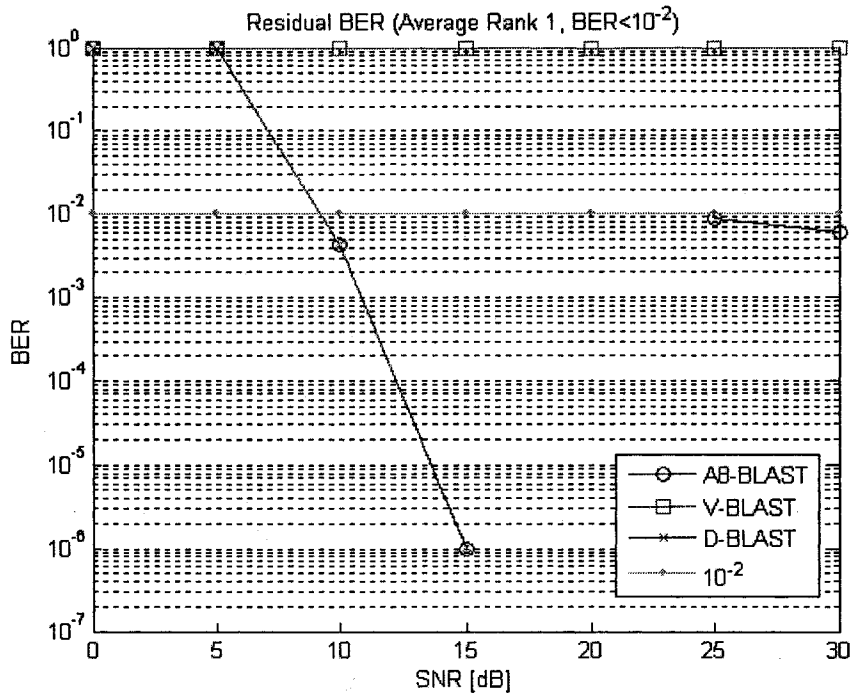


Figure 5-65 A8-BLAST Residual BER (Average Rank 1, BER < 1e-2)

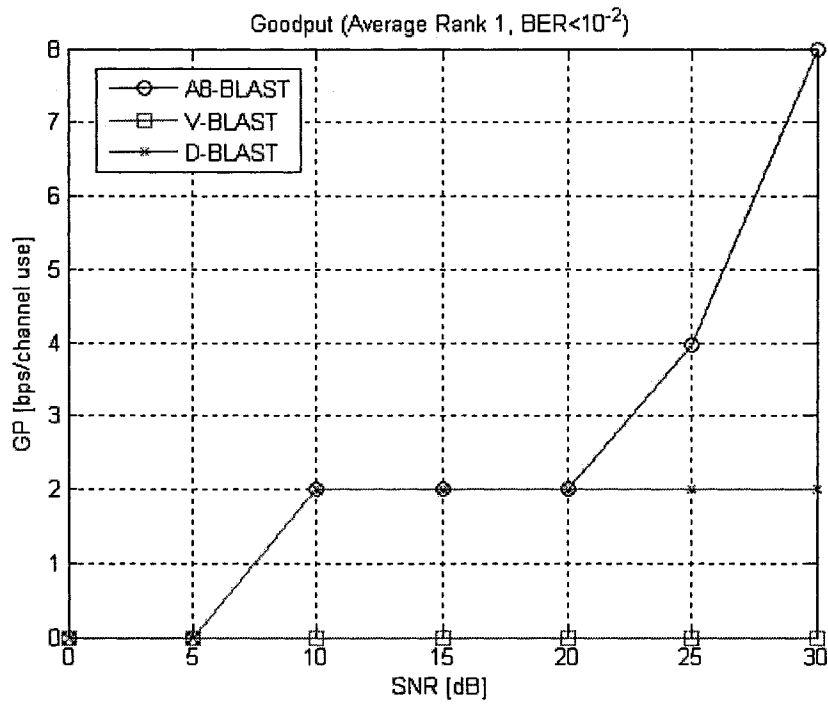


Figure 5-66 A8-BLAST Goodput (Average Rank 1, BER < 1e-2)

5.1.5.1.3 Residual BER Threshold of 10^{-3}

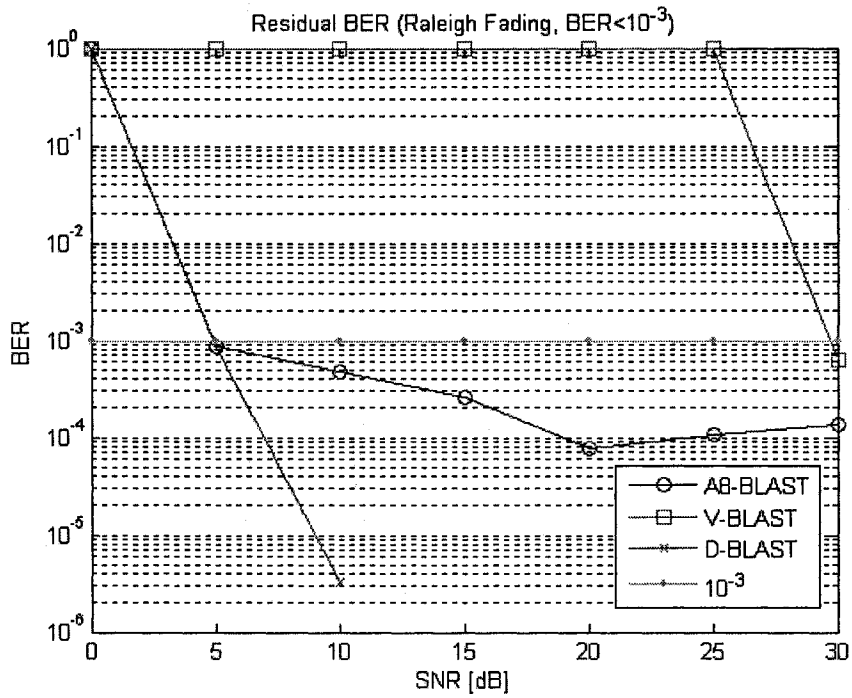


Figure 5-67 A8-BLAST Residual BER (Raleigh Fading, BER < 10^{-3})

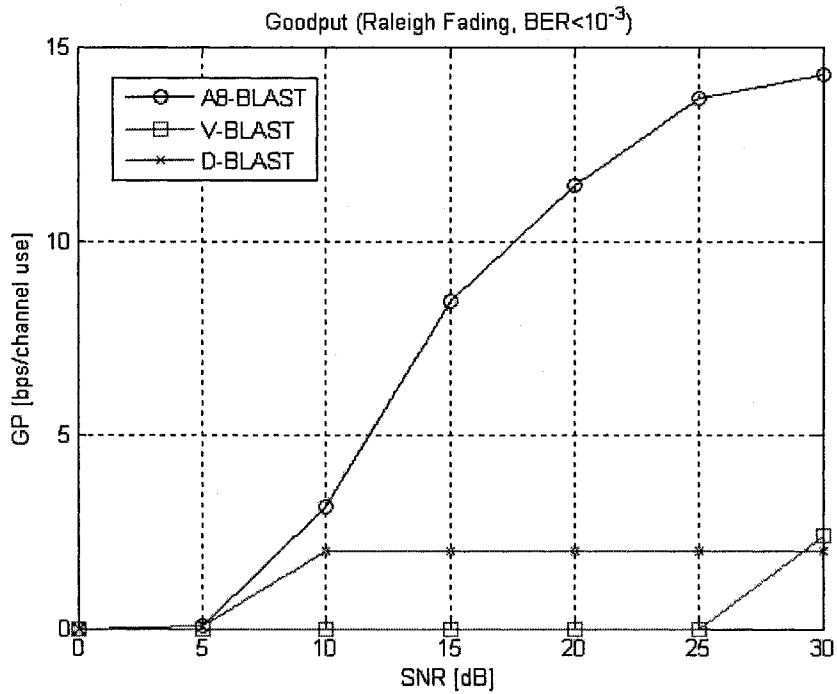


Figure 5-68 A8-BLAST Goodput (Raleigh Fading, BER < 10^{-3})

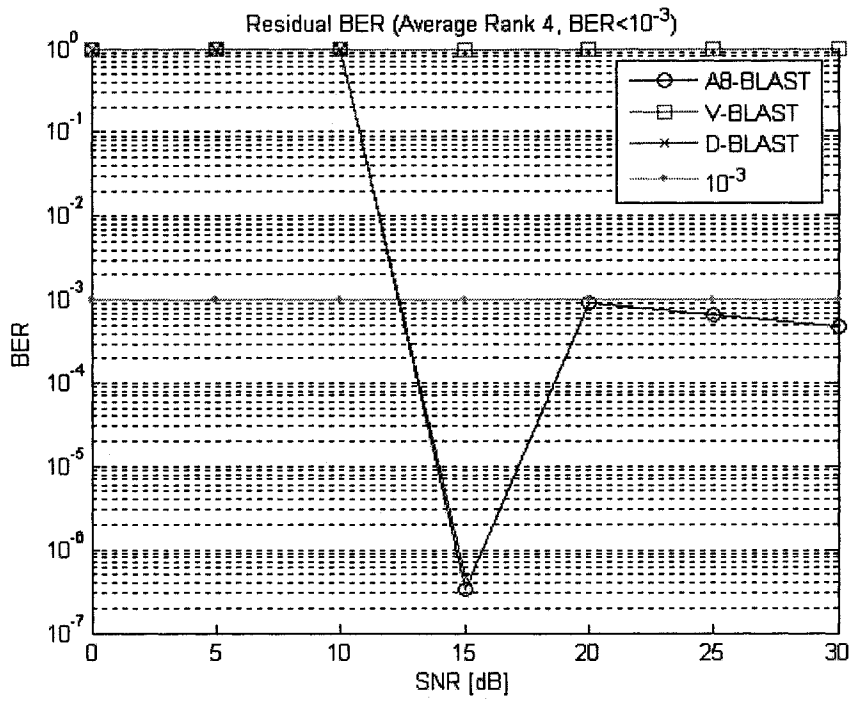


Figure 5-69 A8-BLAST Residual BER (Average Rank 4, BER < 10^{-3})

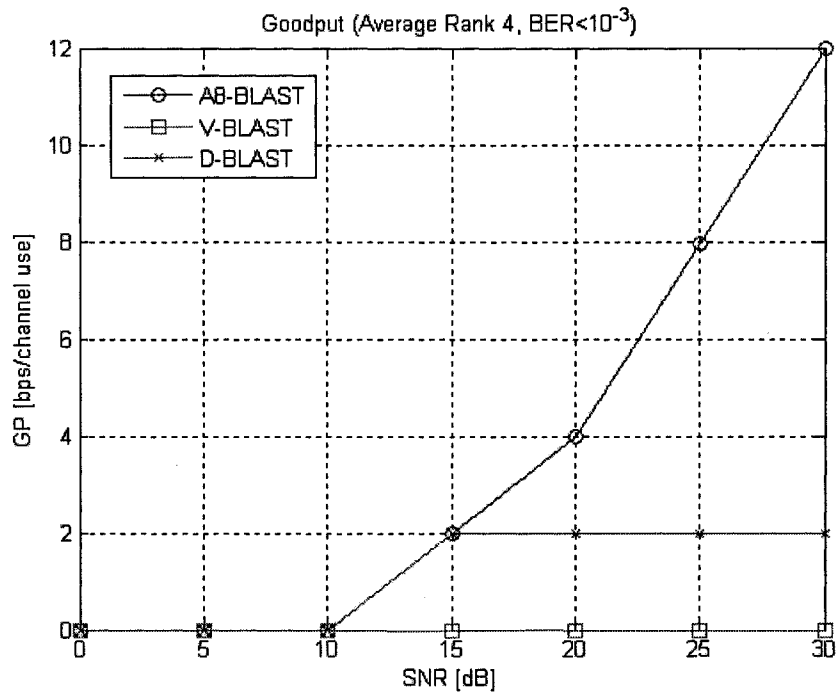


Figure 5-70 A8-BLAST Goodput (Average Rank 4, BER < 10^{-3})

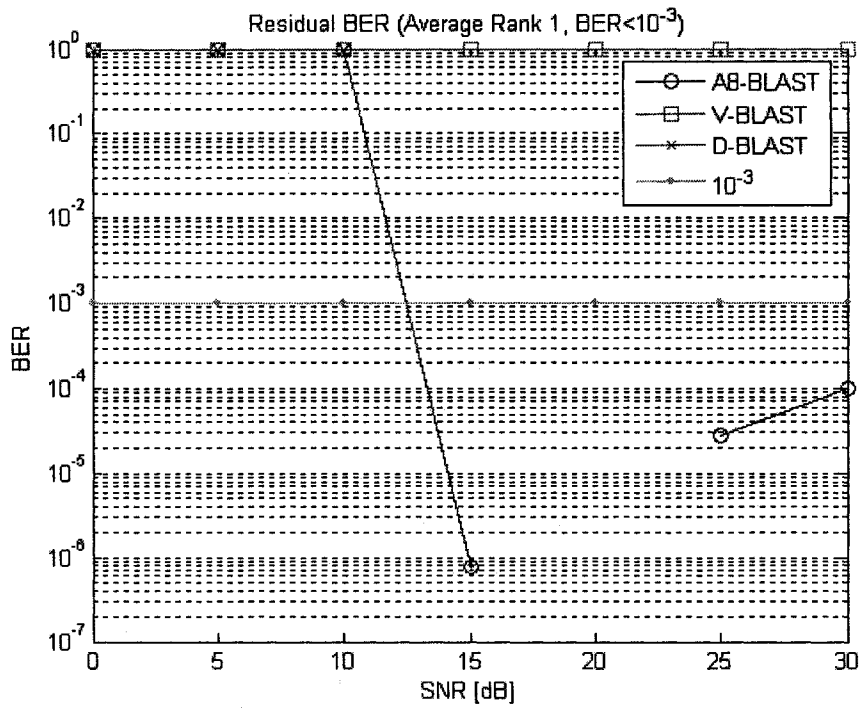


Figure 5-71 A8-BLAST Residual BER (Average Rank 1, BER < 1e-3)

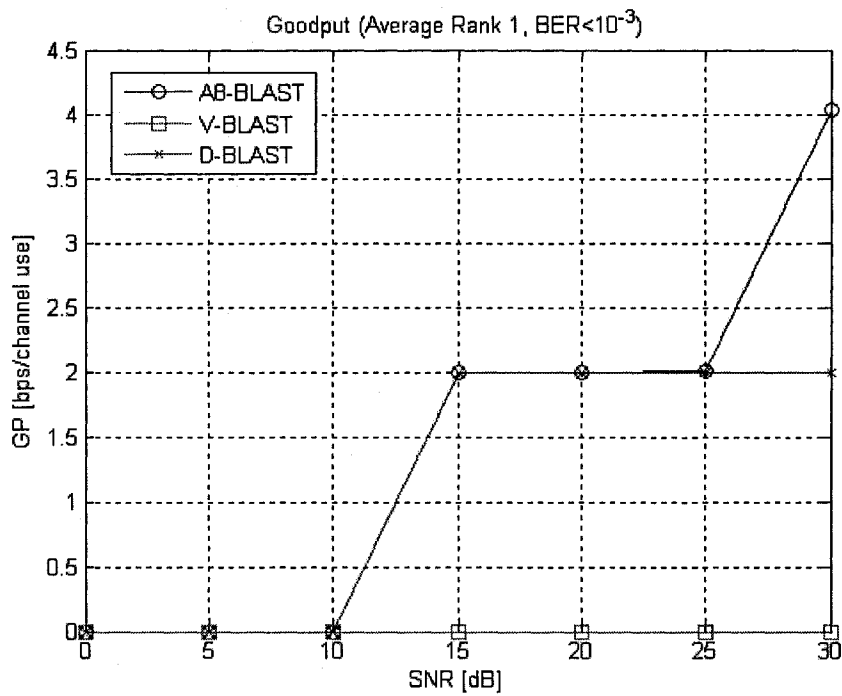


Figure 5-72 A8-BLAST Goodput (Average Rank 1, BER < 1e-3)

5.1.5.2 Summary

The A8-BLAST approach to adaptive space-time processing provides six intermediate modes for adaptation, A8-BLAST2 to A8-BLAST7, the maximum level of granular control over codeword diversity mapping and spectral efficiency of all A-BLAST modes simulated. As evident in the performance results of §5.1.5.1.1-§5.1.5.1.3, A8-BLAST provides improved link goodput relative to the non-adaptive benchmarks V-BLAST and D-BLAST respectively. In addition, employing the six intermediate A8-BLAST modes available for adaptation, residual BER performance may be held below but very close to the tolerable threshold over a wider range of operating environments, thus providing precise control over the adaptive STP performance.

5.1.6 Implementation Issues

As identified in §1.1, throughout the research and development of the A-BLAST approach to adaptive space-time processing, algorithm stability and implementation complexity were important considerations underlying the thesis motivation. In addition to performance alone, for an algorithm to be practical, it must be stable over a wide range of operating environments and be of realizable complexity. The performance results documented in §5.1.3-§5.1.5 take into account the combined signal perturbation effects of imperfect CSI as well as the rank deficient MIMO channel environment arising from the existence of spatial fading correlation.

5.1.6.1 Side Channel Feedback Bandwidth Requirements

The amount of side channel feedback overhead is a concern for any practical MIMO implementation where CSI must be communicated across the channel. Referring to Figure 5-1, in the absence of adaptive modulation, data rate information ($Rate$) may be inferred from the A-BLAST mode selection ($Mode$). As well, diversity combiner weights (CSI_{Rx3}) may be computed entirely at the receiver. Accordingly, the basis CSI requirement for A-BLAST includes the mode information, as well as MIMO permutation and channel QR decomposition (i.e. $Mode, \mathbf{Q}_p^H, \mathbf{L}_p, \mathbf{P}$). Table 5-1 provides a summary of A-BLAST CSI requirements:

CSI Parameter	Data Type	CSI States (M=N)	CSI States (M=N=4)	CSI Weight [bits] (M=N=4)
Mode	Integer	M	4	2
\mathbf{P}	Integer	M!	24	5
\mathbf{L}_p	Complex ²	M ²	16	$16\log_2(q_1)^3$
\mathbf{Q}_p^H	Complex ⁴	2M ²	32	$32\log_2(q_q)^5$

Table 5-1 A-BLAST CSI Summary

In a frequency division duplex (FDD) air interface, following preamble training, the side channel feedback of partial CSI ($Mode, \mathbf{Q}_p^H$) would be sufficient to update the A-BLAST transmitter for upcoming data transfers. In a symmetric MIMO environment employing four element antenna arrays, assuming 8-bit granularity in the coefficients of \mathbf{Q}_p^H , the side channel feedback overhead necessary is estimated as 258 bits per partial CSI update. Figure 5-73 shows the effect of CSI update interval, influenced primarily by MIMO channel coherence time, on the A-BLAST side channel bandwidth requirement for a FDD air interface:

² Coefficients are complex numbers but state count is given in terms of real data type (i.e. real and imaginary).

³ The number of states employed in the quantization of \mathbf{L}_p coefficients is q_1 . \mathbf{L}_p is upper triangular with real coefficients along the main diagonal.

⁴ Coefficients are complex numbers but state count is given in terms of real data type (i.e. real and imaginary).

⁵ The number of states employed in the quantization of \mathbf{Q}_p coefficients is q_q .

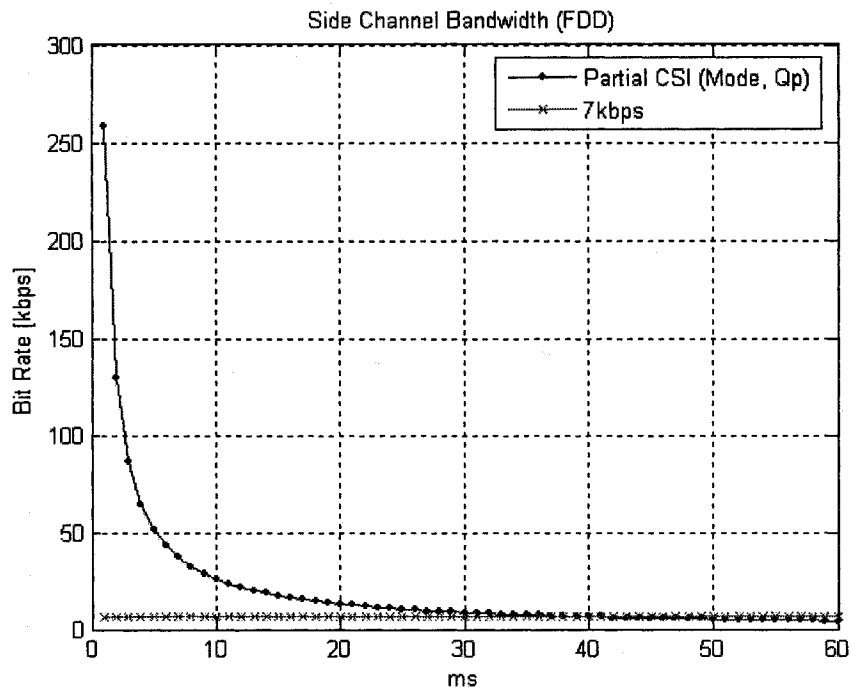


Figure 5-73 Partial CSI Bandwidth (FDD Air Interface, $\log_2(q_q) = 8$, $M=N=4$)

Referring to Figure 5-73, at an update interval of 30ms, suitable for many indoor WLAN environments, the side channel bandwidth is approximately 8.6kbps.

In a time division duplex (TDD) air interface with adequate coherence time (i.e. several milliseconds), where channel reciprocity is assumed to exist [24], preamble training may be synchronized, offset, and performed bi-directionally. In this scenario, again assuming a symmetric MIMO environment employing four element antenna arrays, the side channel feedback may be reduced to simply the partial CSI (Mode, P) and overhead is reduced to 7 bits per partial CSI update, independent of CSI coefficient granularity. Figure 5-74 shows the effect of CSI update interval on A-BLAST side channel bandwidth for the TDD air interface:

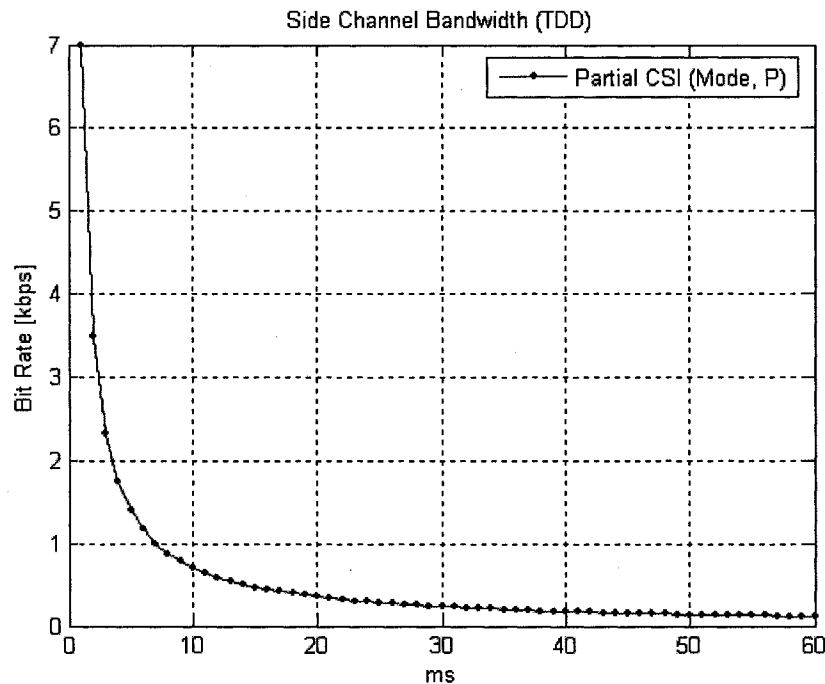


Figure 5-74 Partial CSI Bandwidth (TDD Air Interface, M=N=4)

Clearly, when the exchange of MIMO channel coefficients is not required, side channel feedback overhead is reduced substantially. At an update interval of 37ms, the side channel feedback bandwidth requirement is approximately 7kbps for the four-by-four FDD system, assuming 8-bit channel coefficient granularity. The equivalent update interval in the TDD based air interface requires a side channel bandwidth of approximately 200bps (i.e. approximately 3%), independent of channel coefficient granularity.

5.1.6.2 Channel Estimation

5.1.6.2.1 Effect of Noise Perturbation

Integral to the A-BLAST algorithm is the requirement for CSI. CSI is obtained through preamble training using a known OSTBC transmission and LS based estimation [18]. Assuming $M=N=4$ antennas, if $\mathbf{S}_{G4} \in C^{4 \times 8}$ is the OSTBC training codeword such that $\mathbf{S}_{G4} \mathbf{S}_{G4}^H = \mathbf{S}_{G4}^H \mathbf{S}_{G4} = k \mathbf{I}_4$, where k is a scalar (see §**Error! Reference source not found.**), then the LS solution [18] for channel estimation is:

$$\begin{aligned} \mathbf{H}_{\text{est}} &= \mathbf{R} \frac{\mathbf{S}_{G4}^H}{k} \in C^{4 \times 4} \Rightarrow \\ \mathbf{H}_{\text{est}} &= (\mathbf{H} \mathbf{S}_{G4} + \mathbf{N}) \frac{\mathbf{S}_{G4}^H}{k} \Rightarrow \\ \mathbf{H}_{\text{est}} &= \mathbf{H} + \mathbf{N} \frac{\mathbf{S}_{G4}^H}{k} \end{aligned} \quad (33)$$

In (33), $\mathbf{R} \in C^{4 \times 8}$ is the received training codeword as seen at the receiver. $\mathbf{N} \in C^{4 \times 8}$ is the receiver ZMCSCG noise matrix. As SNR levels lower, the perturbation do to noise dominates and CSI errors arising from LS estimation increase on average. Additional channel estimation techniques exists including MMSE and Fast Fourier Transform (FFT) based methods [18], each capable of reducing CSI estimation errors relative to the LS method at the expense of higher implementation complexity. Relative error is measured in terms of the resulting channel realization error matrix

$\mathbf{E} = \mathbf{H} - \mathbf{H}_{\text{est}}$ as $e = \frac{\|\mathbf{E}\|_F}{\|\mathbf{H}\|_F} = \frac{\|\mathbf{H} - \mathbf{H}_{\text{est}}\|_F}{\|\mathbf{H}\|_F}$. Figure 5-75 shows how CSI errors due to LS channel

estimation grow as average receiver SNR levels lower:

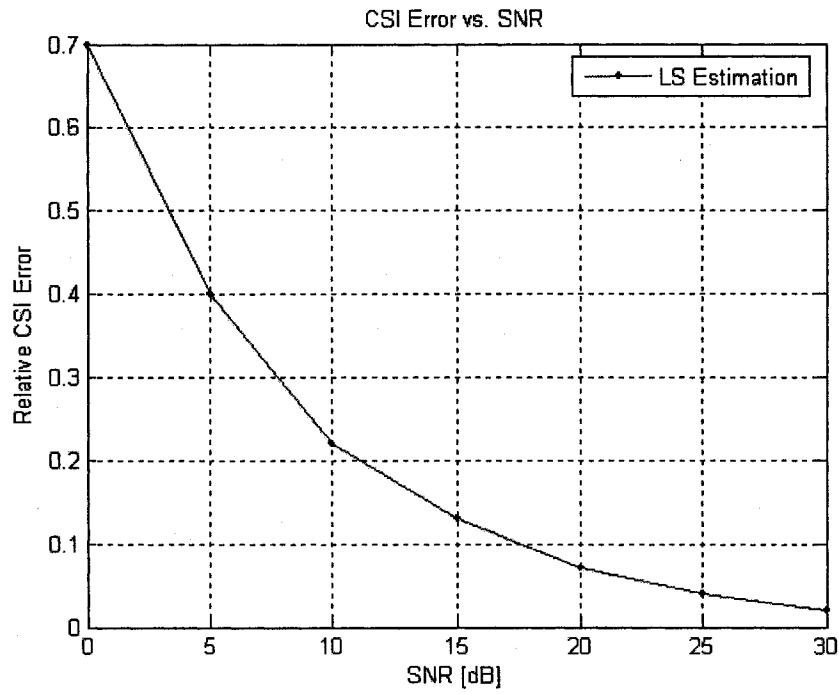


Figure 5-75 Average CSI Error (LS Estimation, Raleigh Fading, M=N=4)

Clearly, the perturbation effects of imperfect CSI are most pronounced at low SNR. The A-BLAST adaptation somewhat mitigates this perturbation through code rate reduction by weighting diversity encoding more heavily than spatial multiplexing encoding as SNR levels lower. Referring to Figure 5-76, CSI errors due to imperfect channel estimation degrades BER performance across the entire SNR range under test:

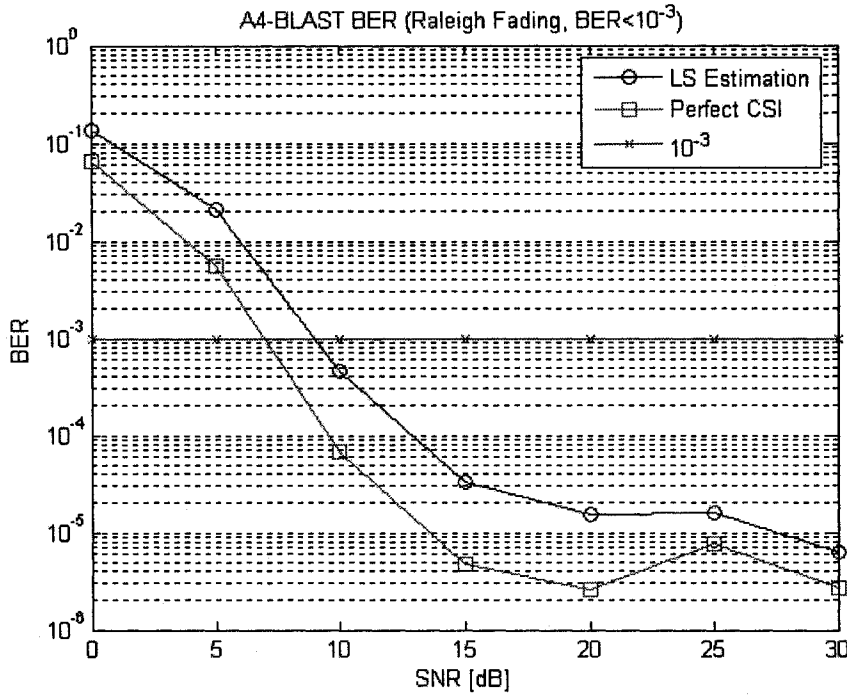


Figure 5-76 Effect of CSI Error on BER (A4-BLAST)

At SNR levels above approximately 9dB, the effect of imperfect CSI is a degradation link goodput. Below 9dB average SNR, A4-BLAST employing LS channel estimation is in an outage condition since the BER has risen above the allowable threshold of 10^{-3} , a degradation of approximately 1.9dB in receive sensitivity versus A4-BLAST employing perfect CSI.

5.1.6.3 Rank Estimation

5.1.6.3.1 Effect of Noise Perturbation

The performance of A-BLAST in rank deficient MIMO channels is important. In a highly scattered wireless environment, typical of many indoor WLAN deployments, as conditions vary due to user mobility, changes in location and amount of local scattering, etc., rank deficiency in \mathbf{H} and therefore \mathbf{H}_{est} is inevitable in practice. Accordingly, the stability of QR factorization in rank deficient environments is important since even in a highly rank deficient channel, which may be ill conditioned to channel inversion, it is desirable and necessary that the A-BLAST algorithm function, enabling diversity encoding with acceptably low probability of symbol detection error.

For the MIMO channel realization estimate $\mathbf{H}_{\text{est}} \in \mathbb{C}^{N \times M}$, the 2-norm condition number is given as the ratio of maximum to minimum singular values [19]:

$$\kappa = \frac{\sigma_{\max}}{\sigma_{\min}} \quad (34)$$

It has been shown that in highly rank deficient environments, a $O(\varepsilon)$ relative error in the channel estimate \mathbf{H}_{est} induces a $O(\varepsilon\kappa)$ relative error in the QR factorization of \mathbf{H}_{est} [38].

As identified in §5.1.2, knowledge of MIMO channel rank is important when determining the weighting of spatial multiplexing encoding selected through A-BLAST. Following the eigenvalue decomposition of the channel estimate \mathbf{H}_{est} , an estimate of the channel rank (r_{est}) is obtained from the descending eigenvalue set $\{\lambda_1 \cdots \lambda_{\min(N,M)}\}$ as the number of eigenvalues necessary to exceed a predefined threshold (τ) of available channel power gain:

$$r_{\text{est}} = r : \sum_{x=1}^{r \leq \min(N,M)} \lambda_x \geq \tau \|\mathbf{H}_{\text{est}}\|_F^2 \quad (35)$$

Figure 5-77 shows how rank estimation using (35) for a MIMO system with $M=N=4$ antennas and a power threshold of 99% varies with Ricean Power Factor (K):

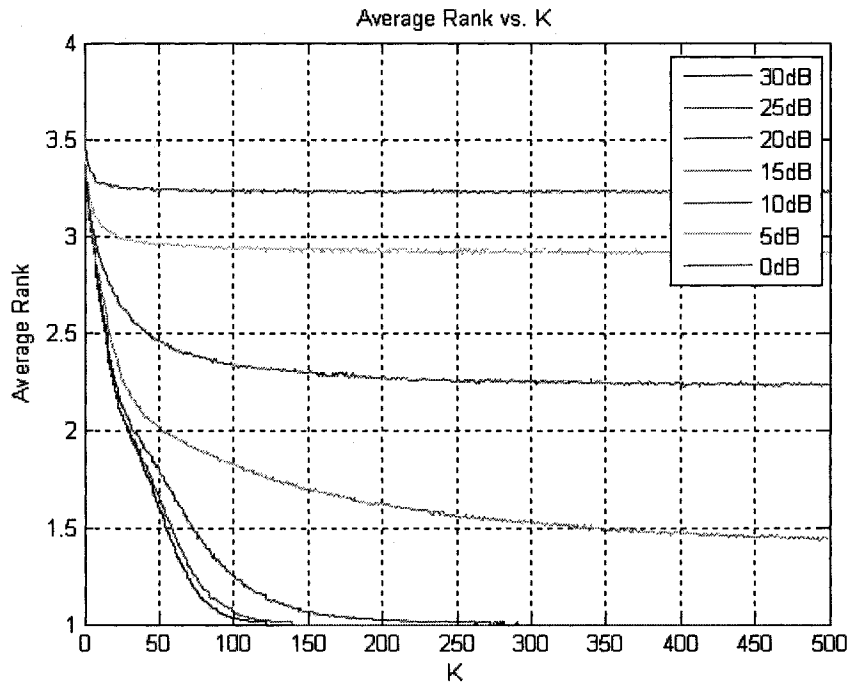


Figure 5-77 Average Rank vs. K ($\tau=0.99$, $M=N=4$)

As shown in Figure 5-77, the ability to accurately estimate the rank of spatially correlated MIMO channel realizations diminish as average receiver SNR levels lower. This is a result of the spatially white perturbation effects of receiver AWGN. In high SNR environments, at levels of $K > 100$, fading correlation introduces linear dependence and therefore rank deficiency in \mathbf{H}_{est} , reducing the average rank to one. As SNR levels lower, the receiver becomes desensitized and channel estimation through preamble training results in increased CSI errors as shown previously in Figure 5-75. In addition, the AWGN perturbation is spatially white across the receive antenna array. The result is noise power spread across all channel eigenvalues and a rank estimate obtained using (35) approaching $r_{\text{est}} \rightarrow \min(N, M)$ at low SNR. Figure 5-78 shows the resulting error in average rank estimation due to receiver desensitization:

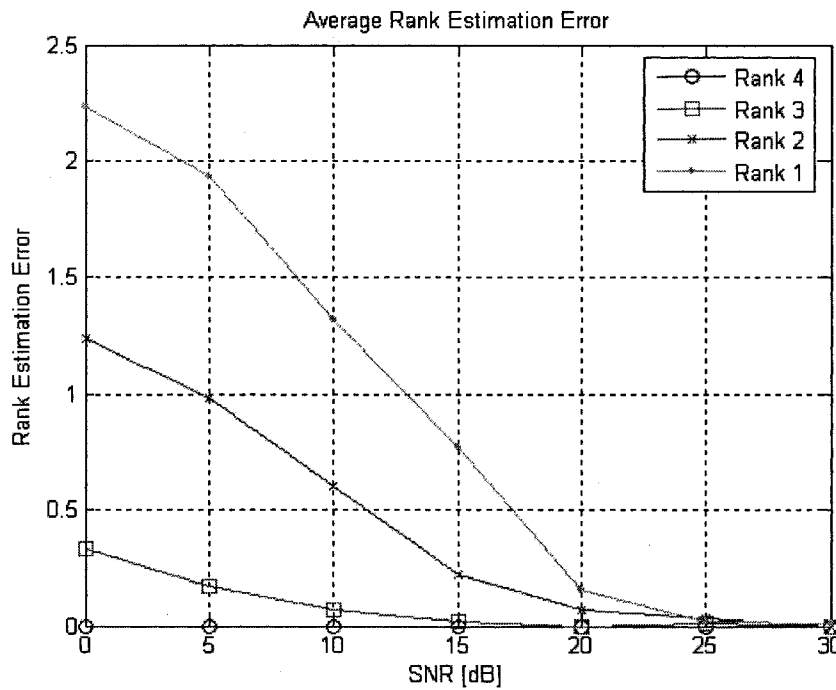


Figure 5-78 Average Rank Estimation Error ($\tau=0.99$, $M=N=4$)

Clearly, rank estimation errors increase as receive SNR levels lower and as the MIMO channel becomes highly rank deficient due to LOS propagation or spatial correlation effects. The negative effects of rank estimation error are mitigated somewhat through adaptation since at low SNR A-BLAST adapts naturally to reduce code rate and more heavily weight diversity encoding over spatial multiplexing encoding to exploit array gain and achieve an SNR improvement.

5.1.6.3.2 Effect of Reducing Rank Percentage Power Threshold (τ)

As discussed in §2.3.3, the MIMO channel rank identifies the number of spatial eigenmodes available for spatial multiplexing. In a similar manner to that identified in [13], referring to (35), A-BLAST adaptation obtains an estimate of the MIMO channel rank using a percentage (τ) of total available channel power. The performance results documented in §5.1.3.1, §5.1.4.1, and §5.1.5.1 are with respect to a percentage power threshold of $\tau = 0.99$.

The effect of reducing τ is a lowering of the average rank estimate as fewer eigenvalues are necessary to exceed the percentage power threshold defining the available eigenmodes useable for spatial multiplexing. As the rank estimate is lowered, A-BLAST adaptation selects space-time mapping modes that weight more heavily diversity order rather than spatial multiplexing gain. Imposing a lower power threshold and therefore lower average rank estimate essentially results in a conservative selection of A-BLAST mode, a selection favoring link reliability over spectral efficiency.

Figure 5-79 illustrates, for A4-BLAST in Rayleigh fading and BER threshold of 10^{-3} , the effect on link goodput from lowering the rank percentage power threshold (τ) to 0.95 and 0.90:

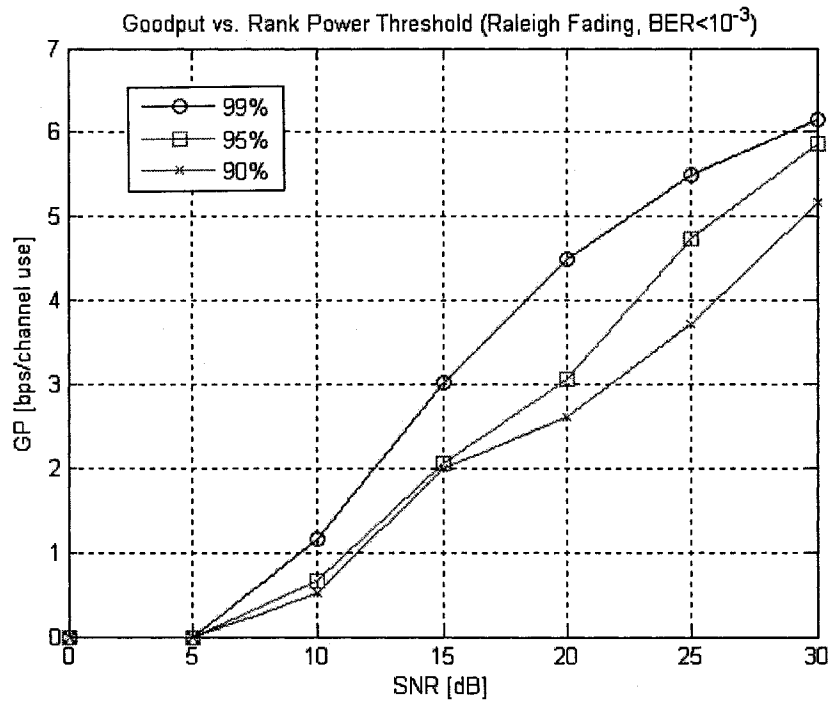


Figure 5-79 Goodput vs. Rank Power Threshold (A4-BLAST)

A change in τ is more pronounced at high SNR levels where the ability exist greatest for A4-BLAST to exploit spatial multiplexing. As SNR levels lower, A4-BLAST adaptation naturally tends toward diversity based space-time mapping in order to preserve BER performance.

In a similar manner, Figure 5-80 illustrates how reducing τ improves residual BER performance:

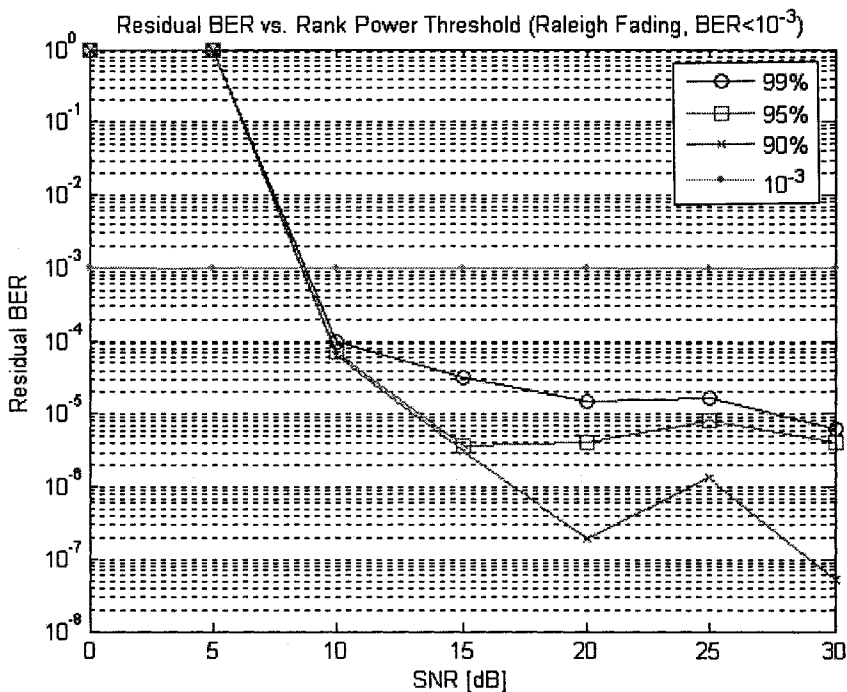


Figure 5-80 Residual BER vs. Rank Power Threshold (A4-BLAST)

Above approximately 10dB SNR, where useable modes exist for adaptation, conservative A4-BLAST mode selection produces superior error performance. Below 10dB, no useable A4-BLAST modes exist and reducing τ provides no improvement in residual BER performance.

5.1.6.4 Antenna Array Mutual Coupling and Spatial Correlation

In many practical MIMO deployments, mutual coupling between antenna array elements and lack of local scattering in the propagation environment makes the existence of spatial correlation unavoidable. It is therefore important to both understand and demonstrate how the A-BLAST adaptation performs under such non-optimal but highly relevant channel conditions. The simulated MIMO channel of the SMWE supports the introduction of spatial correlation through transmitter and receiver spatial covariance matrices (see §3.2.3.3). Simulations were carried out using A4-BLAST with spatial correlation introduced at the receiver through the spatial covariance matrix (\mathbf{R}_r):

$$\mathbf{R}_r = \begin{bmatrix} 1 & 0.75 & 0.5 & 0.25 \\ 0.75 & 1 & 0.75 & 0.5 \\ 0.5 & 0.75 & 1 & 0.75 \\ 0.25 & 0.5 & 0.75 & 1 \end{bmatrix} \quad (36)$$

The spatial covariance matrix of (36) emulates the rather severe correlation distribution of 0.75, 0.5, and 0.25 across adjacent receive antenna array elements [18]. Figure 5-81 illustrates the resulting effect of this spatial correlation on average MIMO channel rank estimation (35):

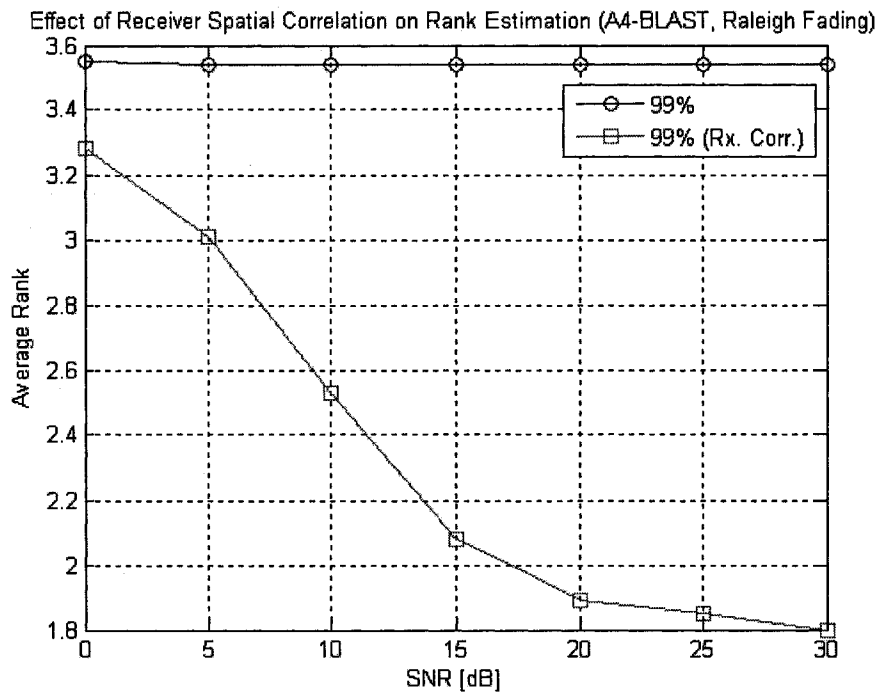


Figure 5-81 Effect of Spatial Correlation on Rank Estimation (A4-BLAST)

It is clear the effect of spatial correlation is most visible at high receive SNR levels. At these SNR levels above approximately 15dB, it acts to lower the average rank estimation by introducing linear dependence between the columns of the channel estimate \mathbf{H}_{est} . As SNR levels lower below 15dB, the influence of the spatially white AWGN again dominates, reducing the visible spatial correlation in the channel estimate \mathbf{H}_{est} .

Similar to the discussion of §5.1.6.3.2, the effect of reduced rank estimation is a conservative A4-BLAST mode selection, emphasizing diversity order over spatial multiplexing gain. In §5.1.6.3.2, the lower average rank estimation was intentionally imposed by reducing the adaptation power threshold parameter (τ). Here, the rank reduction is imposed by a suboptimal channel environment or antenna array geometry. Figure 5-82 illustrates the resulting performance degradation in A4-BLAST link goodput. Conservative A4-BLAST mode selection is clearly evident in the reduced throughput offered to the channel under midrange SNR levels and degraded link goodput:

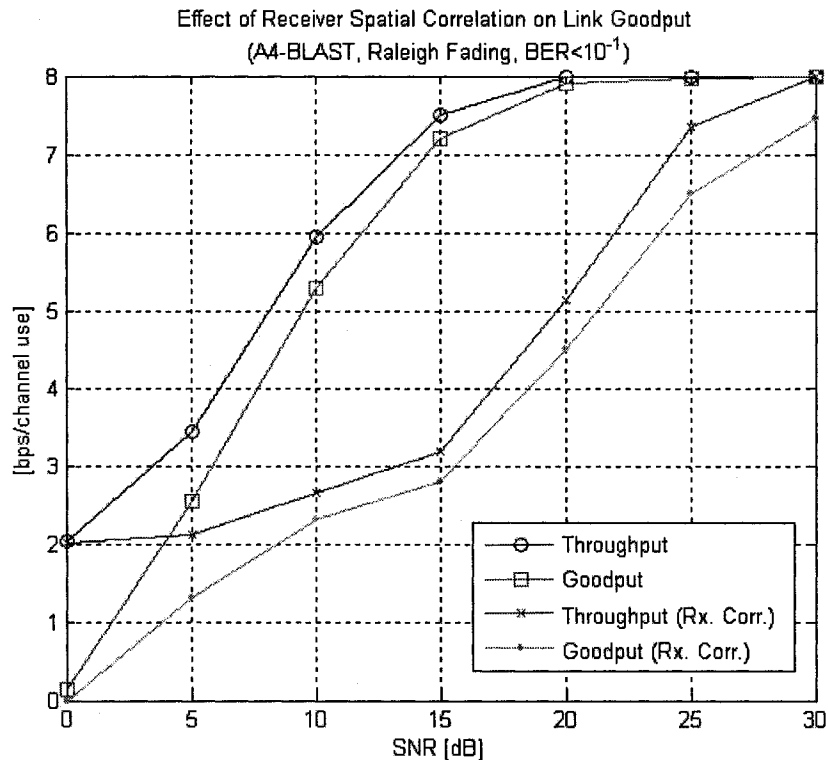


Figure 5-82 Effect of Spatial Correlation on Goodput (A4-BLAST)

Figure 5-83 shows the effect of this receive spatial correlation on BER levels. BER performance is dependent both on the channel environment as well as the A4-BLAST mode selection. As fading

becomes spatially correlated, spatial diversity gain is reduced and susceptibility to microscopic fading increases. This is evident in the increased BER levels when spatial correlation exists:

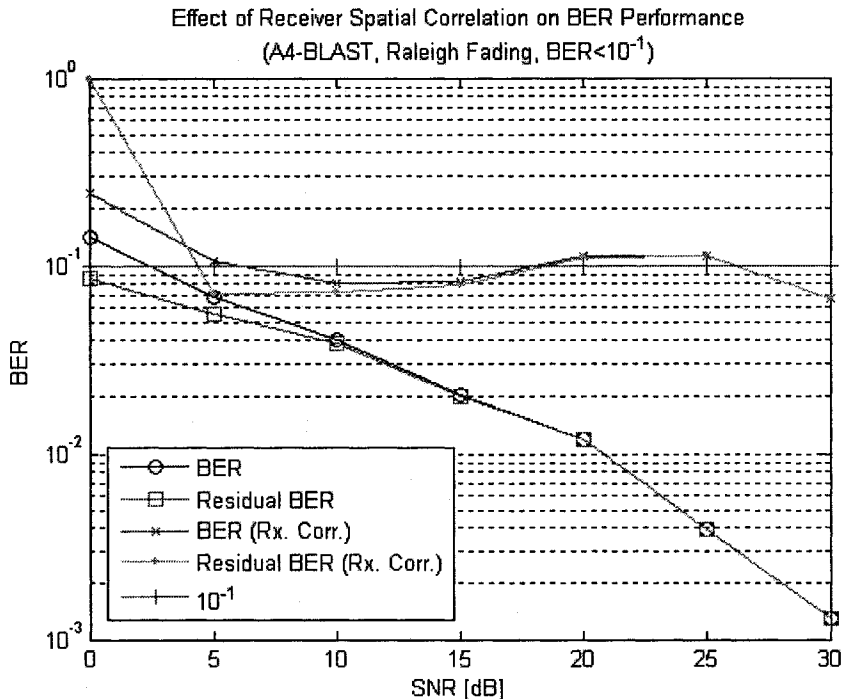


Figure 5-83 Effect of Spatial Correlation on Residual BER (A4-BLAST)

A-BLAST adaptation attempts to maximize performance by selecting a mode which provides just enough diversity order to ensure adequate residual BER performance while maximizing link goodput. Referring to Figure 5-83, at SNR levels between approximately 20dB to 25dB, residual BER performance marginally exceeded the system imposed BER threshold of 10^{-1} . This indicates a need for some level of adaptation calibration specific to the deployment environment. Alternatively, some safety margin may be built into the adaptation algorithm to allow for variance in residual BER levels due to spatial correlation.

Referring to Figure 5-81, the effect of receiver spatial correlation (16) reduces the average rank estimate to between two and three at levels of receive SNR above 15dB. As mentioned previously, in practice this could be a result of mutual coupling between antenna elements due to element separation below the channel coherence distance (D_c). A-BLAST adaptation sees this environment no differently than when rank deficiency is introduced in the MIMO channel estimate due to appropriate levels LOS propagation and Ricean fading. It is therefore expected that the performance of A4-BLAST be similar to that when LOS existing in the propagation environment introduced Ricean fading, lowering the average rank

estimate in a similar manner (see Figure 5-27 and Figure 5-28). The following figures illustrate the expected similarities in residual BER and goodput performance:

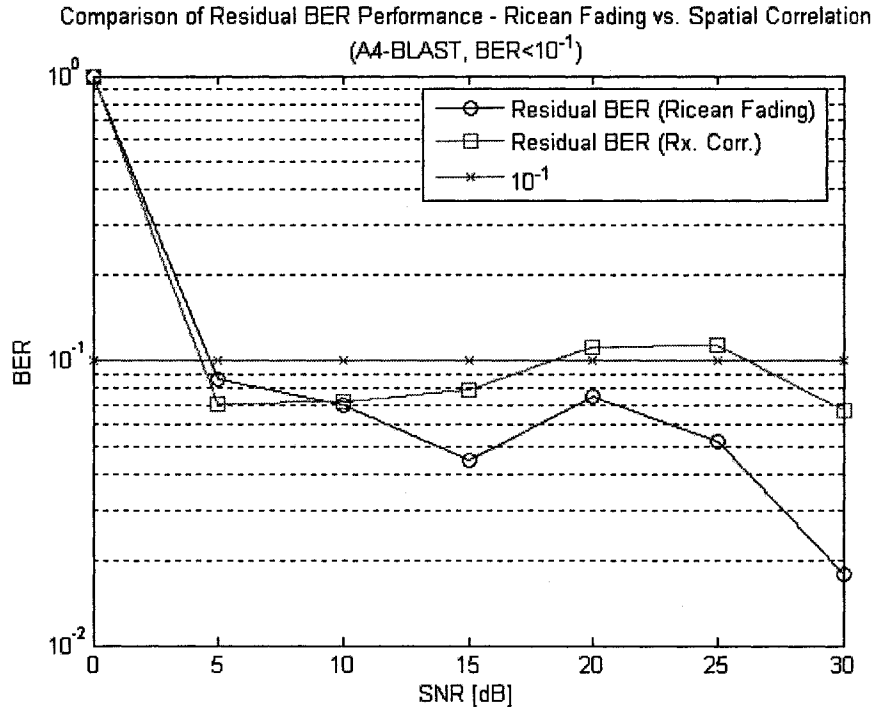


Figure 5-84 Residual BER Performance - Ricean Fading vs. Spatial Correlation (A4-BLAST)

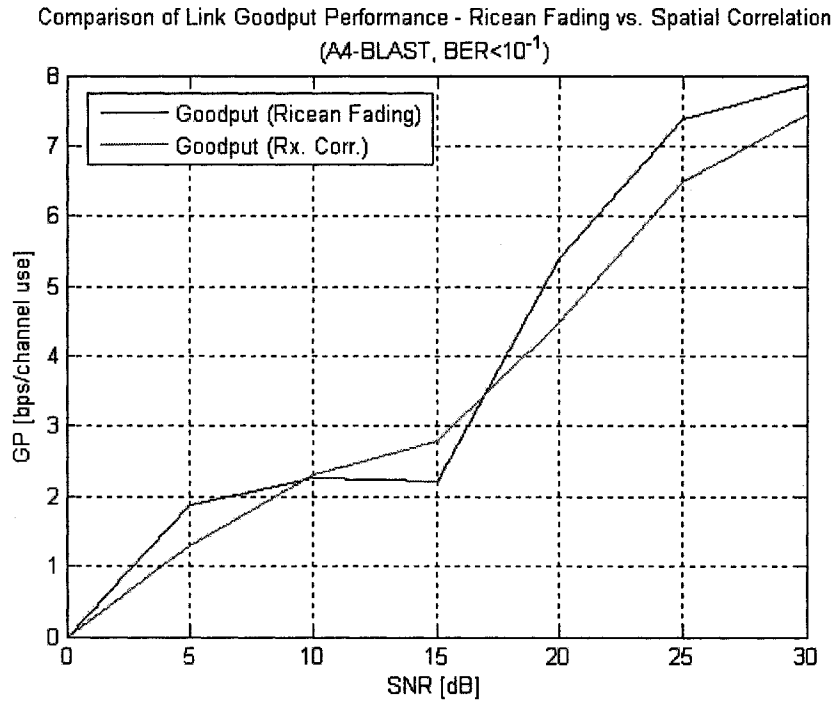


Figure 5-85 Goodput Performance - Ricean Fading vs. Spatial Correlation (A4-BLAST)

In a practical deployment, rank deficiency from ideal Raleigh fading will most certainly be due to the combined degenerative contributions of LOS propagation as well as antenna mutual coupling. Calibration of adaptation to the deployed environment is necessary to ensure expected performance.

5.1.6.5 Implementation Complexity

The importance of the implementation complexity of any adaptive space-time processing method cannot be overstated when considering its usefulness in a practical deployment environment, the A-BLAST technique developed is no different in this regard. With today's fixed point DSP devices capable of achieving upwards of several thousands of millions instructions per second (MIPS) and floating point devices approaching a billion floating point operations per second (GFLOPS), the feasibility of implementation is becoming less dependent on available processing power and more on wireless deployment environmental parameters such as LOS versus NLOS, mobile versus stationary or nomadic, single user versus multi-user, transceiver size, battery power, channel coherence time, channel coherence bandwidth, and media access control layer (MAC) and physical layer (PHY) protocols employed. The A-BLAST adaptation algorithm attempts to minimize processing complexity by employing a table look-up approach to select the A-BLAST codeword to use for a given channel environment and target residual BER. This approach is analogous to adaptive modulation methods where the tables define the BER performance for the particular digital modulation method and channel environment. In the case of A-BLAST adaptive space-time processing, the addition of the MIMO channel spatial rank as an input parameter for table lookup exist. The MIMO channel spatial rank may be efficiently estimated using the eigenvalue decomposition as discussed in §5.1.6.3. The feasibility of the A-BLAST approach depends primarily on the following MIMO environmental and deployment conditions:

- 1) Equally sized antenna arrays at each end of the MIMO channel.
- 2) A narrowband frequency flat fading channel.
- 3) A channel coherence time in excess of the adaptation and feedback interval.

In a fixed wireless access (FWA) or WLAN environment it is certainly possible to provision both the base station (BS), or access point (AP), as well as customer premise equipment (CPE) (e.g. laptop computer, exterior mounted antenna array and RF unit with interior network module) with equally sized antenna arrays. The channel coherence time as well as coherence bandwidth is largely dependent on the level of user mobility and symbol transmission rates offered to the MIMO channel. In a stationary or

relatively low nomadic user environment, typical of many FWA and WLAN deployments, the channel coherence time is typically on the order of tens of milliseconds [39]. In a BWA environment, in order to assume frequency flat fading conditions, achieving a channel coherence bandwidth in excess of the system bandwidth is possible by employing an orthogonal frequency division multiplexed (OFDM) air interface, providing many narrowband frequency flat fading sub-channels over which adaptive space-time processing may occur [39]. Accordingly, the complexity of an A-BLAST implementation in such an environment grows with the number of OFDM sub-channels employing adaptive space-time processing and level of user mobility respectively.

6 CONCLUSIONS AND FUTURE WORK

Consistent with the Introduction of §1, this thesis has approached the questions ‘*What is an optimal MIMO system?*’ and ‘*How much improvement is provided by an optimal MIMO system?*’ through the research of adaptive MIMO space-time processing methods. This thesis proposes an adaptive LST coding method, applicable to any symmetric MIMO system with $M=N$ antennas, called A-BLAST. The space-time codeword of the well known BLAST LST coding method was adapted and combined with channel estimate permutation, as well as, transmitter precoding based on the unitary QR matrix decomposition. By doing so, the performance gap is bridged between the diversity and spatial multiplexing benchmarks of D-BLAST and V-BLAST respectively. The intermediate A-BLAST modes provide more granular control over the diversity and spatial multiplexing codeword weighting and subsequently are better suited to a broader range of operating environments.

Implementations of A-BLAST using two, four, and eight element antenna arrays has been simulated using the SMWE with performance results documented in §5.1.3.1, §5.1.4.1, and §5.1.5.1 for residual BER thresholds of 10^{-1} , 10^{-2} , and 10^{-3} . The A-BLAST results demonstrate the ability to adapt and maintain superior link performance, defined as link *goodput*, in comparison to equivalent non-adaptive implementations of V-BLAST and D-BLAST, as environmental conditions change. Implementation issues such as side channel feedback bandwidth requirements, resiliency to channel state and rank estimation errors, as well as, a discussion on the performance degenerative effects of spatial correlation are included in §5.1.6.4.

Opportunities for further research exist and provide motivation for additional investigation across several fronts. These include such areas as i) improved channel estimation methods for the fast fading MIMO environment, ii) joint optimization of adaptive space-time encoding with adaptive modulation, iii) resiliency to partial CSI quantization error, and iv) extension to the asymmetric MIMO environment.

At time of writing, several important OFDM based wireless air interface standards are under development with others anticipated to soon enter the marketplace. These include revisions of the popular IEEE 802.11 standard for WLAN networks called IEEE 802.11a/g/n. As well, products supporting a NLOS variant of IEEE 802.16 standard for BWA, called IEEE 802.16d/e (a.k.a. WiMAX), are expected to soon be available, allowing deployments of IEEE 802.16d/e wireless metropolitan area (MAN) networks to occur. Accordingly, an investigation toward obtaining a thorough understanding of these standards is important in order to gauge the implementation complexity and potential for

performance improvement arising from the integration, on a per OFDM sub-channel basis, of an adaptive MIMO space-time processing codec, such as A-BLAST.

To conclude, the A-BLAST approach to adaptive space-time processing, as described, successfully demonstrates an ability to outperform the known non-adaptive LST coding benchmarks V-BLAST and D-BLAST. This performance enhancement stems from additional codeword mapping functions which provide more granular control over diversity order and spatial multiplexing gain not available otherwise. In addition, the channel estimate is intelligently permuted and decomposed using a unitary QR decomposition in such a way that increased levels of SINR are maintained at A-BLAST codeword layers with minimal diversity encoding. The A-BLAST adaptation, analogous to that of adaptive modulation, utilize reference BER curves providing conceptually simple and moderately accurate switching between available A-BLAST modes such that throughput is maximized while achieving a target BER performance.

References

- [1] Parker, S., Sandell, M., Yee, M., Sun, Y., Ismail, M., Strauch, P., McGeehan, J., "Space-Time Codes for Future WLANs: Principles, Practice, and Performance", IEEE Communications, December 2004, pp. 96-103.
- [2] Nanda, S., Walton, R., Ketchum, J., Wallace, M., Hsoward, S., "A High-Performance MIMO OFDM Wireless LAN", IEEE Communications, February 2005, pp. 101-109.
- [3] Juntti, M., Vehkaperä, M., Leinonen, J., Li, Z., Tujkovic, D., "MIMO MC-CDMA Communications for Future Cellular Systems", IEEE Communications, February 2005, pp. 118-124.
- [4] Kaiser, T., et al, "When Will Smart Antennas Be Ready for the Market? – Part I", IEEE Signal Processing, March 2005, pp. 87-92.
- [5] Foschini, G., Chizhik, D., Gans, M., Papadias, C., Valenzuela, R., "Analysis and Performance of Some Basic Space-Time Architectures", IEEE Journal on Selected Areas in Communications, Volume 21, Issue 3, April 2003, pp. 48-53.
- [6] Alamouti, S. M., "A Simple Transmit Diversity Technique for Wireless Communications", IEEE Journal Select. Areas Comm., Volume 16, Number 8, October 1998, pp. 1451-1458.
- [7] Mietzner, J., Hoehner, P., "Boosting the Performance of Wireless Communications Systems: Theory and Practice of Multiple Antenna Techniques", IEEE Communications, October 2004, pp. 40-47.
- [8] Jelitto, J., Fettweis, G., "Reduced Dimension Space-Time Processing for Multi-Antenna Wireless Systems", IEEE Wireless Comm., Volume 9, Number 6, December 2002, pp. 18-25.
- [9] Lozano, A., Tulino, A., Verdu, S., "Multiple-Antenna Capacity in the Low-Power Regime", IEEE Transactions on Information Theory, Volume 49, Issue 10, October 2003, pp. 2527-2544.
- [10] Rao, C., Hassibi, B., "Analysis of Multiple-Antenna Wireless Links at Low SNR", IEEE Transactions on Information Theory, Volume 50, Issue 9, September 2004, pp. 2123-2130.
- [11] Damen, M., El Gamel, H., "On the Diversity-vs-Rate Tradeoff in MIMO Systems", IEEE Proceedings of the Information Theory Workshop, April 2003, pp. 357-360.

- [12] Zheng, L., Tse, D., "Diversity and Multiplexing: A Fundamental Tradeoff in Multiple-Antenna Channels", IEEE Transactions on Information Theory, Volume 49, Issue 5, May 2003, pp. 1073-1096.
- [13] Shim, S., Choi, J., Lee, C., Youn, D., "Rank Adaptive Transmission to Improve the Detection Performance of the BLAST in Spatially Correlated MIMO Channel", Proc. IEEE Vehicular Technology Conference, September 2002, Volume 1, pp. 195-198.
- [14] Heath, R., Paulraj, A., "Switching Between Multiplexing and Diversity Based on Constellation Distance", Proc. Allerton Conference on Communication & Control Computing, October 2000, pp. 212-219.
- [15] Heath, R., Paulraj, A., "Linear Dispersion Codes for MIMO Systems Based on Frame Theory", IEEE Transactions on Signal Processing, Volume 50, Issue 10, October 2002, pp. 2429-2441.
- [16] Damen, O., Chkeif, A., Belfore, J., "Lattice Code Decoder for Space-Time Codes", IEEE Communications Letters, Volume 4, Number 5, May 2000, pp. 161-163.
- [17] Bourles-Hamon, M., El Gamal, H., "On the Design of Adaptive Space-Time Codes", IEEE Transactions on Communications, Volume 52, Issue 10, October 2004, pp. 1670-1674.
- [18] Jankiraman, M., Space-Time Codes & MIMO Systems, Boston: Artech House, 2004.
- [19] Golub, G., Van Loan, C., Matrix Computations, Baltimore: John Hopkins University Press, 1996.
- [20] Chizhik, K., Ling, J., Wolniansky, P., Valenzuela, R., Costa, N., Huber, K., "Multiple-Input Multiple-Output Measurements and Modeling in Manhattan", IEEE Journal on Selected Areas in Communications, Volume 21, Issue 3, April 2003, pp. 321-330.
- [21] Gibson, J., et al, The Communications Handbook, Second Edition, CRC Press, 2002.
- [22] Brennan, D., "Linear Diversity Combining Techniques", Proceedings of the IEEE, Volume 91, Number 2, February 2003, pp. 331-356.
- [23] Andersen, J., "Antenna Arrays in Mobile Communications: Gain, Diversity, and Channel Capacity", IEEE Antennas and Propagation, Volume 42, Number 2, April 2000, pp. 12-16.
- [24] Balanis, C., Antenna Theory: Analysis and Design, New York: John Wiley & Sons, 1997.

- [25] Shannon, C., "A Mathematical Theory of Communication", Bell Systems Technical Journal, Volume 27, 1948, pp. 379-423, pp. 623-657.
- [26] Foschini, G., "Layered Space-Time Architecture for Wireless Communication in a Fading Environment When Using Multielement Antennas", Bell Labs Technical Journal, 1996, pp. 41-59.
- [27] Tarokh, V., Jafarkhani, H., Calderbank, A., "Space-Time Block Codes From Orthogonal Designs", IEEE Transactions on Information Theory, Volume 45, Number 5, July 1999, pp. 1456-1467.
- [28] Golden, G., et al, "Detection Algorithm and Initial Laboratory Results Using the V-BLAST Space-Time Communication", Electronic Letters, Volume 35, Issue 1, January 7th, 1999, pp. 14-16.
- [29] Hassibi, B., Hochwald, B., "High-Rate Codes that are Linear in Space and Time", IEEE Transactions on Information Theory, Volume 48, Number 7, October 2000, pp. 1804-1824.
- [30] Ghaderipoor, A., Beygi, L., Jamali, S., "Analytical Survey on the Design of Linear Dispersion Space-Time Codes", ICASSP 2002, Volume 3, May 2002, pp. 2433-2436.
- [31] Salamah, S., Falconer, D., Yanikomeroglu, H., "Transmit Power Control in Fixed Cellular Broadband Wireless Systems", Broadband Communications and Wireless Systems (BCWS) Centre, Carleton University, Ottawa, Canada.
- [32] Liberti, J., Rappaport, T., Smart Antennas for Wireless Communications: IS-95 and Third Generation CDMA Applications, Prentice Hall, 1999.
- [33] Spencer, Q., Peel, C., Swindlehurst, A., Haardt, M., "An Introduction to the Multi-User MIMO Downlink", IEEE Communications Magazine, October 2004, pp. 60-66.
- [34] Molisch, A., Win, M., "MIMO Systems with Antenna Selection", IEEE Microwave Magazine, March 2004, pp. 46-56.
- [35] Sanayei, S., Norratinia, A., "Antenna Selection in MIMO Systems", IEEE Communications Magazine, October 2004, pp. 68-72.
- [36] Sklar, B., Digital Communications – Fundamentals and Applications, Prentice Hall, 1988.
- [37] Wells, R., Applied Coding and Information Theory for Engineers, Prentice Hall, 1999.

- [38] Stewart, G., "On the Perturbation Analysis of LU Cholesky, and QR Factorizations", *SIAM J. Matrix Anal. Appl.* 14, pp. 1141-1145.
- [39] Hanzo, L., Munster, M., Choi, B., Keller, T., *OFDM and MC-CDMA for Broadband Multi-User Communications, WLANs, and Broadcasting*, IEEE Press, 2004.

Appendix A – SMWE Source File Listing

Source File Name	RCS Version	File Type	Description
AMIMOConstants.m	1.17	Script	Defines various constants used throughout the SMWE.
AMIMOCtrl.m	1.14	Script	Implements the adaptive controller functionality.
AMIMOInitCtrl.m	1.12	Script	Initializes the adaptive controller at start up.
AMIMOInitPerf.m	1.1	Script	Initializes performance monitoring at start up.
AMIMOInitTrain.m	1.4	Script	Initializes the controller for training mode.
AMIMOPerfGen.m	1.20	Script	Implements the performance log generation.
AMIMOPerfMon.m	1.15	Script	Implements the performance monitoring functionality.
AMIMOSimDef.m	1.7	Script	Defines the simulation parameters controlling the SMWE execution.
AMIMOSimDisp.m	1.10	Script	Dumps SMWE parameters to stdout at start of each simulation run.
AMIMOTimerTic.m	1.2	Script	Tics simulation timers at each iteration of the simulation loop.
AMIMO_DemodS.m	1.4	Function	Implements symbol demodulation functionality.
AMIMO_EstH.m	1.5	Function	Implements MIMO channel estimation functionality.
AMIMO_EstRank.m	1.6	Function	Implements channel rank estimation functionality.
AMIMO_GCBCnv.m	1.2	Function	Performs GCB baud conversion.
AMIMO_GenH.m	1.5	Function	Implements MIMO channel realization generation.
AMIMO_GenDivWt.m	1.1	Function	Computes diversity combiner weights.
AMIMO_GenH.m	1.5	Function	MIMO channel generator.
AMIMO_GenPrec.m	1.6	Function	Generates required transmitter and receiver ST precoding.
AMIMO_GenS.m	1.4	Function	Implements symbol generation functionality.
AMIMO_GenW.m	1.4	Function	Implements AWGN generation.
AMIMO_GetCodeRate	1.1	Function	Computes code rate in symbols per channel use.
AMIMO_GetOutSNR.m	1.4	Function	Computes outage SNR for given BER target and ABLAST mode.
AMIMO_ModeSel.m	1.14	Function	Implements adaptive mode selection functionality.

AMIMO_ModS.m	1.5	Function	Implements symbol modulation functionality.
AMIMO_ModSel.m	1.3	Function	Implements adaptive modulation functionality.
AMIMO_PSKDet.m	1.5	Function	Implements MPSK symbol detection functionality.
AMIMO_RxPrecode.m	1.4	Function	Implements receiver ST precoding functionality.
AMIMO_StcSel.m	1.6	Function	Implements adaptive STC selection functionality.
AMIMO_STDemapper.m	1.4	Function	Implements receiver ST demapping functionality.
AMIMO_STMapper.m	1.4	Function	Implements transmitter ST mapping functionality.
AMIMO_TxPrecode.m	1.4	Function	Implements transmitter ST precoding functionality.
AMIMO_TxRx.m	1.4	Function	Implements MIMO channel ST transmission/reception.
GetAWGN.m	1.1	Function	Utility function for AWGN generation.
GetH.m	1.1	Function	Utility function for Raleigh MIMO channel generation.
ModConstants.m	1.3	Script	Defines various modulation constants.
STMapConstants.m	1.4	Script	Defines various ST mapping constants.
TestAMIMO.m	1.14	Script	Main routine defining the SMWE execution.
Toeplitz.m	1.1	Function	Utility function to generate Toeplitz form matrices.

Table 2 SMWE Source File Listing

All files are archived on the server `jaguar.cs.mun.ca` at the following locations:

Functions → `/users/palab/student2/jasonlee/matlab/AMIMO/bin/RCS`

Scripts → `/users/palab/student2/jasonlee/matlab/AMIMO/script/RCS`

Utilities → `/users/palab/student2/jasonlee/matlab/util/RCS`

Appendix B – Supplementary A-BLAST Mode Summary Data

Example Calculation of Code Rate [s/cu] and Diversity Order

Example) A6-BLAST4:

$$\text{Code Rate} = 18 \text{ [symbol/codeword]} * 1/6 \text{ [codeword/channel-use]} = 3 \text{ [s/cu]}$$

$$\text{Diversity Order} = 12/18 \text{ [symbol / (symbol / codeword)]} * 6 \text{ [T/R diversity path]} + (18 - 12)/18 \text{ [symbol / (symbol / codeword)]} * 24 \text{ [T/R diversity path]} = 12$$

A2-BLAST (M = N = 2)

Mode	Code Rate [s/cu]	Diversity Order	Codeword
A2-BLAST1	2	2	$s_1 \quad s_3$ $s_2 \quad s_4$
A2-BLAST2	1	4	$s_1 \quad s_2$ $s_2 \quad s_1$

Table 3 A2-BLAST Mode Summary (M=N=2)

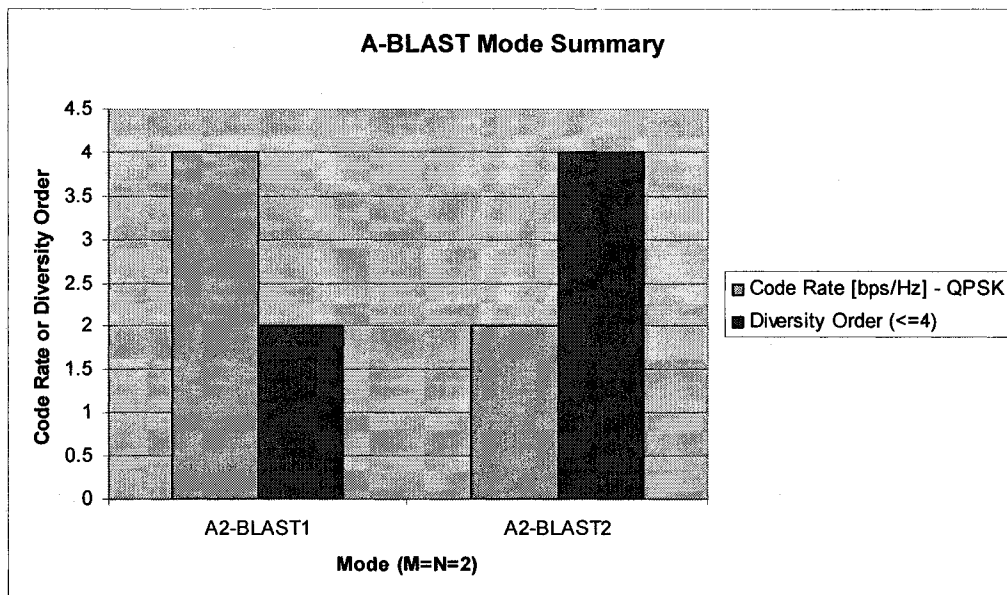


Figure 86 A2-BLAST Mode Summary (M=N=2)

A3-BLAST ($M = N = 3$)

Mode	Code Rate [s/cu]	Diversity Order	Codeword
A3-BLAST1	3	3	$s_1 \ s_4 \ s_7$ $s_2 \ s_5 \ s_8$ $s_3 \ s_6 \ s_9$
A3-BLAST2	2	4.5	$s_1 \ s_4 \ s_6$ $s_2 \ s_5 \ s_3$ $s_3 \ s_2 \ s_5$
A3-BLAST3	1	9	$s_1 \ s_3 \ s_2$ $s_2 \ s_1 \ s_3$ $s_3 \ s_2 \ s_1$

Table 4 A3-BLAST Mode Summary ($M=N=3$)

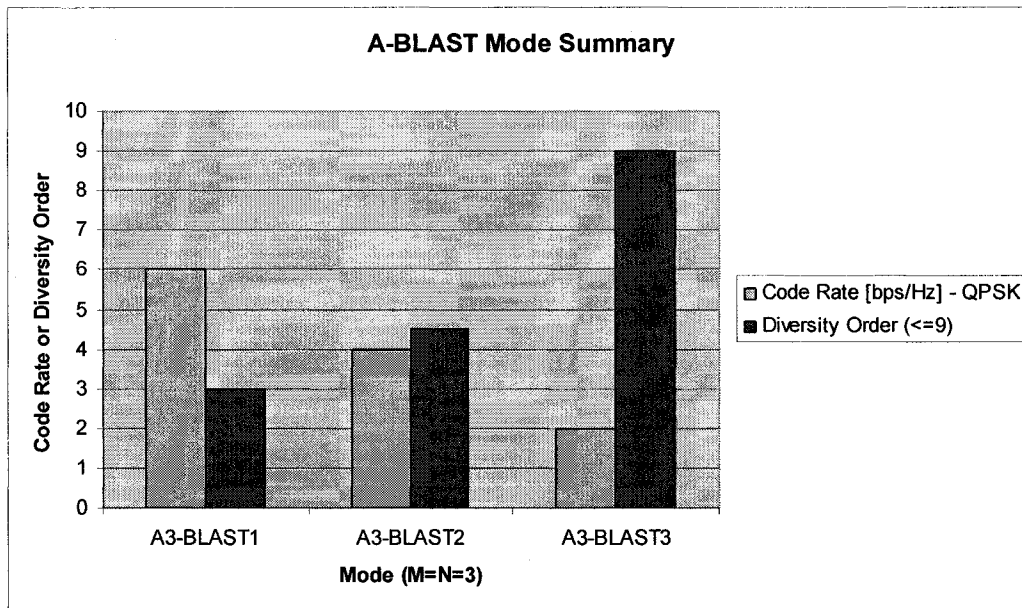


Figure 87 A3-BLAST Mode Summary ($M=N=3$)

A4-BLAST (M = N = 4)

Mode	Code Rate [s/cu]	Diversity Order	Codeword
A4-BLAST1	4	4	s_1 s_5 s_9 s_{13} s_2 s_6 s_{10} s_{14} s_3 s_7 s_{11} s_{15} s_4 s_8 s_{12} s_{16}
A4-BLAST2	3	5.3	s_1 s_5 s_8 s_{11} s_2 s_6 s_9 s_{12} s_3 s_7 s_{10} s_4 s_4 s_3 s_7 s_{10}
A4-BLAST3	2	8	s_1 s_5 s_7 s_8 s_2 s_6 s_4 s_3 s_3 s_2 s_6 s_4 s_4 s_3 s_2 s_6
A4-BLAST4	1	16	s_1 s_4 s_3 s_2 s_2 s_1 s_4 s_3 s_3 s_2 s_1 s_4 s_4 s_3 s_2 s_1

Table 5 A4-BLAST Mode Summary (M=N=4)

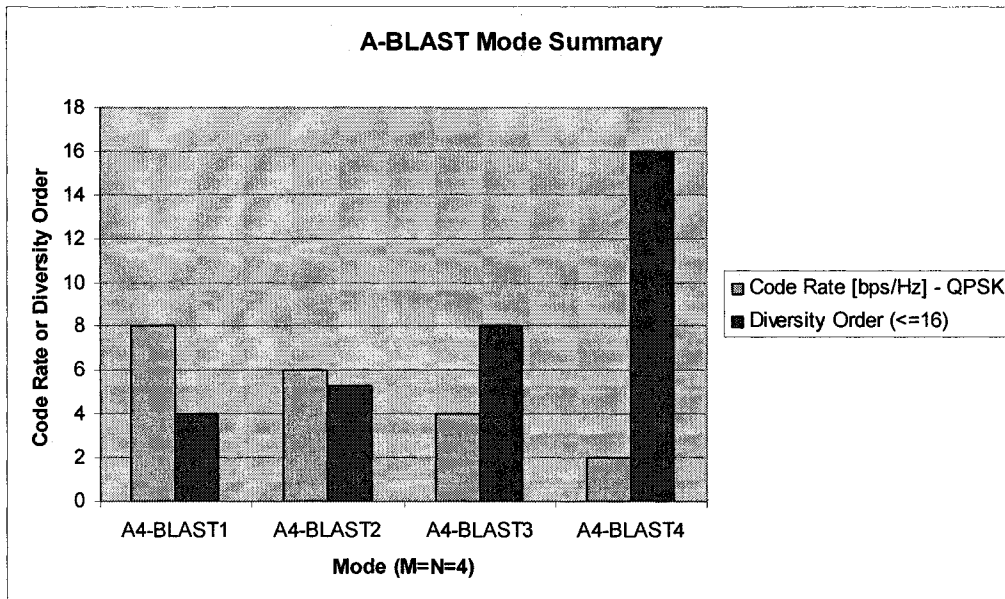


Figure 88 A4-BLAST Mode Summary (M=N=4)

A5-BLAST ($M = N = 5$)

Mode	Code Rate [s/cu]	Diversity Order	Codeword
A5-BLAST1	5	5	s_1 s_6 s_{11} s_{16} s_{21} s_2 s_7 s_{12} s_{17} s_{22} s_3 s_8 s_{13} s_{18} s_{23} s_4 s_9 s_{14} s_{19} s_{24} s_5 s_{10} s_{15} s_{20} s_{25}
A5-BLAST2	4	6.25	s_1 s_6 s_{10} s_{14} s_{18} s_2 s_7 s_{11} s_{15} s_{19} s_3 s_8 s_{12} s_{16} s_{20} s_4 s_9 s_{13} s_{17} s_5 s_5 s_4 s_9 s_{13} s_{17}
A5-BLAST3	3	8.33	s_1 s_6 s_9 s_{12} s_{21} s_2 s_7 s_{10} s_{13} s_{22} s_3 s_8 s_{11} s_5 s_4 s_4 s_3 s_8 s_{11} s_5 s_5 s_4 s_3 s_8 s_{11}
A5-BLAST4	2	12.5	s_1 s_6 s_8 s_9 s_{10} s_2 s_7 s_5 s_8 s_9 s_3 s_2 s_7 s_5 s_8 s_4 s_3 s_2 s_7 s_5 s_5 s_4 s_3 s_2 s_7
A5-BLAST5	1	25	s_1 s_5 s_4 s_3 s_2 s_2 s_1 s_5 s_4 s_3 s_3 s_2 s_1 s_5 s_4 s_4 s_3 s_2 s_1 s_5 s_5 s_4 s_3 s_2 s_1

Table 6 A5-BLAST Mode Summary ($M=N=5$)

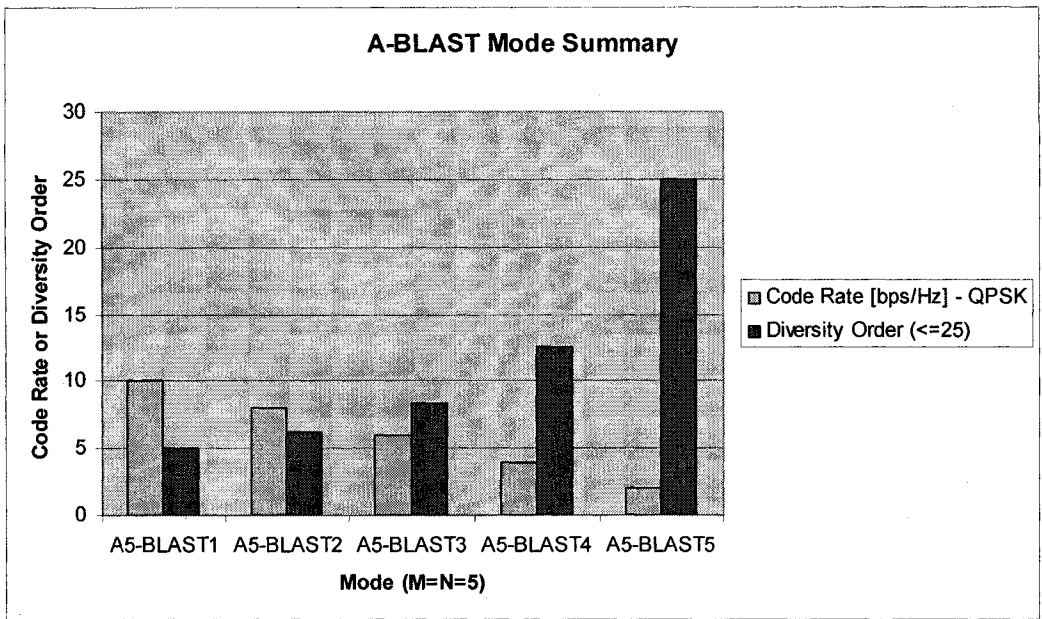


Figure 89 A5-BLAST Mode Summary (M=N=5)

A6-BLAST ($M = N = 6$)

Mode	Code Rate [s/cu]	Diversity Order	Codeword
A6-BLAST1	6	6	s_1 s_7 s_{13} s_{19} s_{25} s_{31} s_2 s_8 s_{14} s_{20} s_{26} s_{32} s_3 s_9 s_{15} s_{21} s_{27} s_{33} s_4 s_{10} s_{16} s_{22} s_{28} s_{34} s_5 s_{11} s_{17} s_{23} s_{29} s_{35} s_6 s_{12} s_{18} s_{24} s_{30} s_{36}
A6-BLAST2	5	7.2	s_1 s_7 s_{12} s_{17} s_{22} s_{27} s_2 s_8 s_{13} s_{18} s_{23} s_{28} s_3 s_9 s_{14} s_{19} s_{24} s_{29} s_4 s_{10} s_{15} s_{20} s_{25} s_{30} s_5 s_{11} s_{16} s_{21} s_{26} s_6 s_6 s_5 s_{11} s_{16} s_{21} s_{26}
A6-BLAST3	4	9	s_1 s_7 s_{11} s_{15} s_{19} s_{22} s_2 s_8 s_{12} s_{16} s_{20} s_{23} s_3 s_9 s_{13} s_{17} s_{21} s_{24} s_4 s_{10} s_{14} s_{18} s_6 s_5 s_5 s_4 s_{10} s_{14} s_{18} s_6 s_6 s_5 s_4 s_{10} s_{14} s_{18}
A6-BLAST4	3	12	s_1 s_7 s_{10} s_{13} s_{15} s_{17} s_2 s_8 s_{11} s_{14} s_{16} s_{18} s_3 s_9 s_{12} s_6 s_5 s_4 s_4 s_3 s_9 s_{12} s_6 s_5 s_5 s_4 s_3 s_9 s_{12} s_6 s_6 s_5 s_4 s_3 s_9 s_{12}
A6-BLAST5	2	18	s_1 s_7 s_9 s_{10} s_{11} s_{12} s_2 s_8 s_6 s_5 s_4 s_3 s_3 s_2 s_8 s_6 s_5 s_4 s_4 s_3 s_2 s_8 s_6 s_5 s_5 s_4 s_3 s_2 s_8 s_6 s_6 s_5 s_4 s_3 s_2 s_8

A6-BLAST6	1	36	s_1 s_6 s_5 s_4 s_3 s_2 s_2 s_1 s_6 s_5 s_4 s_3 s_3 s_2 s_1 s_6 s_5 s_4 s_4 s_3 s_2 s_1 s_6 s_5 s_5 s_4 s_3 s_2 s_1 s_6 s_6 s_5 s_4 s_3 s_2 s_1
-----------	---	----	--

Table 7 A6-BLAST Mode Summary (M=N=6)

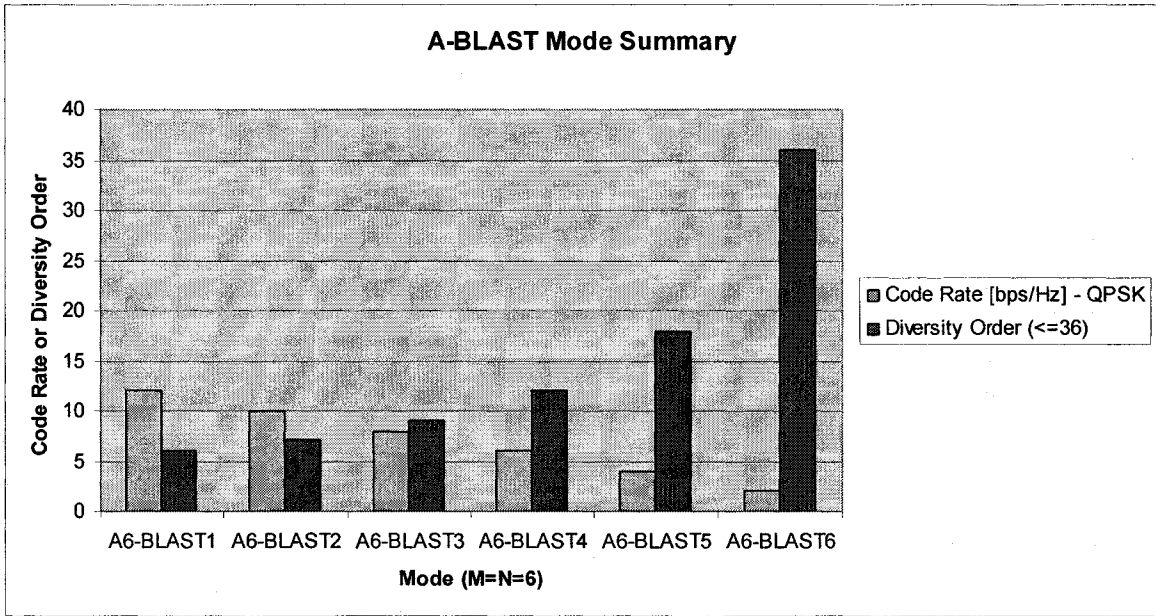


Figure 90 A6-BLAST Mode Summary (M=N=6)

A7-BLAST ($M = N = 7$)

Mode	Code Rate [s/cu]	Diversity Order	Codeword
A7-BLAST1	7	7	s_1 s_8 s_{15} s_{22} s_{29} s_{36} s_{43} s_2 s_9 s_{16} s_{23} s_{30} s_{37} s_{44} s_3 s_{10} s_{17} s_{24} s_{31} s_{38} s_{45} s_4 s_{11} s_{18} s_{25} s_{32} s_{39} s_{46} s_5 s_{12} s_{19} s_{26} s_{33} s_{40} s_{47} s_6 s_{13} s_{20} s_{27} s_{34} s_{41} s_{48} s_7 s_{14} s_{21} s_{28} s_{35} s_{42} s_{49}
A7-BLAST2	6	8.2	s_1 s_8 s_{14} s_{20} s_{26} s_{32} s_{38} s_2 s_9 s_{15} s_{21} s_{27} s_{33} s_{39} s_3 s_{10} s_{16} s_{22} s_{28} s_{34} s_{40} s_4 s_{11} s_{17} s_{23} s_{29} s_{35} s_{41} s_5 s_{12} s_{18} s_{24} s_{30} s_{36} s_{42} s_6 s_{13} s_{19} s_{25} s_{31} s_{37} s_7 s_7 s_6 s_{13} s_{19} s_{25} s_{31} s_{37}
A7-BLAST3	5	9.8	s_1 s_8 s_{13} s_{18} s_{23} s_{28} s_{32} s_2 s_9 s_{14} s_{19} s_{24} s_{29} s_{33} s_3 s_{10} s_{15} s_{20} s_{25} s_{30} s_{34} s_4 s_{11} s_{16} s_{21} s_{26} s_{31} s_{35} s_5 s_{12} s_{17} s_{22} s_{27} s_7 s_6 s_6 s_5 s_{12} s_{17} s_{22} s_{27} s_7 s_7 s_6 s_5 s_{12} s_{17} s_{22} s_{37}
A7-BLAST4	4	12.25	s_1 s_8 s_{12} s_{16} s_{20} s_{23} s_{26} s_2 s_9 s_{13} s_{17} s_{21} s_{24} s_{27} s_3 s_{10} s_{14} s_{18} s_{22} s_{25} s_{28} s_4 s_{11} s_{15} s_{19} s_7 s_6 s_5 s_5 s_4 s_{11} s_{15} s_{19} s_7 s_6 s_6 s_5 s_4 s_{11} s_{15} s_{19} s_7 s_7 s_6 s_5 s_4 s_{11} s_{15} s_{19}

A7-BLAST5	3	16.3	s_1 s_8 s_{11} s_{14} s_{16} s_{18} s_{20} s_2 s_9 s_{12} s_{15} s_{17} s_{19} s_{21} s_3 s_{10} s_{13} s_7 s_6 s_5 s_4 s_4 s_3 s_{10} s_{13} s_7 s_6 s_5 s_5 s_4 s_3 s_{10} s_{13} s_7 s_6 s_6 s_5 s_4 s_3 s_{10} s_{13} s_7 s_7 s_6 s_5 s_4 s_3 s_{10} s_{13}
A7-BLAST6	2	24.5	s_1 s_8 s_{10} s_{11} s_{12} s_{13} s_{14} s_2 s_9 s_7 s_6 s_5 s_4 s_3 s_3 s_2 s_9 s_7 s_6 s_5 s_4 s_4 s_3 s_2 s_9 s_7 s_6 s_5 s_5 s_4 s_3 s_2 s_9 s_7 s_6 s_6 s_5 s_4 s_3 s_2 s_9 s_7 s_7 s_6 s_5 s_4 s_3 s_2 s_9
A7-BLAST7	1	49	s_1 s_7 s_6 s_5 s_4 s_3 s_2 s_2 s_1 s_7 s_6 s_5 s_4 s_3 s_3 s_2 s_1 s_7 s_6 s_5 s_4 s_4 s_3 s_2 s_1 s_7 s_6 s_5 s_5 s_4 s_3 s_2 s_1 s_7 s_6 s_6 s_5 s_4 s_3 s_2 s_1 s_7 s_7 s_6 s_5 s_4 s_3 s_2 s_1

Table 8 A7-BLAST Mode Summary (M=N=7)

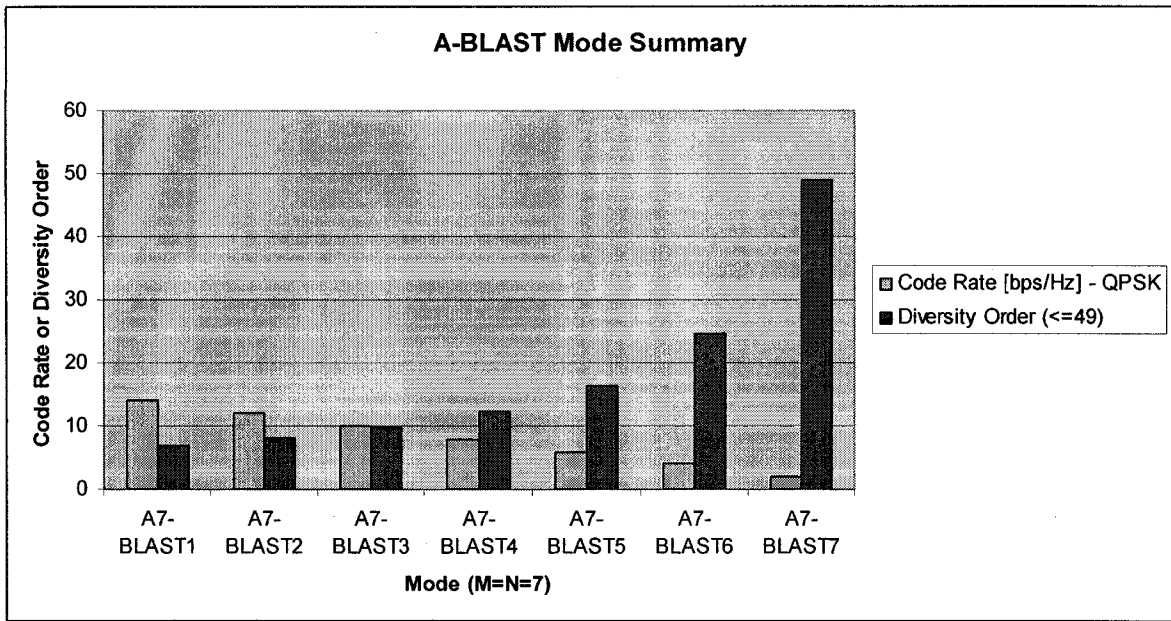


Figure 91 A7-BLAST Mode Summary (M=N=7)

A8-BLAST ($M = N = 8$)

Mode	Code Rate [s/cu]	Diversity Order	Codeword
A8-BLAST1	8	8	s_1 s_9 s_{17} s_{25} s_{33} s_{41} s_{49} s_{57} s_2 s_{10} s_{18} s_{26} s_{34} s_{42} s_{50} s_{58} s_3 s_{11} s_{19} s_{27} s_{35} s_{43} s_{51} s_{59} s_4 s_{12} s_{20} s_{28} s_{36} s_{44} s_{52} s_{60} s_5 s_{13} s_{21} s_{29} s_{37} s_{45} s_{53} s_{61} s_6 s_{14} s_{22} s_{30} s_{38} s_{46} s_{54} s_{62} s_7 s_{15} s_{23} s_{31} s_{39} s_{47} s_{55} s_{63} s_8 s_{16} s_{24} s_{32} s_{40} s_{48} s_{56} s_{64}
A8-BLAST2	7	9.1	s_1 s_9 s_{16} s_{23} s_{30} s_{37} s_{44} s_{51} s_2 s_{10} s_{17} s_{24} s_{31} s_{38} s_{45} s_{52} s_3 s_{11} s_{18} s_{25} s_{32} s_{39} s_{46} s_{53} s_4 s_{12} s_{29} s_{26} s_{33} s_{40} s_{47} s_{54} s_5 s_{13} s_{20} s_{27} s_{34} s_{41} s_{48} s_{55} s_6 s_{14} s_{21} s_{28} s_{35} s_{42} s_{49} s_{56} s_7 s_{15} s_{22} s_{29} s_{36} s_{43} s_{50} s_8 s_8 s_7 s_{15} s_{22} s_{29} s_{36} s_{43} s_{50}
A8-BLAST3	6	10.7	s_1 s_9 s_{15} s_{21} s_{27} s_{33} s_{39} s_{44} s_2 s_{10} s_{16} s_{22} s_{28} s_{34} s_{40} s_{45} s_3 s_{11} s_{17} s_{23} s_{29} s_{35} s_{41} s_{46} s_4 s_{12} s_{18} s_{24} s_{30} s_{36} s_{42} s_{47} s_5 s_{13} s_{19} s_{25} s_{31} s_{37} s_{43} s_{48} s_6 s_{14} s_{20} s_{26} s_{32} s_{38} s_8 s_7 s_7 s_6 s_{14} s_{20} s_{26} s_{32} s_{38} s_8 s_8 s_7 s_6 s_{14} s_{20} s_{26} s_{32} s_{38}
A8-BLAST4	5	12.8	s_1 s_9 s_{14} s_{19} s_{24} s_{29} s_{33} s_{37} s_2 s_{10} s_{15} s_{20} s_{25} s_{30} s_{34} s_{38} s_3 s_{11} s_{16} s_{21} s_{26} s_{31} s_{35} s_{39} s_4 s_{12} s_{17} s_{22} s_{27} s_{32} s_{36} s_{40} s_5 s_{13} s_{18} s_{23} s_{28} s_8 s_7 s_6 s_6 s_5 s_{13} s_{18} s_{23} s_{28} s_8 s_7 s_7 s_6 s_5 s_{13} s_{18} s_{23} s_{28} s_8 s_8 s_7 s_6 s_5 s_{13} s_{18} s_{23} s_{28}

A8-BLAST5	4	16	s_1 s_9 s_{13} s_{17} s_{21} s_{24} s_{27} s_{30} s_2 s_{10} s_{14} s_{18} s_{22} s_{25} s_{28} s_{31} s_3 s_{11} s_{15} s_{19} s_{23} s_{26} s_{29} s_{32} s_4 s_{12} s_{16} s_{20} s_8 s_7 s_6 s_5 s_5 s_4 s_{12} s_{16} s_{20} s_8 s_7 s_6 s_6 s_5 s_4 s_{12} s_{16} s_{20} s_8 s_7 s_7 s_6 s_5 s_4 s_{12} s_{16} s_{20} s_8 s_8 s_7 s_6 s_5 s_4 s_{12} s_{16} s_{20}
A8-BLAST6	3	21.3	s_1 s_9 s_{12} s_{15} s_{17} s_{19} s_{21} s_{23} s_2 s_{10} s_{13} s_{16} s_{18} s_{20} s_{22} s_{24} s_3 s_{11} s_{14} s_8 s_7 s_6 s_5 s_4 s_4 s_3 s_{11} s_{14} s_8 s_7 s_6 s_5 s_5 s_4 s_3 s_{11} s_{14} s_8 s_7 s_6 s_6 s_5 s_4 s_3 s_{11} s_{14} s_8 s_7 s_7 s_6 s_5 s_4 s_3 s_{11} s_{14} s_8 s_8 s_7 s_6 s_5 s_4 s_3 s_{11} s_{14}
A8-BLAST7	2	32	s_1 s_9 s_{11} s_{12} s_{13} s_{14} s_{15} s_{16} s_2 s_{10} s_8 s_7 s_6 s_5 s_4 s_3 s_3 s_2 s_{10} s_8 s_7 s_6 s_5 s_4 s_4 s_3 s_2 s_{10} s_8 s_7 s_6 s_5 s_5 s_4 s_3 s_2 s_{10} s_8 s_7 s_6 s_6 s_5 s_4 s_3 s_2 s_{10} s_8 s_7 s_7 s_6 s_5 s_4 s_3 s_2 s_{10} s_8 s_8 s_7 s_6 s_5 s_4 s_3 s_2 s_{10}
A8-BLAST8	1	64	s_1 s_8 s_7 s_6 s_5 s_4 s_3 s_2 s_2 s_1 s_8 s_7 s_6 s_5 s_4 s_3 s_3 s_2 s_1 s_8 s_7 s_6 s_5 s_4 s_4 s_3 s_2 s_1 s_8 s_7 s_6 s_5 s_5 s_4 s_3 s_2 s_1 s_8 s_7 s_6 s_6 s_5 s_4 s_3 s_2 s_1 s_8 s_7 s_7 s_6 s_5 s_4 s_3 s_2 s_1 s_8 s_8 s_7 s_6 s_5 s_4 s_3 s_2 s_1

Table 9 A8-BLAST Mode Summary (M=N=8)

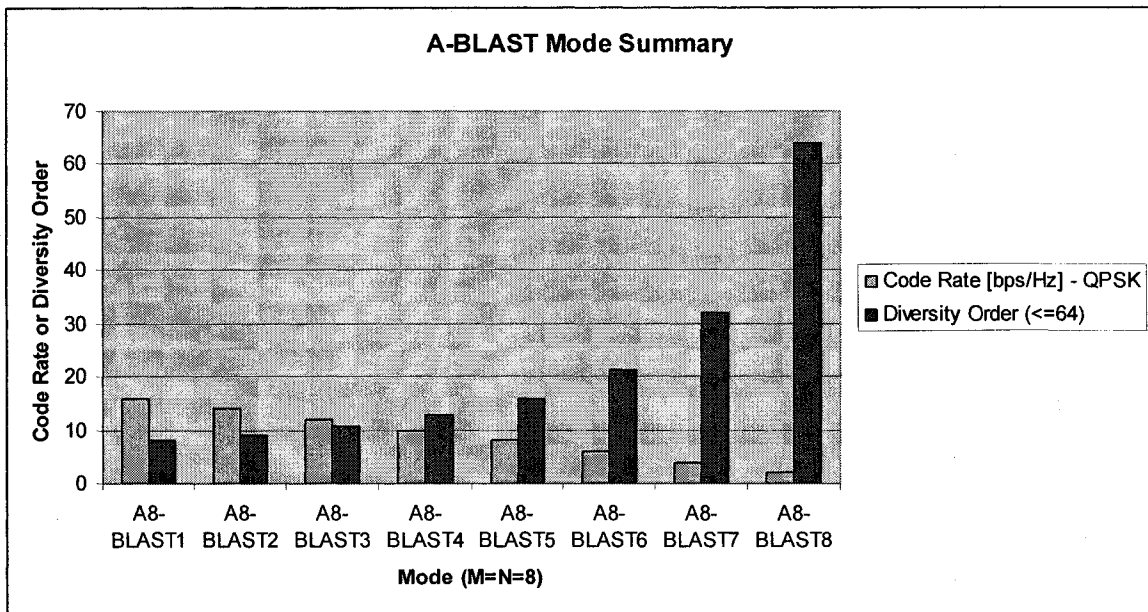


Figure 92 A8-BLAST Mode Summary (M=N=8)



